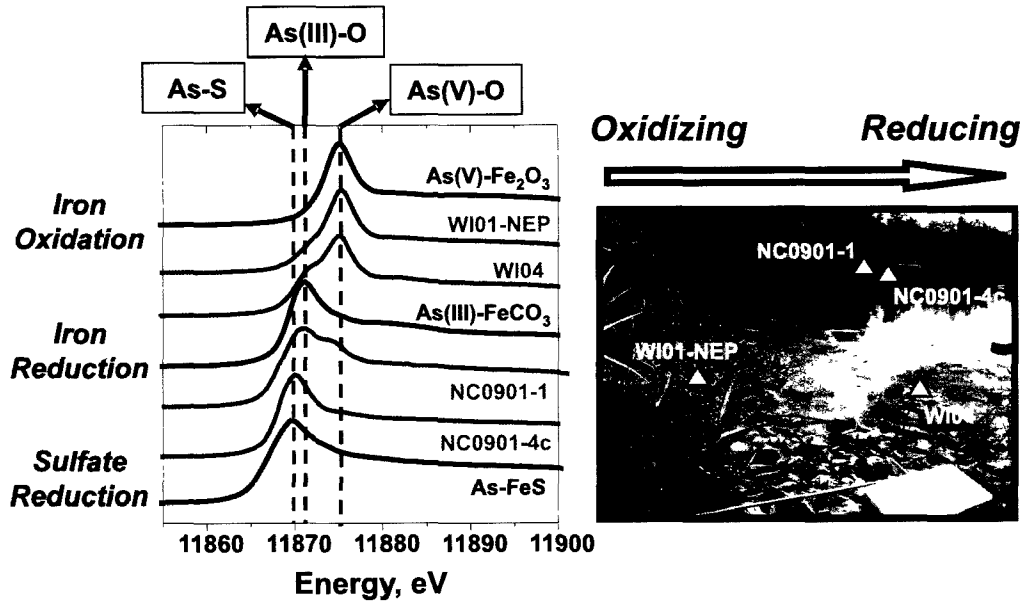
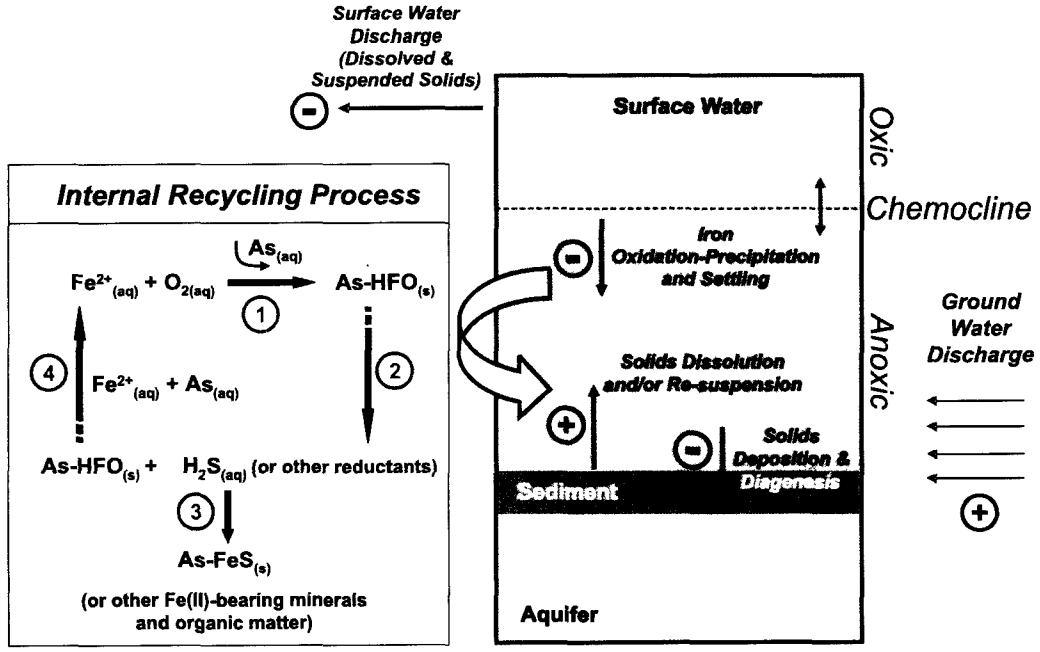
United States Environmental Protection Agency

600R05161

Field Study of the Fate of Arsenic, Lead, and Zinc at the Ground-Water/Surface-Water Interface



Redox Controls on Contaminant Speciation and Mobility



EPA/600/R-05/161
December 2005

Field Study of the Fate of Arsenic, Lead, and Zinc at the Ground-Water/ Surface-Water Interface

Robert G. Ford, Richard T. Wilkin,
Cynthia J. Paul, Frank Beck, Jr., and Tony Lee
U.S. Environmental Protection Agency
Office of Research and Development
National Risk Management Research Laboratory
Ground Water and Ecosystems Restoration Division
Ada, Oklahoma 74820

Kirk G. Scheckel
U. S. Environmental Protection Agency
Office of Research and Development
National Risk Management Research Laboratory
Land Remediation and Pollution Control Division
Cincinnati, Ohio 45268

Patrick Clark
U. S. Environmental Protection Agency
Office of Research and Development
National Risk Management Research Laboratory
Technology Transfer and Support Division
Cincinnati, Ohio 45268

National Risk Management Research Laboratory
Office of Research and Development
U.S. Environmental Protection Agency
Cincinnati, Ohio 45268

Notice

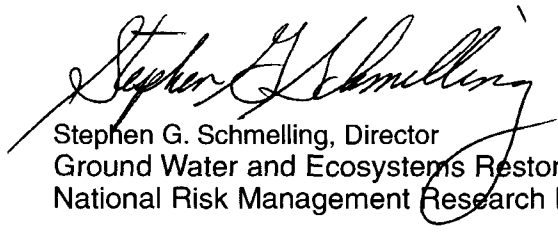
The U. S. Environmental Protection Agency through its Office of Research and Development funded the research described herein. This report has been subjected to the Agency's peer and administrative review and has been approved for publication as an EPA document. Mention of trade names or commercial products does not constitute endorsement or recommendation for use. All research projects making conclusions or recommendations based on environmental data and funded by the U.S. Environmental Protection Agency are required to participate in the Agency Quality Assurance Program. This project was conducted under an approved Quality Assurance Project Plan. The procedures specified in this plan were used without exception. Information on the plan and documentation of the quality assurance activities and results are available from the Principal Investigator.

Foreword

The U.S. Environmental Protection Agency is charged by Congress with protecting the Nation's land, air, and water resources. Under a mandate of national environmental laws, the Agency strives to formulate and implement actions leading to a compatible balance between human activities and the ability of natural systems to support and nurture life. To meet this mandate, EPA's research program is providing data and technical support for solving environmental problems today and building a science knowledge base necessary to manage our ecological resources wisely, understand how pollutants affect our health, and prevent or reduce environmental risks in the future.

The National Risk Management Research Laboratory is the Agency's center for investigation of technological and management approaches for preventing and reducing risks from pollution that threatens human health and the environment. The focus of the Laboratory's research program is on methods and their cost-effectiveness for prevention and control of pollution to air, land, water, and subsurface resources; protection of water quality in public water systems; remediation of contaminated sites, sediments and ground water; prevention and control of indoor air pollution; and restoration of ecosystems. NRMRL collaborates with both public and private sector partners to foster technologies that reduce the cost of compliance and to anticipate emerging problems. NRMRL's research provides solutions to environmental problems by: developing and promoting technologies that protect and improve the environment; advancing scientific and engineering information to support regulatory and policy decisions; and providing the technical support and information transfer to ensure implementation of environmental regulations and strategies at the national, state, and community levels.

This publication has been produced as part of the Laboratory's strategic long-term research plan. It is published and made available by EPA's Office of Research and Development to assist the user community and to link researchers with their clients. Characterization of contaminant transport across the ground-water/surface-water transition zone is an important component of risk characterization for sites that are a source of contaminants within an urban watershed. Defining the chemical and biological factors that control the fate of ground-water contaminants that are discharged into surface water is critical to the design of effective risk management strategies. This report summarizes findings from an extensive field investigation conducted to determine the fate of inorganic contaminants within the headwaters of an urban watershed and to support the design and evaluation of remedial strategies to mitigate exposure to contaminants in surface water and sediments.



Stephen G. Schmelling, Director
Ground Water and Ecosystems Restoration Division
National Risk Management Research Laboratory

Contents

Foreword iii
Figures vii
Tables ix
Acknowledgments xi
Executive Summary xiii

Chapter 1
- Purpose 1
- Study Scope 3

Chapter 2
- Site Background 5
- Study Approach 5
- Site Characterization Methods 9
  - Field Measurements 9
    - Ground Water 9
    - Surface Water 9
  - Laboratory Measurements 10
    - Water Chemistry 10
    - Sediments 10
  - Sediment Chemistry and Mineralogy 10
  - Mineralogical Characterization 11
  - X-ray Absorption Spectroscopy 11
    - Arsenic XAS 11
    - Pb and Zn XAS 11
  - Sediment Extraction Procedures 12
    - Surficial Sediments 12
    - Buried Sediments 12
  - Scanning Electron Microscopy-Energy Dispersive Spectroscopy 12

Chapter 3
- Site Hydrology 15
- Media-Specific Contaminant Distributions 24
  - Ground Water 24
  - Surface Water 24
  - Sediments 27
- Chemical Speciation of Metals in Sediments 32
  - Sediment Extractions 32
    - Surficial Sediments 32
    - Buried Sediments 33
- Element Speciation by X-ray Absorption Spectroscopy 38
- Scanning Electron Microscopy 43

Chapter 4
- Stability of Contaminants in HBHA Pond Sediments 47
- Monitoring Long-Term Behavior (or Performance) of HBHA Pond 49
- Relevance to Other Sites 49

References 51
Appendix A 55
Appendix B 57
Appendix C 63

Figures

Figure 1 Conceptual model of geochemical zones that play a dominant role in governing solid-liquid partitioning of arsenic (lead and zinc) across the GW/SW transition zone at the Industri-Plex Superfund Site. 2

Figure 2 Prominent land features within the Industri-Plex Superfund Site and adjacent to the HBHA Pond. 6

Figure 3 (A) Arsenic (As), benzene (Bz), and toluene (Tl) concentrations (ppb) from temporary ground-water sampling locations as a function of depth below ground surface (feet) for the study site. 7

Figure 4 (A) Close-up view of permanent ground-water monitoring network; arrows show approximate centerline of arsenic and BTEX plumes discharging into HBHA Pond. 8

Figure 5 (A) Patterns in surface water and ground-water flow budgets within the HBHA Pond as documented by Aurilio et al. (1994) and Wick et al. (2000). 16

Figure 6 Aerial distribution and time-dependent variability for total dissolved arsenic concentrations (ppb) detected in tubing wells established adjacent to the HBHA Pond. 17

Figure 7 Aerial distribution and time-dependent variability for total dissolved zinc concentrations (ppb) detected in tubing wells established adjacent to the HBHA Pond. 18

Figure 8 Aerial distribution and time-dependent variability for benzene concentrations (ppb) detected in tubing wells established adjacent to the HBHA Pond. 19

Figure 9 Vertical patterns in water quality within the northern part of the HBHA Pond on sampling dates in April 2000, August 2000, and April 2001. 20

Figure 10 Vertical patterns in water quality within the central part of the HBHA Pond on sampling dates in April 2000, August 2000, and April 2001. 21

Figure 11 Vertical patterns in water quality within the southern part of the HBHA Pond on sampling dates in April 2000, August 2000, and April 2001. 22

Figure 12 Evidence of water column mixing within the HBHA Pond as a result of a large surface water flow event. 23

Figure 13 The concentration distribution of (A) alkalinity, (B) sulfate, (C) ammonia-nitrogen, and (D) total organic carbon (TOC) and benzene in ground water. 25

Figure 14 The distribution of dissolved As, Zn, Fe, and total S in shallow ground water adjacent to the northern and eastern margins of the HBHA Pond. 26

Figure 15 Temporal trends in water chemistry for the NML sampling station and adjacent ground-water monitoring locations (TW07 and TW02). 27

Figure 16 The distribution of arsenic (As) in sediments collected from the HBHA Pond. 28

Figure 17 The distribution of lead (Pb) and zinc (Zn) in sediments collected from the HBHA Pond. 29

Figure 18 The distribution of chromium (Cr) and iron (Fe) in sediments collected from the HBHA Pond. 30

Figure 19 The distribution of sulfur (S) and organic carbon (OC) in sediments collected from the HBHA Pond. 31

Figure 20 The ratio of As, Fe, Pb, and Zn extracted by HCl for unoxidized and oxidized sediments collected from suboxic zones within the HBHA Pond. 37

Figure 21 (A-D) Comparison of the amount of As and Fe extracted by an ascorbate solution as a function of total Fe and S content in sediments (oxic = open symbols, suboxic = filled symbols). 37

Figure 22 X-ray diffraction data showing the relative proportion of hematite and ferrihydrite in the <2 μm size fraction isolated from surficial sediment samples WI01, WI01-NEP, and WI02-NEP collected near the north-northwestern margin of the HBHA Pond. 38

Figure 23 Locations of a selection of sediments collected from oxic and suboxic zones within the HBHA Pond. 40

Figure 24 XANES data for (A) a series of reference compounds and (B) a selection of sediments collected within the HBHA Pond. 41

Figure 25 XANES data for (A) a series of reference compounds and (B) a selection of sediments collected within the HBHA Pond. 41

Figure 26 Aerial distribution of contaminant sediment speciation within the HBHA Pond based on LCF-XANES analysis; contour lines delineate depth to sediment (meters). 42

Figure 27 Characterization of the mineralogy of the clay-sized sediment fraction and zinc speciation in the silt-sized fraction of surficial sediment sample WI02-NEP before and after incubation for a period of 2.5 years. 43

Figure 28 Representative compositional spectra for samples imaged using SEM-EDS; UP = unidentified peak 45

Figure 29 Image of a pyrite framboid observed in a surficial (oxic) sediment (WI02-NEP, clay-sized fraction) 45

Figure 30 Images of iron (hydr)oxide precipitates collected near the chemocline within the water column of the HBHA Pond (PS-3) 46

Figure 31 Illustration of the apparent geochemical processes controlling solid-solution partitioning of arsenic, lead, and zinc within the HBHA Pond. 48

Figure C.1 Location of XANES and EXAFS regions of an XAS spectrum. 64

Figure C.2 Aerial photo and architectural diagram of the Advanced Photon Source at Argonne National Laboratory, Chicago, IL 65

Figure C.3 Experimental configuration for transmission data collection. 65

Figure C.4 Experimental configuration for fluorescence data collection 65

Figure C.5 Standard raw XAFS spectra illustrating the three regions: (A) pre-edge, (B) edge step, and (C) EXAFS. 66

Figure C.6 Solid sample sandwiched between pieces of Kapton tape 67

Figure C.7 Sample backfilled into opening of a Teflon block and secured with tape 67

Figure C.8 Autosampler template for multi-sample analysis 67

Figure C.9 Fluorescence data collection of metal hyperaccumulation in plant leaves. 68

Figure C.10 Raw fluorescence data Pb sorption on ferrihydrite. 68

Figure C.11 Background corrected spectra of Figure C.10. 69

Figure C.12 k-space conversion of spectra in Figure C.11 69

Figure C.13 The k^3-weighted -function of Figure C.12. 70

Figure C.14 Radial distribution (or structure) function of Fourier transformed k-space data for Figure C.13 70

Figure C.15 ATOMS input file for magnetoplumbite listing crystallographic information. 71

Figure C.16 FEFF file used to determine fitting paths for EXAFS modeling showing the interaction of a central Pb atom (Pb1) with two different oxygen atoms (O5 and O3) and three different iron atoms (Fe2, Fe5, and Fe4). 71

Figure C.17 Structural data derived from ab-initio calculated fitting paths for Pb sorption on ferrihydrite. 72

Figure C.18 XANES spectra (thin line) and derivative of XANES spectra (thick line) for aqueous Zn^{2+} (blue) and ZnS (red) 73

Figure C.19 XANES spectra for arsenite [As(III) - blue] and arsenate [As(V) - red]. 73

Figure C.20 Linear combination fitting of X-ray absorption near edge spectroscopy data (LCF-XANES) for a sediment (Sediment1) sample with multiple Zn species. 74

Tables

Table 1 Percent of Total Element Released by Selected Wet Chemical Extraction Tests. 35

Table 2 Percent of Total Element Released by Selected Wet Chemical Extraction Tests. 36

Table 3 Atomic Percentages of Elements in 5 Samples Determined by SEM-EDS. 44

Table A.1 Analytical Methods, Detection Limits, Precision, and Accuracy for Measurement of Aqueous Chemistry 55

Table A.2 Analytical Methods, Detection Limits, Precision, and Accuracy for Measurement of Solid Phase Chemistry 56

Table B.1 Concentrations of Selected Elements in Halls Brook Holding Area Pond Core NC01 57

Table B.2 Concentrations of Selected Elements in Halls Brook Holding Area Pond Core CC02 58

Table B.3 Concentrations of Selected Elements in Halls Brook Holding Area Pond Core SC02 58

Table B.4 Concentrations of Selected Elements in Halls Brook Holding Area Pond Grab Sediment Samples 59

Table B.5 Concentrations of Selected Elements in Halls Brook Holding Area Pond Cores 60

Table B.6 Results from LCF-XANES Fits of the Pb XANES Data Collected for Sediments from Suboxic and Oxic Zones within the HBHA Pond 61

Table B.7 Results from LCF-XANES Fits of the Zn XANES Data Collected for Sediments from Suboxic and Oxic Zones within the HBHA Pond 62

Acknowledgments

Joseph LeMay (U.S. EPA-Region 1, Boston, MA), Thomas Holdsworth (U.S. EPA/ORD-Cincinnati), and Tim Bridges (U.S. EPA-Region 1 Laboratory, Chelmsford, MA) provided valuable assistance and guidance during field sampling. Ning Xu, Sandra Saye, and Jihua Hong provided analytical support for determination of metals and arsenic speciation; Lynda Pennington, Kelly Bates, and Brad Scroggins provided analytical support for determination of aqueous carbon, nitrogen species and major anions (Contracts #68-C-98-138 and #68-C-03-097). Becky Butler (U.S. EPA/ORD-Ada) along with Martha Williams and Trina Perry (Contract #68-W-01-032) assisted with editing and formatting for publication. The authors greatly appreciate support provided by the staff of DND-CAT and PNC-CAT. DND-CAT is supported by the E.I. DuPont de Nemours & Co., The Dow Chemical Company, the U.S. National Science Foundation through Grant DMR-9304725, and the State of Illinois through the Department of Commerce and the Board of Higher Education Grant IBHE HECA NWU 96. PNC-CAT is supported by the U.S. Department of Energy, Basic Energy Sciences, under Contract DE-FG03-97ER45628, the University of Washington, and grants from the Natural Sciences and Engineering Research Council of Canada. Use of the Advanced Photon Source was supported by the U.S. Department of Energy, Basic Energy Sciences, Office of Energy Research under Contract W-31-102-Eng-38. This document benefited significantly from critical and constructive reviews from Christopher Impellitteri (U.S. EPA), Janet Hering (California Institute of Technology), Madeline Schreiber (Virginia Polytechnic Institute & State University), and Sonia Nagorski (University of Alaska Southeast).

Executive Summary

Physical and chemical interactions between adjacent ground-water and surface-water bodies are important factors impacting water budget and contaminant transport within a watershed. These interactions are also of importance for hazardous waste site cleanup within the United States, since about 75% of sites regulated under the Resource Conservation and Recovery Act (RCRA) and the Comprehensive Environmental Response, Compensation, and Liability Act (CERCLA, or Superfund) are located within a half mile of a surface water body. The boundary between adjacent ground-water and surface-water bodies is referred to as the ground-water/surface-water (GW/SW) transition zone. The transition zone plays a critical role in governing contaminant exchange and transformation during water exchange between the two water bodies. The transition zone is host to a wide diversity of aquatic organisms, and it also can serve as a sink for contaminants transported in surface water or ground water. Ultimately, the potential for human exposure within a watershed and the health of the ecosystem inhabiting the transition zone will depend on the bioavailability of accumulated contaminants. The extent of contaminant bioavailability will, in part, be dictated by partitioning reactions that control the distribution and speciation of contaminants within water and sediments in the GW/SW transition zone.

The purpose of this document is to illustrate some of the chemical processes that govern contaminant transport and speciation during water exchange across the GW/SW transition zone. The focus of this document is the assessment of metal speciation transformations in contaminated sediments. Results from a field investigation of the fate of arsenic, lead, and zinc transported across the GW/SW transition zone at a contaminated site are presented in order to illustrate the importance of using a site conceptual model and to provide an example of approaches that may be used to characterize the spatial and temporal distributions of inorganic contaminant speciation. The field site described in this report is located immediately downgradient from the Industri-Plex Superfund Site in Woburn, MA and is characterized by a ground-water contaminant plume that discharges into the Halls Brook Holding Area (HBHA) Pond resulting in contamination of surface water and sediments.

The results from this field investigation provide insight into the source of inorganic contaminants within the HBHA Pond and present a conceptual framework relative to the design of strategies to mitigate human exposure to site-derived contaminants. Spatial and temporal trends in ground-water data indicate that arsenic and zinc observed within surface water and sediments of the HBHA Pond are primarily derived from continuing ground-water discharge. In contrast, lead observed in sediments appears either to be derived from historical discharges or is currently derived from sediment transport or soil erosion from upgradient source areas. In addition, the vertical distribution and temporal patterns in arsenic concentrations within the water column of the HBHA Pond indicate that sediment dissolution/desorption processes contribute to the overall dissolved concentration of this contaminant. The fate of these inorganic contaminants is coupled to the fate of iron and sulfate derived from ground-water discharge. Iron (hydr)oxides are actively produced in oxic portions of the HBHA Pond, while iron sulfides are produced in suboxic/anoxic portions of the HBHA Pond. The generation of iron (hydr)oxides is a result of oxidation and precipitation of ferrous iron upon contact with oxygen within oxic portions of the HBHA Pond. The generation of iron sulfides is tied to microbial sulfate reduction coupled with degradation of anthropogenic and naturally occurring dissolved organic compounds in discharging ground water within suboxic/anoxic portions of the HBHA Pond. These newly formed precipitate phases possess significant sorption capacity for arsenic, lead, and zinc. The retention of these solids within deeper portions of the HBHA Pond water column and/or sediments helps to mitigate downgradient transport of these freshly deposited contaminants through the watershed. Analytical data are presented to define the spatial distribution and chemical speciation of arsenic, lead, and zinc within HBHA Pond sediments relative to the spatial distribution of predominant redox processes throughout the pond.

While the observed distributions of arsenic, lead, and zinc in ground water, sediments, and surface water described in this report are ultimately unique to site-specific characteristics, some observed patterns in contaminant geochemistry are likely relevant to other sites of contamination. Specifically, the results of this study may have application to sites where an anoxic iron-rich ground-water plume encounters an oxygenated environment (e.g., anoxic landfill leachates or organic contaminant plumes). The results of this intensive field investigation provide useful information on technical approaches to characterize inorganic contaminant transport through subsurface redox gradients that are frequently established at sites with co-occurring organic and inorganic contaminant plumes. As demonstrated for this particular site, the ultimate fate of inorganic contaminants will depend on both site-specific characteristics (e.g., hydrology and soil/sediment mineralogy) and the chemical properties of the contaminant in question.

Chapter 1

Purpose

Physical and chemical interactions between adjacent ground-water and surface-water bodies are important factors impacting water budget and nutrient/contaminant transport within a watershed (Winter et al., 1998). These interactions are also of importance for hazardous waste site cleanup within the United States, since about 75% of sites regulated under the Resource Conservation and Recovery Act (RCRA) and the Comprehensive Environmental Response, Compensation, and Liability Act (CERCLA, or Superfund) are located within a half mile of a surface water body (Tomassoni, 2000; Biksey and Gross, 2001). The boundary between adjacent ground-water and surface-water bodies is referred to as the ground-water/surface-water (GW/SW) transition zone. The transition zone plays a critical role in governing contaminant exchange and transformation during water exchange between the two water bodies. The transition zone is host to a wide diversity of aquatic organisms, and it also can serve as a sink for contaminants transported in surface water or ground water. Ultimately, the health of the ecosystem inhabiting the transition zone will depend on the bioavailability of accumulated contaminants. The extent of contaminant bioavailability will, in part, be dictated by partitioning reactions that control the distribution and speciation of contaminants within water and sediments in the GW/SW transition zone.

The purpose of this document is to illustrate some of the chemical processes that govern contaminant transport and speciation during water exchange across the GW/SW transition zone. The focus of this document is the assessment of metal speciation transformations in contaminated sediments. Results from a field investigation of the fate of arsenic, lead, and zinc transported across the GW/SW transition zone at a contaminated site are presented in order to illustrate the importance of using a site conceptual model and to provide an example of approaches that may be used to characterize the spatial and temporal distributions of inorganic contaminant speciation. The field site described in this report is characterized by a ground-water contaminant plume that discharges into a pond resulting in contamination of surface water and sediments. While the observed distributions of arsenic, lead, and zinc in ground water, sediments, and surface water described in this report are ultimately unique to site-specific characteristics, some observed patterns in contaminant geochemistry are likely relevant to other sites of contamination. Specifically, the results of this study may have application to sites where an anoxic iron-rich ground-water plume encounters an oxygenated environment (e.g., anoxic landfill leachates or contaminant plumes).

Assessment of the factors controlling contaminant transport and distribution between interacting ground-water and surface-water bodies will be guided by the conceptual model that delineates the relevant hydrologic and biogeochemical processes. Typically, a conceptual model is developed based on site-specific data, which is subsequently revised in an iterative fashion with continued accumulation of data that document relevant processes active on site. The complexity of the conceptual model and the extent of required refinement or revision will be dictated by site heterogeneity and process variability in time and space.

In a companion publication, a site conceptual model was developed for the GW/SW transition zone at the Industri-Plex Superfund Site largely based on temporal measurements of surface water chemistry adjacent to the region of contaminated ground-water discharge within the Halls Brook Holding Area (HBHA) Pond (see Figures 6 and 11 in Ford, 2005; http://www.epa.gov/ahaazvuc/pubs/rschbrief.html). In general, three geochemical zones that played an important role in governing the partitioning of arsenic between liquid and solids across the GW/SW transition zone were identified within the proposed site conceptual model as depicted below in Figure 1. The emphasis of the initial report was directed towards illustration of the importance of surface water hydrologic dynamics on observed temporal variations in contaminant concentrations in a setting where contaminated ground water was suspected as the primary contaminant source. The spatial and temporal dynamics observed for arsenic concentrations within the HBHA Pond water column were best explained by considering joint contributions from both contaminated ground-water discharge and sediment dissolution/desorption reactions. However, the characteristics of arsenic partitioning to sediments within the HBHA Pond were not specifically explored in that document. Additional data are provided in this report to provide greater understanding of the characteristics of sediments deposited within the HBHA Pond and the processes that control the solid-phase partitioning of arsenic, lead, and zinc.

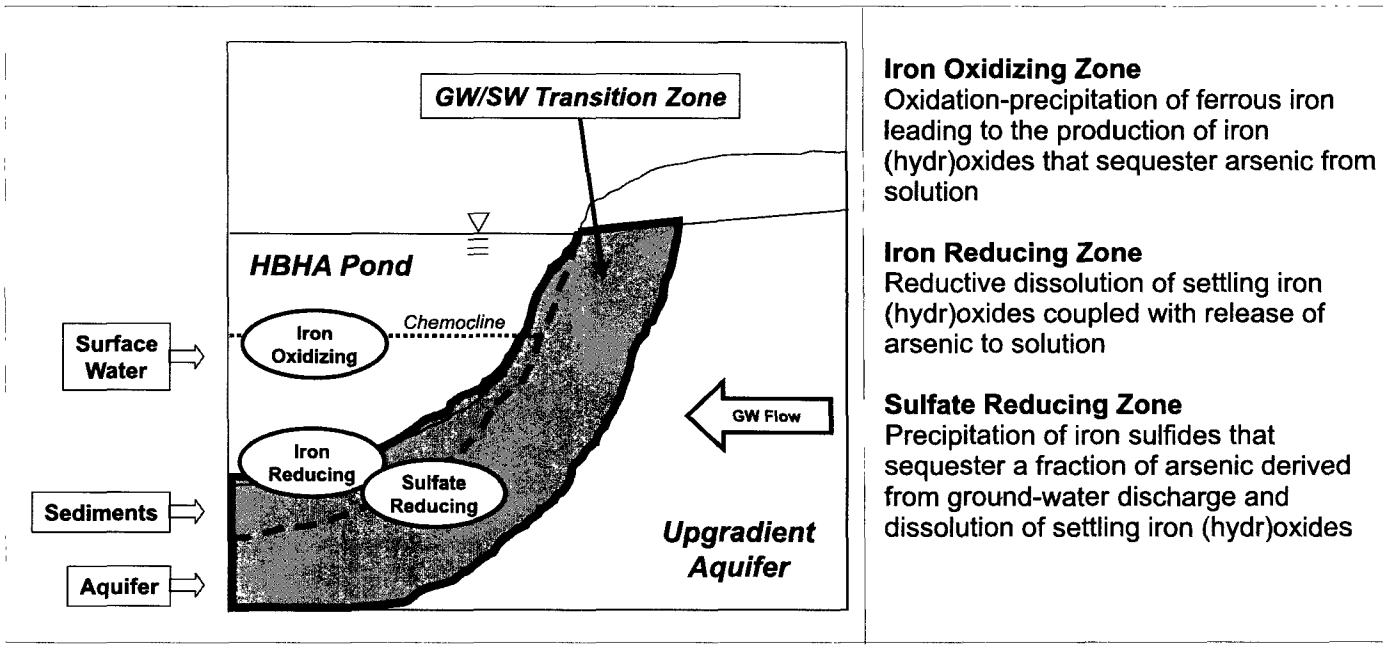


Figure 1 *Conceptual model of geochemical zones that play a dominant role in governing solid-liquid partitioning of arsenic (lead and zinc) across the GW/SW transition zone at the Industri-Plex Superfund Site.*

The issue of contaminated sediments within the HBHA Pond is important relative to the desire to reduce contaminant exposure and potential health risks. While elimination of the ground-water plume would benefit site restoration, this action alone would not eliminate all risks associated with historical contamination due to the recalcitrance of inorganic contaminants within the HBHA Pond. Based on the simplified conceptual model of the geochemical processes controlling the fate of arsenic, lead, and zinc shown in Figure 1, three key questions were posed relative to the information needed to characterize the site:

1) What is the chemical composition of the ground water discharging into the HBHA Pond and how does this vary spatially and temporally?
2) What are the specific processes that result in the partitioning of arsenic, lead, and zinc to solids that are deposited within the HBHA Pond?
3) What is the stability of these solids (and their associated contaminants) and what physicochemical processes can disturb the functionality of the HBHA Pond relative to the downgradient migration of contaminants?

Site characterization data on the temporal and spatial distributions of dissolved arsenic in the northern portion of the HBHA Pond and the upgradient aquifer were reported by Ford (2005). This information provided partial answers to the three questions posed above. Specifically, water chemistry data indicated that: 1) nearly continuous stratification (i.e., development of a stable chemocline) within the HBHA Pond caused by discharge of contaminated ground water with elevated dissolved solids content lead to the development of an internal redox process that controlled arsenic and iron precipitation-dissolution reactions, 2) the concentration of dissolved arsenic within the water column of the HBHA Pond was controlled by the balance between ferrous iron oxidation coupled with precipitation of iron (hydr)oxides near the chemocline and the reductive dissolution of the newly formed iron (hydr)oxides as they settled through the anoxic hypolimnion, and 3) the apparently stable stratification within the HBHA Pond could be disrupted by an exceptionally high surface water influx, although the chemocline was re-established through time and the arsenic-iron redox cycle restored. However, the results documented by Ford (2005) provided limited detail of the chemical composition of ground water, and they provided no specific insight into the extent and characteristics of arsenic (lead and zinc) partitioning to sediments for dissolved and particulate contaminants accumulated within the hypolimnion. Accordingly, the objectives of this report are to elaborate on the physicochemical processes controlling arsenic, lead, and zinc partitioning to sediments within the HBHA Pond and to evaluate the stability of sediment-associated contaminants along with overall performance of the HBHA Pond in mitigating contaminant migration.

Study Scope

As will be discussed later, the fate of arsenic, lead, and zinc is tied to the interaction between ground water and surface water within the HBHA Pond. Sediments within the HBHA Pond play a critical role in the biogeochemical linkage of these two water sources. These sediments originate from two sources: 1) mineral precipitates derived from discharging ground water, e.g., due to ferrous iron oxidation and precipitation of iron (hydr)oxides, and 2) deposition of particulates derived from terrestrial sources, e.g., biotic sources within the water column and along the margin of the HBHA Pond and eroded soils. Several studies have been conducted to examine the fate of arsenic and other metals across the sediment-water interface within the water column of lakes and reservoirs (e.g., Aggett and O'Brien, 1985; Aggett and Kriegman, 1988; Seyler and Martin, 1989; Balistrieri et al., 1994; Spliethoff et al., 1995; Sohrin et al., 1997; Kneebone et al., 2002; Martin and Pederson, 2002; Senn and Hemond, 2002). In many of these studies, it has been shown that the fate of arsenic is tied to the chemical cycling of iron. Iron may be continuously recycled within the water body for systems in which anoxia develops within the hypolimnion or underlying sediments. Reduced iron generated in the lower regions of a lake can diffuse upward within the water column and re-precipitate upon contact with oxygen or other oxidants (e.g., Davison et al., 1982; Sholkovitz and Copland, 1982). Dissolved arsenic within the water column can partition to the newly-formed iron (hydr)oxides either through coprecipitation at the time of formation or adsorption to settling iron (hydr)oxide particles (Seyler and Martin, 1989; Balistrieri et al., 1994; Spliethoff et al., 1995; Sohrin et al., 1997; Senn and Hemond, 2002). Arsenic partitioned to the settling iron (hydr)oxides can subsequently be remobilized during reductive dissolution within the hypolimnion or following sedimentation depending on the spatial distribution of reducing conditions within the lake system. This 'natural' biogeochemical cycle may overlap with hydrologically-driven contaminant fluxes across the GW/SW transition zone, which can cause misleading interpretations of the environmental risk that is directly attributable to discharge of contaminated ground water (See 'Summary and Conclusions' in Sholkovitz and Copland, 1982.).

The purpose of this study was to evaluate the fate of arsenic, lead, and zinc within the HBHA Pond system immediately downgradient from the Industri-Plex Superfund Site, which hosts contaminated soils and ground water resulting from industrial activities dating back to the mid-1800s (Davis et al., 1994; Aurilio et al., 1995; Wick and Gschwend, 1998). The fate of arsenic and other inorganic contaminants in this system is coupled to the chemical cycling of iron, sulfur, and carbon due to the characteristics of the ground-water plume discharging into the surface water system. The results of field measurements to ascertain the spatial and temporal variations of the geochemistry within the GW/SW transition zone and the chemical speciation of arsenic, lead, and zinc across redox gradients within HBHA Pond sediments are examined below to identify the factors controlling the mobility of these contaminants.

Chapter 2

Site Background

The Aberjona Watershed is an industrialized 65-km^2 watershed located in northeastern Massachusetts. The watershed boundary lies within the towns of Reading, Woburn, Winchester, and Medford. The Aberjona Watershed extends to the Mystic Lakes, which drain into the Boston Harbor via the Mystic River. Historic industrial activities have resulted in contamination within the northern extent of the watershed. Specifically, activities at the Industri-Plex Superfund Site, a 245-acre industrial park located in Woburn, Massachusetts, resulted in the deposition of inorganic and organic contaminants in soils, sediments, and ground water. In response to public health concerns, a Record of Decision (ROD) for the Industri-Plex Superfund Site was signed in 1986, addressing on-site soil, sediment, and hot spot ground water contamination.

Contamination at the Industri-Plex Superfund Site was a result of historical industrial activity. From the mid-1800s to the 1930s, leather tanning was the dominant industry in Woburn, and the Aberjona River and its tributaries served as the main conduits for tannery wastewater (Durant et al., 1990). During the same period, starting in the late 19th century, sulfuric acid and arsenical pesticide manufacturing took place near the headwaters of the watershed in an area now designated as the Industri-Plex Superfund Site. Estimates suggest that 270 metric tons of arsenic may still exist within the site boundaries (Aurilio, 1995). By-products such as unused portions of animal hides from tanning and glue-manufacturing operations from 1934-1969 were disposed on site. It is hypothesized that leached degradation products from these materials have contributed to the mobilization of arsenic via the ground water from source areas to a wetland that serves as a source of surface water to the Aberjona River (Davis et al., 1994). Ground water that, in part, originates from within the boundaries of the Industri-Plex Superfund Site discharges into a pond known as the Halls Brook Holding Area (HBHA) Pond. This surface water feature was constructed to serve as a hydraulic retention basin to mitigate flooding during periods of peak surface water discharge. Sources of surface water to the HBHA Pond include Halls Brook, a perennial stream located on the western edge of the pond, and an intermittent stream (Atlantic Avenue Drainway) that conveys water from an upgradient wetland and stormwater runoff from Atlantic Avenue and nearby parking facilities. The HBHA Pond is located in the northern-most portion of a wetland area referred to as the Halls Brook Holding Area. An aerial view of the study location, including portions of the Industri-Plex Superfund Site ('hide piles') is provided in Figure 2.

The ground water beneath the Industri-Plex Superfund Site and the study area in North Woburn has been designated as a non-drinking water source area by the state of Massachusetts. This designation may influence selection of remedial alternatives to address the contaminated soils, ground water, surface water, and sediments. It is possible that most, if not all, of contaminated ground water discharges to the HBHA Pond down gradient from the Industri-Plex Superfund Site. If true, this pond may sequester or retard down gradient transport of arsenic, lead, and zinc. However, there is uncertainty as to the speciation of these contaminants in the various environmental media, interactions between the surface water and ground water, and stability of contaminated sediments within the HBHA Pond. A critical aspect to this site investigation was the resolution of these uncertainties prior to considering remedial action alternatives for contamination at the Industri-Plex Superfund Site. This report expands on the description of the contaminated ground-water plume originating from the Industri-Plex Superfund Site and the processes that control the fate of site contaminants as they are transported across the GW/SW transition zone (Ford, 2005).

Study Approach

The field sampling activities and laboratory analyses performed under this study provide a current assessment of arsenic, lead, and zinc distribution in ground water, surface water, and sediments at the Industri-Plex Superfund Site and within the HBHA Pond. Site characterization was directed towards identifying the predominant chemical processes controlling arsenic, lead, and zinc migration to and sequestration within the HBHA Pond. Field-based sampling was carried out over a period of 35 months to assess time-dependent trends in contaminant mobility within the Industri-Plex Superfund Site and the HBHA Pond. The data derived from this effort provide a means for 1) assessing the long-term assimilative capacity within the HBHA Pond, and 2) the potential for future mobilization of arsenic, lead, and zinc partitioned to sediments.

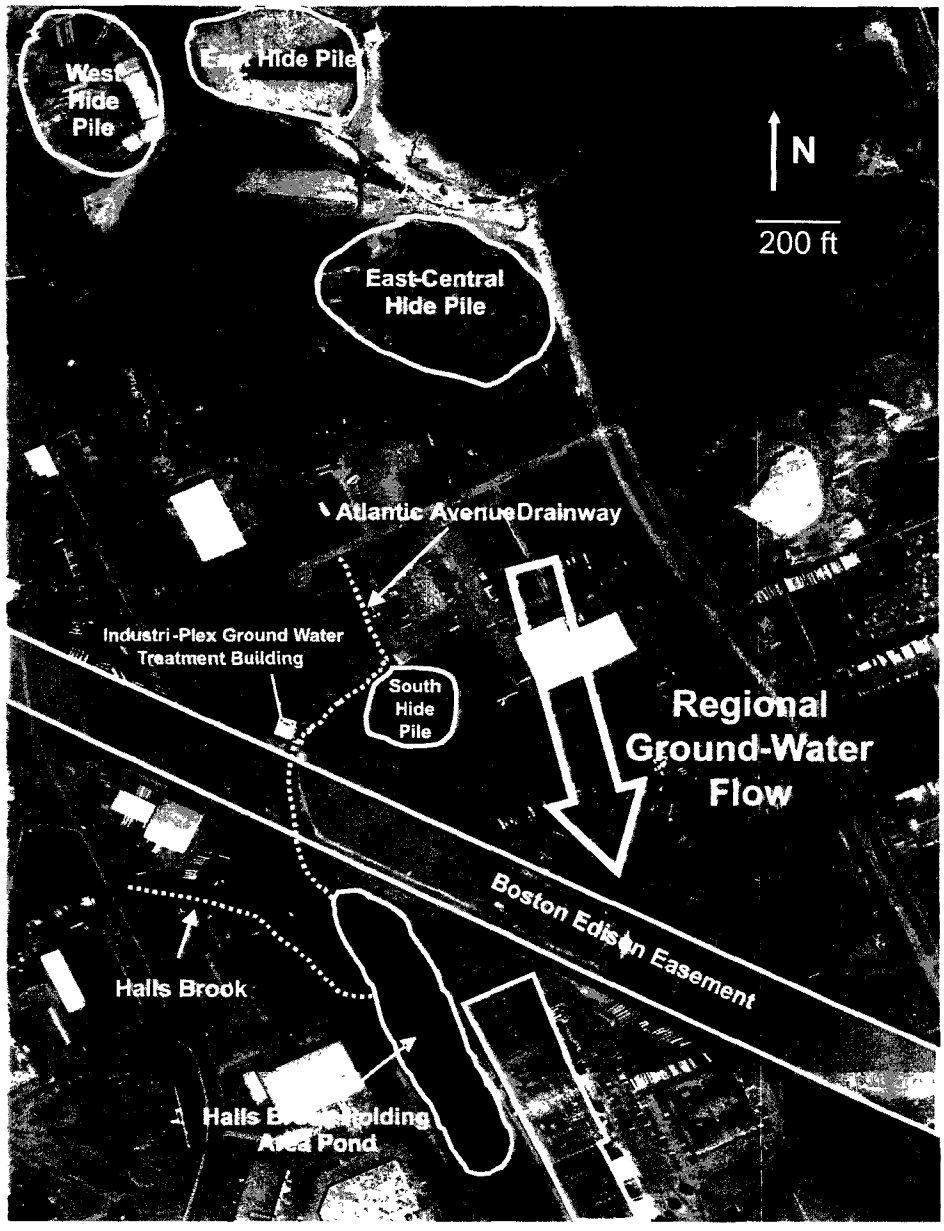


Figure 2 *Prominent land features within the Industri-Plex Superfund Site and adjacent to the HBHA Pond. Land features labeled as 'hide piles' are suspected source terms for metal contaminants within the Industri-Plex Superfund Site. Image was derived from May 1995 aerial photograph obtained from MassGIS.*

Results from ground water, surface water, and sediment sampling and characterization are summarized and evaluated in the sections and appendices that follow. Collection of ground water, surface water, and sediment samples was completed during the following dates: October 13-21, 1999; November 30 - December 3, 1999; March 27 - April 6, 2000; May 16-18, 2000; August 22-30, 2000; March 26 - April 14, 2001; May 11-17, 2001; September 10-21, 2001; and September 20-23, 2004. The study was initiated by defining the extent of the plumes of arsenic and BTEX compounds within the aquifer upgradient to the HBHA Pond. This was accomplished by collecting ground-water samples at temporary wells installed at discrete depths using direct-push equipment (Figure 3A). Patterns in water chemistry data collected from these sampling locations were then used to guide the installation of permanent wells that were used to monitor temporal trends in water chemistry adjacent to and within the HBHA Pond (Figure 3B). An effort was made to capture the vertical heterogeneity anticipated within the GW/SW transition zone by the installation of discrete sampling points at various locations (illustrated in Figure 4).

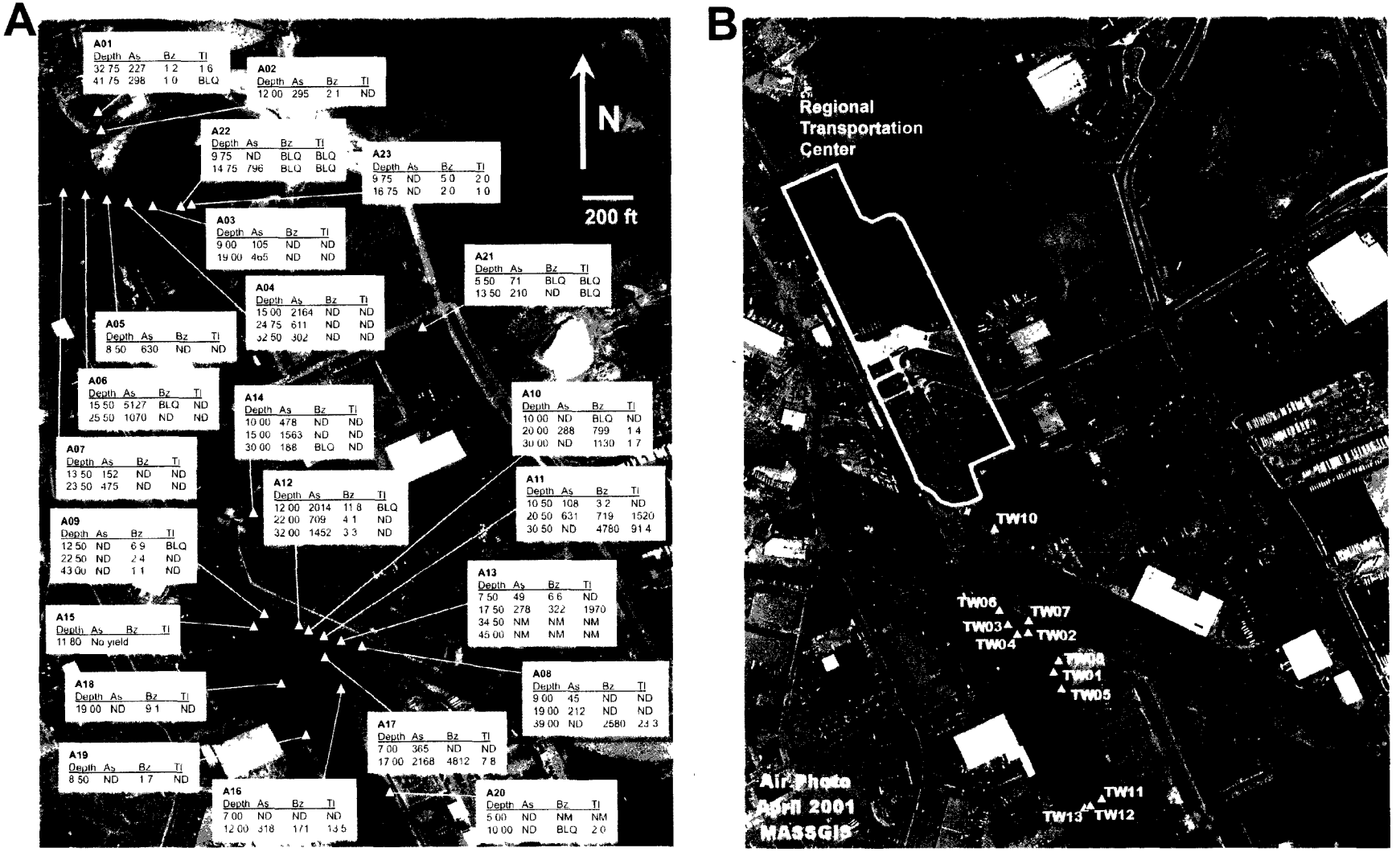


Figure 3 *(A) Arsenic (As), benzene (Bz), and toluene (Tl) concentrations (ppb) from temporary ground-water sampling locations as a function of depth below ground surface (feet) for the study site. ND = not detected, BLQ = below limit of quantitation. Image was derived from May 1995 aerial photograph obtained from MassGIS. (B) Permanent ground-water monitoring locations established adjacent to the HBHA Pond. Images were derived from April 2001 aerial photograph obtained from MassGIS.*

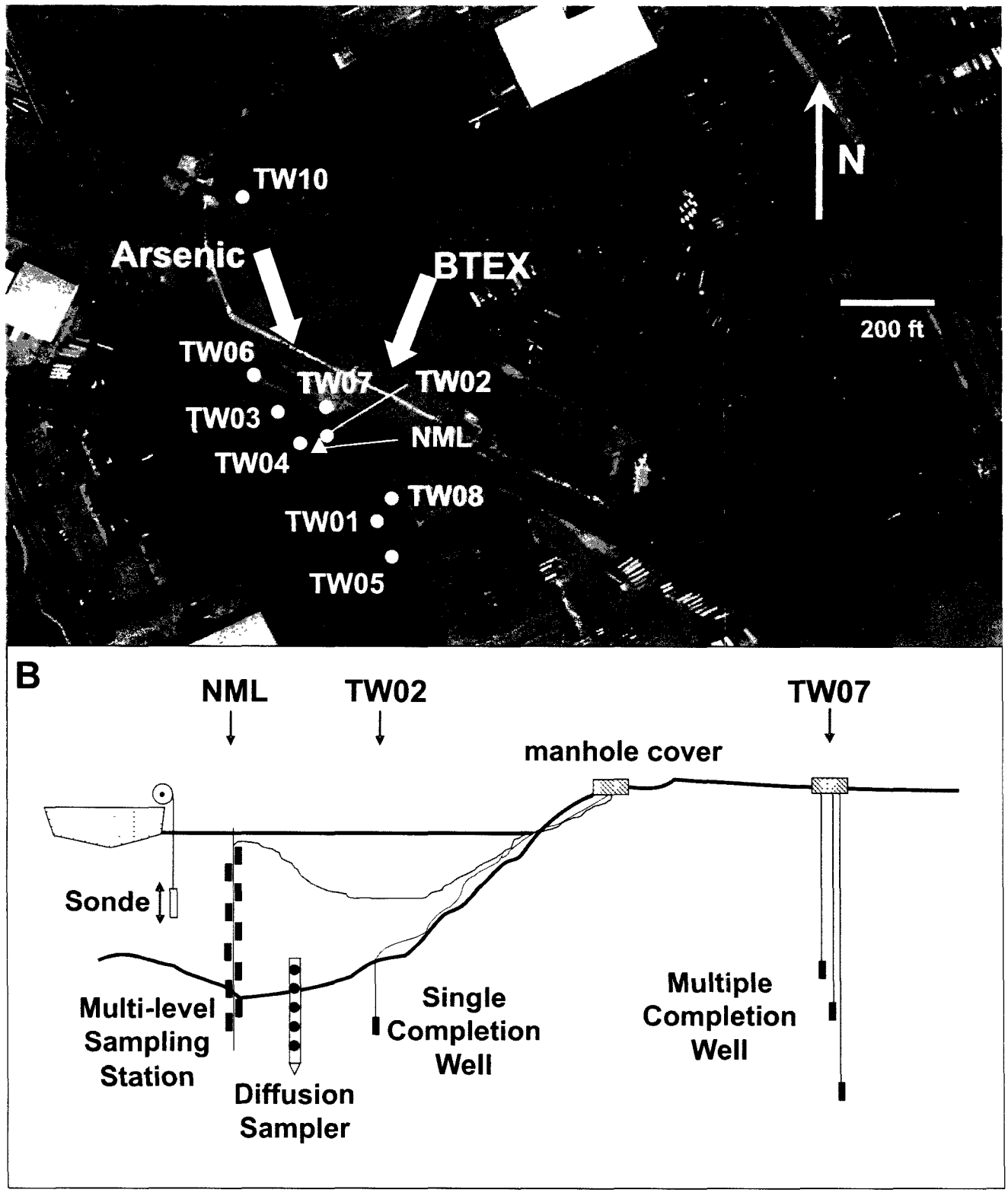


Figure 4 *A) Close-up view of permanent ground-water monitoring network; arrows show approximate centerline of arsenic and BTEX plumes discharging into HBHA Pond. B) Illustration of the approach used to provide depth-resolved spatial coverage of the GW/SW transition zone adjacent to the HBHA Pond. Sampling intervals were completed with 6-inch stainless steel screens connected to 3/8-inch Teflon-lined polyethylene tubing, except for nylon membranes used for cells in diffusion sampler.*

Site Characterization Methods

Water physicochemical parameters were measured in the field along with the collection of water and sediment samples during the sampling dates previously listed. The objective of this effort was to define the chemical structure of the system with particular attention being given to delineation of the GW/SW transition zone. Historical data had been collected as part of previous site characterization efforts to demonstrate a net decrease in arsenic (and other contaminant) concentrations in transitioning from the upgradient aquifer to the outlet of the HBHA Pond. However, limited detailed liquid and solid phase characterization data had been collected to aid in establishing the specific process(es) that controlled the transport of inorganic contaminants through the system (Aurilio et al., 1994; Davis et al., 1996; Ahmann et al., 1997). In particular, insufficient information was available to assess the influence of the seasonal dynamics of water flow and microbial processes on the geochemistry of inorganic contaminants within the HBHA Pond. Wick and others (Wick and Gschwend, 1998a; Wick and Gschwend, 1998b; Wick et al., 2000) had characterized the HBHA Pond system with respect to the fate of synthetic organic compounds that entered the pond via ground-water discharge, and this provided a solid basis from which to design a site characterization program. A range of geochemical data was collected to refine and support the general site conceptual model that had been developed to describe the function of the HBHA Pond relative to arsenic migration, i.e., the sequestration of arsenic, lead, and zinc discharged into the pond via partitioning to Fe-bearing minerals that were continuously deposited onto the sediment layer. Details of sample collection and characterization protocols are described below.

Field Measurements

Ground Water

The major and trace element chemistry and redox characteristics of ground water were assessed through field- and laboratory-based measurements on water samples collected from the aquifer immediately upgradient and below the HBHA Pond. In addition, the concentration distribution of dissolved contaminants was assessed to determine if there were interactions between inorganic and organic contaminants that may influence biogeochemical processes active within and adjacent to the GW/SW transition zone. Sufficient data were collected to define the overall redox chemistry within ground water and how this influenced the chemical speciation of arsenic prior to its discharge into the HBHA Pond. In general, this required measurements to determine the speciation of soluble carbon, iron, and sulfur including the spatial and temporal variability in these constituents.

Ground-water samples were extracted from Teflon-lined tubing wells equipped with 6-inch stainless steel screens that had been driven to depth using direct-push equipment. Samples of ground water were collected using a peristaltic pump through a closed flow cell following stabilization of pH, specific conductance, turbidity, oxidation-reduction potential (ORP), and dissolved oxygen (Puls and Paul, 1995). Filtered (0.45-μm, cellulose acetate membrane) ground-water samples were collected for laboratory analyses. The concentration of ferrous iron was determined by spectrophotometric detection of its complex with 1,10-phenanthroline at 510 nm (Hach, 1992a). The concentration of ferrous iron plus dithionite-reducible ferric iron (total iron) was also assessed by spectrophotometric detection of the ferrous iron complex with 1,10-phenanthroline at 510 nm following reduction with dithionite (Hach, 1992b). The alkalinity of water samples was determined by titration with standardized sulfuric acid to a colorimetric endpoint near pH 4.5.

Surface Water

Depth profiling within the northern, central, and southern regions of the HBHA Pond was carried out at various times of the year to assess the chemical structure of the water column and to delineate the processes controlling contaminant partitioning between solution and solids that subsequently deposit onto the underlying sediments. General water chemistry measurements were conducted as a function of depth either by lowering an instrumented sonde down through the water column or by pumping water to the surface through an enclosed and instrumented flow cell (Figure 4B). The sonde or flow cell was instrumented to collect readings of temperature, dissolved oxygen, pH, specific conductance, and ORP (platinum electrode). Water samples were collected as a function of depth within the water column by pumping water to the surface for field determinations (ferrous iron and alkalinity) or laboratory measurements to determine the major and trace element chemistry. A permanent multi-screened sampling station (NML) was installed within the northern end of the HBHA Pond to facilitate multiple sampling rounds during or following storm events. As shown below and by the work of Wick and others (Wick and Gschwend, 1998a; Wick et al., 2000), depth-resolved measurements within the HBHA Pond water column were critical towards developing a clear understanding of the physicochemical processes that controlled the fate of contaminants discharged from the upgradient aquifer.

Depth-resolved surface water chemistry within the HBHA Pond was assessed using a YSI 6820 Multi-Parameter Water Quality Monitor to measure temperature, pH, specific conductance, ORP, and dissolved oxygen. Water samples were collected at each depth for determination of turbidity and dissolved/particulate concentrations of arsenic, iron, and organic carbon. Suspended solids were collected by in-line pressure filtration using a peristaltic pump from various depths within the HBHA Pond water column for mineralogical characterization.

Surveys of the distribution of specific conductance throughout the HBHA Pond were conducted prior to and following a storm event to understand the dynamics of physicochemical stratification throughout the water column. Continuous measurements of specific conductance as a function of depth were collected using a Geoprobe Direct Image® Electrical Conductivity System that had been adapted for deployment from a pontoon boat. Transects of specific conductance were developed by contouring data from multiple vertical profiles collected within northern and southern portions of the HBHA Pond. The locations of vertical profiles were recorded using a Trimble Navigation GeoExplorer GPS Receiver with post-processing correction of locational data. Data collection events occurred on April 5, 2001 and May 11, 2001 following a major surface water flow event at the end of March 2001 (Ford, 2005).

Laboratory Measurements

Water Chemistry

Dissolved metals in ground water were determined by ICP-OES or ICP-MS for filtered samples acidified to pH<2 with concentrated nitric acid (Fisher Optima). The concentration of benzene was determined by purge-and-trap gas chromatography for filtered samples acidified to pH<2 with concentrated sulfuric acid (Fisher Optima). Dissolved sulfate was determined by capillary electrophoresis with indirect UV detection (Standard Methods, 1999). Nitrate and ammonium were determined by flow injection analysis with a Lachat Quikchem 800 Analyzer (U.S. EPA, 1983; Methods 353.2 and 350.1, respectively). Dissolved organic carbon was determined by UV catalyzed persulfate digestion with infrared detection of evolved CO_2 (U.S. EPA, 1983; Method 415.2).

Dissolved (0.2-µm filter, nylon membrane) and total concentrations of metals in surface water samples were determined by ICP-OES or ICP-MS for samples acidified to pH<2 with concentrated nitric acid (Fisher Optima). Samples for particulate metals were microwave-digested in 10% v/v nitric acid prior to analysis. Dissolved arsenic speciation (0.2-µm filter, nylon membrane) was determined by ion chromatography-hydride generation-atomic fluorescence spectrophotometry (IC-HG-AFS) for samples acidified to pH<2 with concentrated hydrochloric acid (Optima) in amber polyethylene containers and stored at 4°C for a period of less than five days (McCleskey et al., 2004). Separate holding time studies using a representative range of site-specific water chemistries demonstrated that changes in inorganic arsenic speciation were less than the analytical error for a holding time of seven days or less (data not shown). The speciation method was optimized for detection of As(III), As(V), MMA(V), and DMA(V) using gradient elution with a phosphate mobile phase (Gomez-Ariza et al., 2000).

Sediments

The major element and contaminant chemistry was defined in sediments collected from various locations within the HBHA Pond during different times of the year. Locations that were deemed important included regions of obvious ground-water discharge, i.e., ground-water seeps evidenced by the precipitation of iron (hydr)oxides, as well as regions that represented varying stages along the redox gradient from shallow to deeper water levels within the pond. Shallow sediment grab samples were collected throughout the HBHA Pond to help define the chemical processes that controlled the distribution of contaminants across the sediment-water interface. In addition, sediment cores were collected to greater depth in order to define the depositional history and diagenetic processes that exert an influence on inorganic contaminants accumulated within the system. The predominant sediment mineralogy at various locations across the system redox gradient was assessed along with characterization of the chemical speciation of arsenic, lead, and zinc using chemical extraction tests as well as X-ray absorption spectroscopy on preserved sediment samples. Previous work had shown that iron monosulfides were a significant component in sediments deposited/formed within suboxic regions of the HBHA Pond (Wilkin and Ford, 2002). Results documented below demonstrated the predominance of iron (hydr)oxides in the reactive fraction of sediments deposited/formed within oxic regions of the HBHA Pond.

Sediment samples were collected in December 1999, April 2001, and September 2001 from the HBHA Pond. The greatest density of sampling points was along the center axis and along the northeast shore of the pond, where contaminated ground water discharges into the HBHA Pond. Sediment samples were retrieved from water depths ranging from 0.5 to 4.5 m. Cores were collected using a 5-cm diameter piston-coring device. The cores were capped immediately after their recovery and kept upright before and during freezing. Surface sediments were collected into N_2-purged plastic bags by pumping highly fluidized sediments to the surface using a peristaltic pump. Surface sediments and cores were frozen within 1 h of collection from the pond bottom. While still frozen, sediment cores were sub-sampled by cutting off 2- to 5-cm thick sections, which were immediately bagged and kept frozen for subsequent solid-phase analyses.

Sediment Chemistry and Mineralogy

Surficial (oxic) sediments were dried in air to constant mass prior to chemical measurements or mineralogical determinations. The <2 mm size fraction was isolated from these sediments by sieving prior to further analysis. Buried sediments collected from suboxic zones were thawed and dried at room temperature in an anaerobic glove box (96:4 v/v N_2-H_2 gas mixture). Excess pore water was squeezed out by hand and decanted from the sediments prior to drying.

Dried samples were homogenized with an agate mortar and pestle and retained in the anaerobic glove box. Sample splits were removed from the glove box and allowed to oxidize in an oven at 60°C for 72 hours.

Methods used for determination of the elemental composition of sediments are listed in Appendix A along with method detection limits, analytical accuracy, and precision. All solid-phase concentrations are reported on a dry weight basis. Total carbon and carbonate carbon were determined on oven-dried samples using a UIC (Model CM5014) carbon coulometer system (Huffmann, 1977). Organic carbon content was derived from the difference between total carbon and inorganic carbon. For total carbon analysis, a 20-300 mg aliquot of powdered sediment was combusted at 950 °C. Inorganic carbon was analyzed as carbon dioxide released from a sample after reaction with hot 5% perchloric acid. Total sulfur was determined by mixing oven-dried sediment samples with vanadium pentoxide and combusting the mixture in the presence of high-purity oxygen-gas at 1050 °C (Atkin and Somerfield, 1994). Sulfur dioxide produced is quantitatively titrated using a sulfur coulometer (UIC Model CM5014S). Concentrations of metals and metalloids in the sediments were determined by microwave assisted digestion in 10% HNO_3 (modified EPA Method 3051), followed by inductively coupled plasma optical emission spectrometry (ICP-OES, Perkin Elmer Optima 3300DV). Microwave digestion was carried out using a CEM Mars 5 system at a total pressure of 120 psi (8.5 bar) and maximum temperature of 170 °C. The reliability of this digestion method was continuously checked using international certified reference materials (NIST 2710, NIST 2780, and CCRMP LKSD-1). Arsenic recovery from these reference materials, for example, ranged from 88% to 97% of the certified values.

Mineralogical Characterization

Precipitate mineralogy was determined by powder X-ray diffraction (XRD) using a Rigaku MiniFlex diffractometer. XRD data were collected using Fe Kα radiation via continuous scan in 0.02 °2θ steps with a count time of 12 sec/step. The <2 μm size fraction of surficial sediment samples was isolated via centrifugation of aqueous suspensions. Air-dried samples were prepared as smear mounts with methanol on zero background quartz slides (typically 10-15 mg of sample). Mounted samples were allowed to air dry prior to data collection. External calibration using a smear mount of the NIST SRM 640b (silicon) was carried out on a regular basis to confirm goniometer angular position accuracy and to estimate peak position error due to sample displacement. Peak identification for crystalline phases was achieved by reference to the ICDD Powder Diffraction File database (JCPDS, 1993). Identification of 6-line and 2-line ferrihydrite was carried out by reference to data reported by Stanjek and Weidler (1992).

X-ray Absorption Spectroscopy

Arsenic XAS

The oxidation state and bonding environment of arsenic associated with iron oxidation precipitates was examined using X-ray absorption near edge structure (XANES) spectroscopy. Arsenic *K*-edge spectra were collected at sectors 20-BM (DuPont-Northwestern-Dow Collaborative Access Team; DND-CAT) and 5-BM (Pacific Northwest Consortium Collaborative Access Team; PNC-CAT) at the Advanced Photon Source, Argonne National Laboratory (Argonne, IL). Dried sediment samples were loaded into 1-mm-thick plastic sample holders and sealed with strips of Kapton tape. Absorption spectra were collected at the As K-edge (11,867 eV) in fluorescence mode using a 13-element solid-state Ge-detector. The synchrotron was operated at 7.0 GeV and at a nominal 100 mA fill current. The energy of a Si(220) double-crystal monochromator was calibrated using arsenic or gold foil. The monochromator step size was 0.25 eV per step in the XANES region (11845-11900 eV). Multiple scans were collected and summed for each sample (3 to 9). The XANES fluorescence data were normalized to the edge-jump height, and the *K*-edge inflection point was determined as the energy at the maximum in the first derivative of the normalized spectra. Mineral reference compounds were synthesized in the laboratory, including arsenate adsorbed to hematite (Ford, 2002), arsenite coprecipitated with siderite, and arsenite coprecipitated with mackinawite (Wilkin and Ford, 2002). All fluorescence spectra were collected at room temperature. For surficial (oxic) sediments and the arsenate-hematite reference sample, no attempt was made to exclude sample exposure to air. However, buried (suboxic) sediments and the reference samples prepared using arsenite were protected from oxygen exposure in an inert atmosphere prior to and during collection of fluorescence data in order to prevent sample oxidation. The relative percentages of As(V)-O, As(III)-O, and As-S species in the study samples were assessed by linear combination fitting (LCF) of XANES data employing WinXAS Version 3.1 (Ressler, 1998) using reference spectra for As(V)-hematite, As(III)-siderite, and As(III) coprecipitated with FeS. The LCF-XANES analysis demonstrated that an orpiment-like phase (As_2S_3) was an insignificant component for all examined samples.

Pb and Zn XAS

The sediment samples were analyzed for Pb and Zn by XANES spectroscopy to determine metal speciation parameters. XANES spectroscopic data were collected at beamline 20-BM (Pacific Northwest Consortium - Collaborative Access Team) at the Advanced Photon Source at Argonne National Laboratory, Argonne, IL. The electron storage ring operated at 7 GeV with a top-up fill mode. Three to five scans were collected at ambient temperature in fluorescence mode with a 13-element Ge detector. A 0.5 mm premonochromator slit width and a Si(111) double crystal monochromator detuned

by 20% to reject higher-order harmonics were employed. For XANES analyses, the sediment samples were loaded into Teflon sample holders and sealed with Kapton tape within an oxygen-free glovebox. The samples were transferred to the experimental hutch in a plastic bag which was purged with Ar during transfer and data collection to avoid oxidation from atmospheric oxygen. No beam-induced oxidation was evident. No background Pb or Zn was detected in the purge bag material or the Kapton tape. Energy was calibrated to the first inflection of Zn_K (9.659 keV) or Pb_{LII} (15.200 keV) metal foil standards and was collected simultaneously with the spectrum of each sample for the respective metals. Due to the relative low concentration of Pb and high concentration of As in the samples, the Pb_{LII} edge energy was utilized for Pb data collection rather than the usual Pb_{LIII} edge energy of 13.055 keV. The Pb_{LIII} $L_{\alpha 1}$ fluorescence energy of X-ray emission is 10.552 keV which shouldered on the overwhelming As_K $K_{\alpha 1}$ emission energy peak at 10.544 keV. The collected scans for a particular sample were merged, the data were then normalized, and the background was removed by spline fitting using WinXAS 3.1 (Rehr and Ankudinov, 2001, 2003). The XANES spectra of Pb and Zn in sediment samples and references were then assembled in a format suitable for linear combination fitting (Beauchemin et al., 2002; Roberts et al., 2002; Scheinost et al., 2002; Scheckel and Ryan, 2004) of the X-ray absorption near edge spectroscopy (LCF-XANES) data to identify the major Pb and Zn species present in the sediment samples.

Sediment Extraction Procedures

Surficial Sediments

A series of single-step chemical extractions were employed to assess the relative stability of metals associated with oxic sediments exposed at the surface near visible ground-water seeps along the north-northwestern margin of the HBHA Pond. The extraction steps employed in this procedure are documented below. All stock solutions were prepared using reagent grade chemicals and deionized water (Millipore® Milli-Q3RO/Milli-Q2 system). All glassware had been previously soaked in dilute HNO_3 and rinsed thoroughly with deionized water.

i) *Weakly Adsorbed:* A 20 ml aliquot of 1 M $MgCl_2$ (Baker®) at pH 7.0 was added to 45 ml polyethylene centrifuge tubes containing either 0.1 gm solid for WI01-NEP, WI02, WI02-NEP, and WI04 or 1.0 gm for WI01. Samples were prepared in duplicate. The tubes were continuously shaken for 1 hr (Tessier et al., 1979) and centrifuged for 10 min at 15,000 RPM. The supernatant was carefully pipetted off and filtered through 0.2 um Nuclepore® filter.

ii) *Strongly Adsorbed*: The residue from *(i)* was extracted with 19 ml 0.005 M NaH_2PO_4 (Sigma®) at both pH 4 (Bartlett and James, 1988; Welch and Lico, 1998). Samples were shaken for 24 hours, and supernatants were collected in the same manner as described in step *(i)*.

iii) *Amorphous Iron Oxides*: The ascorbate solution for Step 3 was prepared following the method of Ferdelman (1988). Sodium citrate (0.2 M $C_6H_5Na_3O_7 \cdot 2H_2O$) and sodium bicarbonate (0.6 M $NaHCO_3$) were added to deionized water. The solution was then deaerated with nitrogen and ascorbic acid (0.4 M $C_6H_8O_6$) was added with a resulting pH of 8.0. Sediment samples were extracted for 24 hours with 19 ml of the ascorbate solution, and the supernatants were collected in the same manner as described in step *(i)*.

iv) *Iron Sulfides*: The final step in the sequential extraction scheme involved adding 19 ml 0.5 M HCl (Aldrich®) to the sediment samples and shaking for 1 hour (Kostka and Luther, 1994). Supernatants were collected in the same manner as described in step *(i)*.

Buried Sediments

A series of single-step chemical extractions were performed to better constrain the solid-phase partitioning of arsenic, lead, and zinc in buried sediments collected from the bottom of the HBHA Pond. All solutions were deoxygenated prior to use, and extractions were carried out using unoxidized sediments in an anaerobic glove box. The following solutions were used: 0.5 M $MgCl_2$, 0.1 M Na_2CO_3, 0.02 M ascorbic acid (buffered to pH 7 in 0.6 M $NaHCO_3$), and 1 M HCl. Dilute hydrochloric acid extractions were conducted on both unoxidized and oxidized sediment samples. Supernatant solutions were filtered through 0.22-µm syringe filters and acidified with concentrated nitric acid. The analysis of metals in the solutions obtained following chemical extraction was carried out using ICP-OES.

All liquid extractant samples were acidified to pH < 2 using ultra-pure HNO_3 and analyzed for the elements of interest (arsenic, iron, lead, zinc) by ICP-OES. Samples with low arsenic concentration were also analyzed using GFAAS. Quality assurance measures performed on these analyses included analytical duplicates, known analytical quality controls (AQCs), check standards, and blanks. Non-detect results were observed for all blank samples, and the results for all other QC samples met the required data quality requirements (Appendix A).

Scanning Electron Microscopy-Energy Dispersive Spectroscopy

Scanning Electron Microscopy was used to evaluate the morphology and spatial relationships among mineral precipitates for two surficial sediments, suspended solids collected adjacent to the chemocline within the HBHA Pond, and

one buried sediment sample. In addition, energy dispersive X-ray spectroscopy (EDS) was conducted on polished and unpolished samples to determine the composition of sediments on a semi-quantitative basis. Samples for SEM/EDS analysis were stored in an anaerobic glove box and then embedded in an epoxy resin. The sample mounts (1" diameter round mounts) were ground and polished using diamond abrasives and coated with a thin layer of gold prior to being placed within the SEM sample chamber. The sample of suspended solids was the only unpolished sample analyzed for these studies. The grain mount procedure used for this sample is discussed below.

Secondary electron and back-scattered electron images were obtained using a JEOL 6360 SEM. The instrument was operated using an 18kV and 20 kV accelerating potential and a beam current of about 8.5 nA. Micrographs were obtained at a range of magnifications from 1500X to 10000X. Copper grids obtained from SPI Supplies (West Chester, PA) were used to verify quantitative lengths. EDS spectra were acquired using an OXFORD Instruments Model INCA300/GEM EDS Unit. Elemental concentrations were calculated using INCA software and cobalt metal as a standard reference material to insure semi-quantitative accuracy.

Polished thin-sections were made from sediments that had previously been imbedded in resin. Thin-section samples were sonicated in methanol for 30 minutes prior to mounting, rinsed with RO water, and dried with an air-stream (canned air) before proceeding any further. After the drying process, each prepared thin-section was mounted to an aluminum stub using double-sided carbon tape, and then a strip of silver paint was applied from the aluminum stub to the top of the sample thin-section for conductivity purposes. The silver paint was dried thoroughly with a stream of air before the coating procedures were attempted. A 10-second gold sputter coat was applied to these samples in preparation for SEM analysis. One of the sediment thin-sections was treated differently in the sample preparation because a pyrite framboid was identified under an optical light microscope. The framboid could not be located with the SEM after the first sample preparation. The thin-section was stripped of the first 10-second gold coat with a methanol/sonication process for 30 minutes, rinsed with RO water, and then followed by a 2% potassium iodide/sonication process for 30 minutes. The thin-section sample was then rinsed with RO water, dried with a stream of air (canned air), mounted on an aluminum stub with double-sided carbon tape, two strips of silver paint were applied on opposite sides of the thin-section for conductivity reasons, and finally, a fresh 10-second gold coating was applied. By stripping the first gold coat, we were able to mark the site of interest so that the framboid could be more easily located in the SEM system.

The suspended solid sample collected from the southern portion of the HBHA Pond was stored in an anaerobic glove-box until ready for SEM/EDS sample preparation. A small sample (<1 mg) was suspended in 1 mL of methanol, sonicated for 10 minutes, agitated, and then sonicated a second time for 10 minutes. A carbon planchet was mounted on an aluminum stub with double-sided carbon tape, and then one drop of the suspension was placed on the top surface of the planchet. The sample was immediately placed into a dessicator for 2 days of vacuum drying. The sample was then removed from the dessicator, two strips of silver paint were applied (opposite sides) and dried immediately with an air stream (canned air) before the gold coating could be applied. The sample was then coated with gold for 10 seconds to achieve good conductivity for the SEM/EDS analyses.

Chapter 3

Site Hydrology

A portion of the ground-water plume discharges into the HBHA Pond that also receives surface water inputs from a perennial stream (Halls Brook) on its western edge and an intermittent runoff channel at its northwestern end (Figure 2). The HBHA Pond was built in the early 1970s for flood control. The HBHA Pond has a maximum depth of approximately 5 meters (15 feet), and it discharges into a heavily vegetated wetland area. The HBHA Pond discharge reconstitutes Halls Brook, which meanders through the wetland until discharge into the Aberjona River. Independent estimates of water flux into the HBHA Pond indicate that approximately 7-60% of the water input is derived from ground water throughout the year (Aurilio et al., 1994; Wick et al. 2000). Trends in ground water and surface water inputs into the HBHA Pond documented by these authors are illustrated in Figure 5. Data shown in Figure 5A and Figure 5B indicate that the influx of ground water remains relatively constant, although the fraction of ground-water flow relative to the total system flow varies significantly as a function of surface water inputs. For example, during late January 1998, the relative fraction of ground-water flow varied from an average of approximately 60% down to 10% following an increase in surface-water flow (Figure 5B, see history of water flow in Aberjona River at USGS 01102500). Water level measurements in the HBHA Pond (this study) illustrate rapid fluctuations in water budget in this system in response to changes in surface-water influx (Figure 5C).

Based on salt balance calculations, Wick et al. (2000) have estimated that a contaminated ground-water plume (denoted 'Q_{high}' by the authors) contributes approximately 1- 9% of the water input into the HBHA Pond throughout the year (3-27% of ground-water input). Based on specific conductance measurements throughout the HBHA Pond, these authors concluded that the primary location of contaminated ground-water discharge was within the northern end of the lake. Independent measurements of ground water and lake water chemistry (including dissolved arsenic) from the current study support this finding and show that contaminants are primarily discharged within the north-northeastern portion of the pond (Figures 6-8; Pb below detection in ground water). However, arsenic contamination is derived from a larger portion of the adjacent ground-water aquifer than the hydrocarbon contaminants studied by Wick et al. (1998, 2000). Thus, their estimates of contaminated ground-water flux may be low with respect to the discharging arsenic plume. The distribution of arsenic and benzene as a function of depth for three ground-water monitoring locations proximate to the north-northeastern shoreline of the HBHA Pond (TW06, TW07, TW08) indicates that the hydrocarbon plume occurs over a smaller region than the arsenic plume. While the highest arsenic concentrations were encountered at location TW07, there were still substantial concentrations of arsenic in the vicinity of the hydrocarbon plume (TW08). Since additional hydrologic data were not collected during this study, there is insufficient information to properly constrain an estimate of the flux of arsenic derived from ground water. However, published data of changes in the vertical distribution of dissolved arsenic in the HBHA Pond water column at location NML demonstrate that observed concentrations of arsenic within this pond are derived from a combination of ground-water inputs and sediment dissolution processes (Ford, 2005).

An important component of the conceptual model developed thus far is the maintenance of a stable chemocline within the HBHA Pond that serves to regulate the redox cycling of Fe-bearing solids and associated contaminants. Thus, it was important to assess the relative stability of this physical aspect of the HBHA Pond water column during the period of study. A series of water quality measurements are shown in Figures 9-11 as a function of depth at north, central, and south sampling locations for three sampling dates. In general, the vertical trends in specific conductance, dissolved oxygen, and ORP document relatively uniform stratification (i.e., formation of chemocline) throughout the water column. Dissolved oxygen concentrations are low (limit of detection), and measured ORP is negative near the sediment-water interface. In some instances, a turbidity maximum was observed near the chemocline, which was attributed to iron (hydr)oxides precipitating as a result of ferrous iron oxidation. The chemocline was disrupted in the central and southern portions of the HBHA Pond during the April 2001 sampling date as indicated by a uniform profile for specific conductance as a function of depth (Figures 10 and 11). This was due to a significant increase in surface-water influx

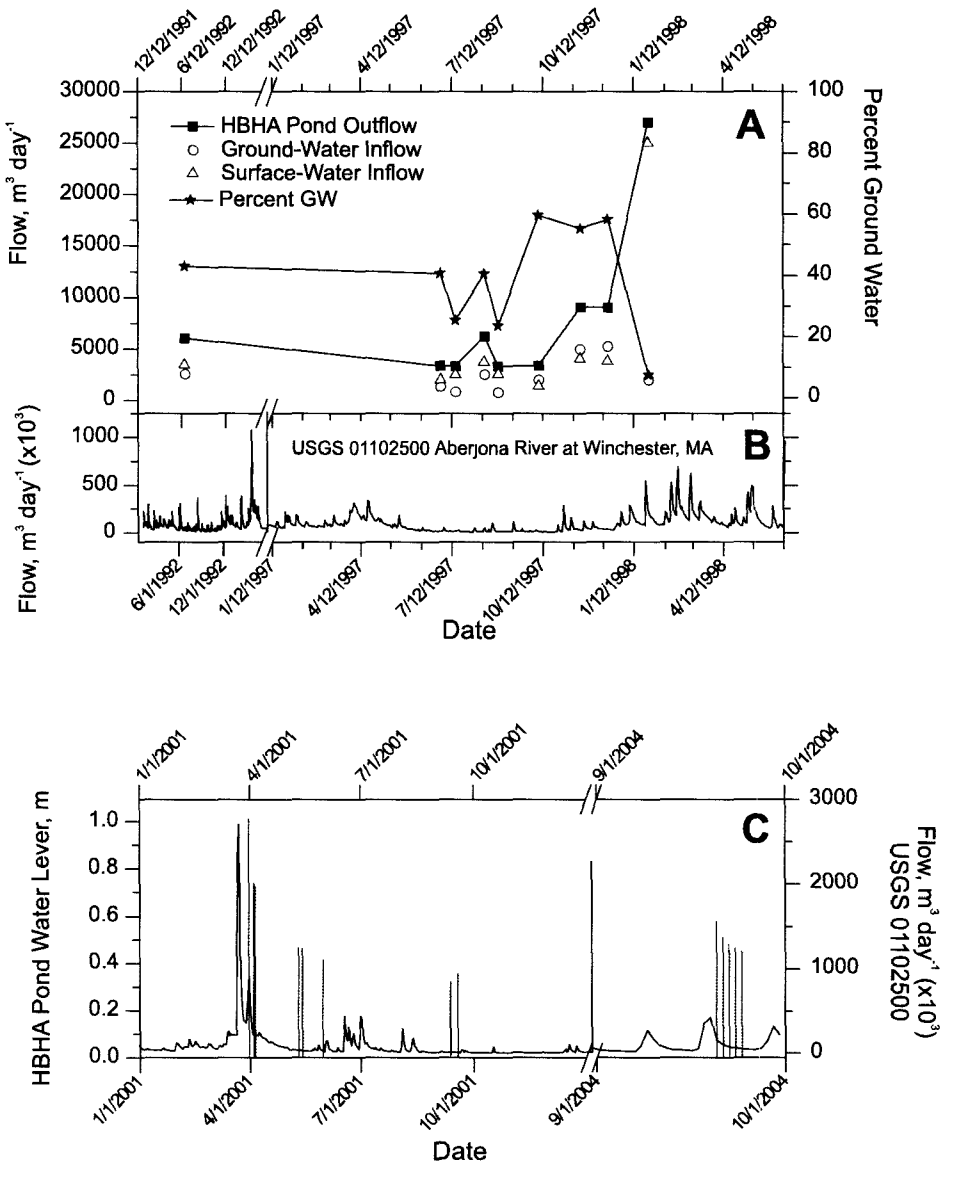


Figure 5 *(A) Patterns in surface water and ground-water flow budgets within the HBHA Pond as documented by Aurilio et al. (1994) and Wick et al. (2000). (B) Concurrent flow variations within the Aberjona River are also shown for the USGS 01102500 gaging station located approximately 2.5 miles south of the HBHA Pond (Winchester, MA). (C) Water level variations (blue columns) recorded within the HBHA Pond (this study) relative to concurrent flow variations observed at the USGS 01102500 gaging station.*

(Figure 5C), a fraction of which was contributed by Halls Brook. The chemocline was depressed to greater depth on this sampling date in the northern portion of the HBHA Pond (Figure 9). Maintenance of stratification in this portion of the pond is likely due to its proximity to the primary point of discharge of contaminated ground water with high dissolved solids. However, as shown in Figure 12 based on contours of specific conductance within the water column in the northern and southern portions of the HBHA Pond, the chemocline is re-established throughout the pond to essentially pre-storm conditions within a period of less than a month. Analysis of historical surface water flow records at the USGS Winchester Monitoring Station indicates that flow events of sufficient magnitude to disrupt the chemocline may occur at a frequency of about every four years (data not shown). Water quality measurements conducted as part of this study indicate that any disruption to the chemocline is relatively short-lived, which is consistent with historical records for the HBHA Pond (Wick et al., 2000).

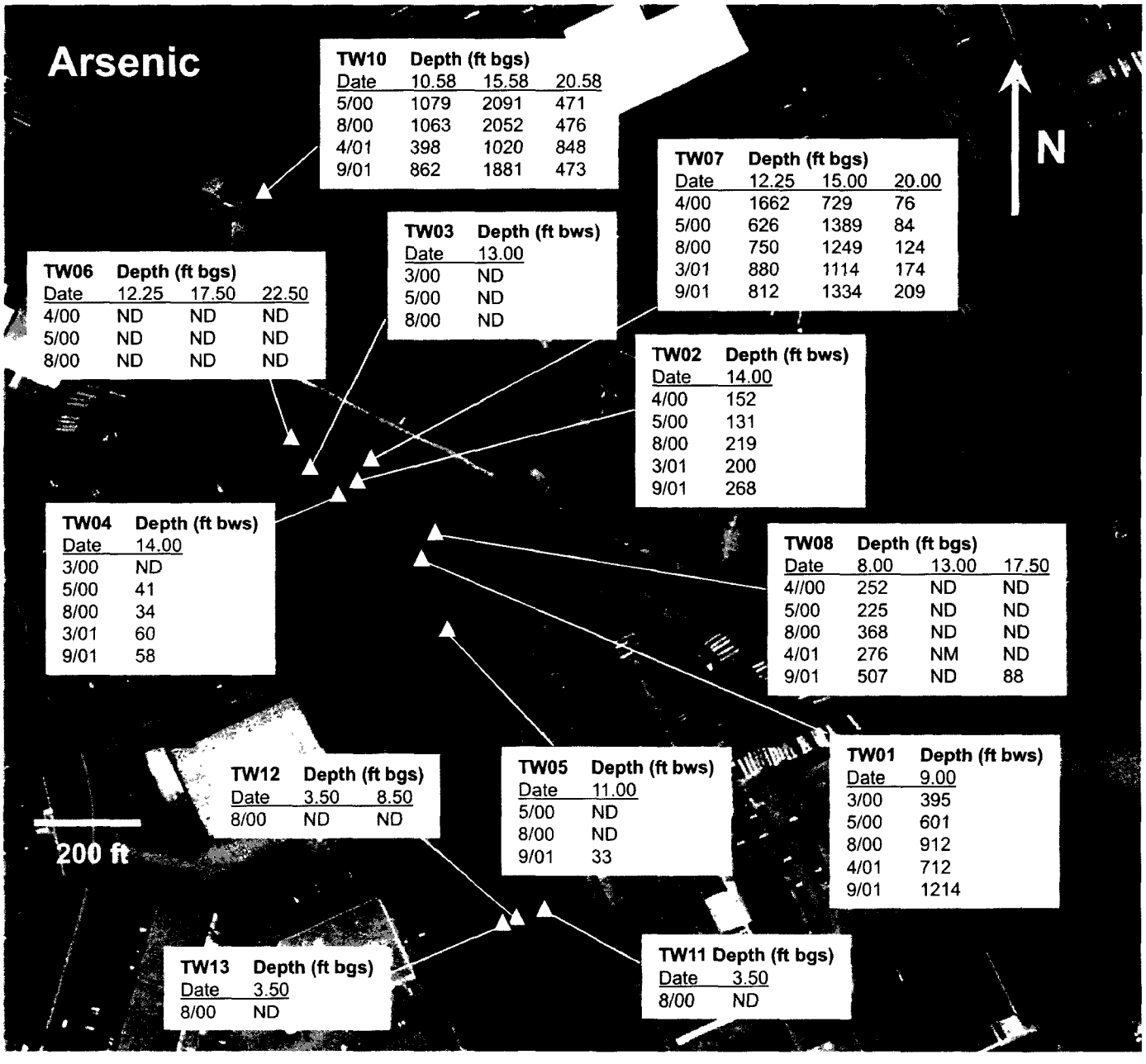


Figure 6 *Aerial distribution and time-dependent variability for total dissolved arsenic concentrations (ppb) detected in tubing wells established adjacent to the HBHA Pond. Depths are shown in feet below ground surface (ft bgs) and feet below water surface (ft bws) for tubing wells installed on land and within the HBHA Pond, respectively. Depths for tubing wells TW01, TW02, TW03, TW04, and TW05 were determined at the time of installation. NM = not measured, ND = not detected (<33 ppb). Image derived from May 1995 aerial photograph obtained from MassGIS.*

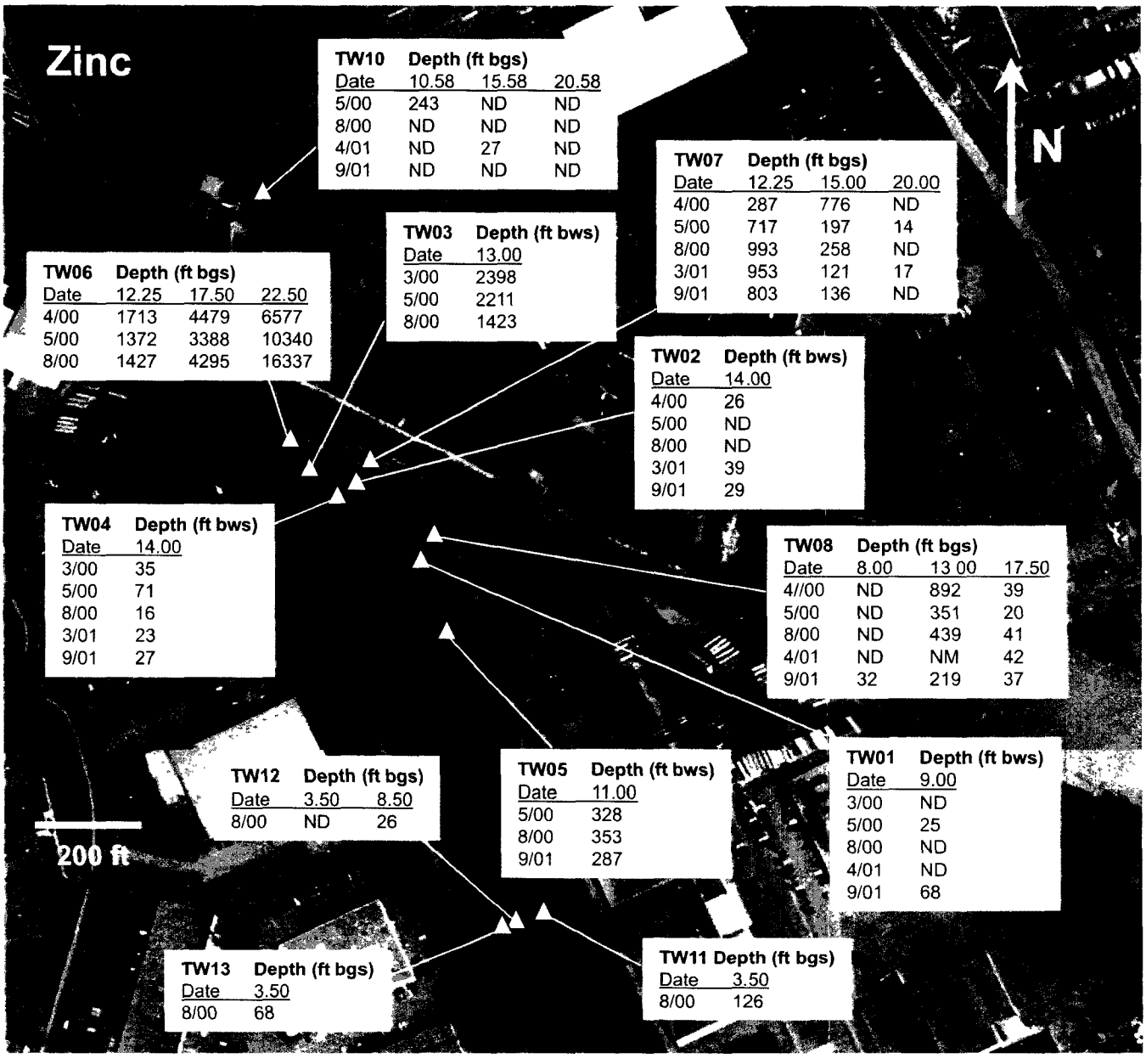


Figure 7 *Aerial distribution and time-dependent variability for total dissolved zinc concentrations (ppb) detected in tubing wells established adjacent to the HBHA Pond. Depths are shown in feet below ground surface (ft bgs) and feet below water surface (ft bws) for tubing wells installed on land and within the HBHA Pond, respectively. Depths for tubing wells TW01, TW02, TW03, TW04, and TW05 were determined at the time of installation. NM = not measured, ND = not detected (<14 ppb). Image derived from May 1995 aerial photograph obtained from MassGIS.*

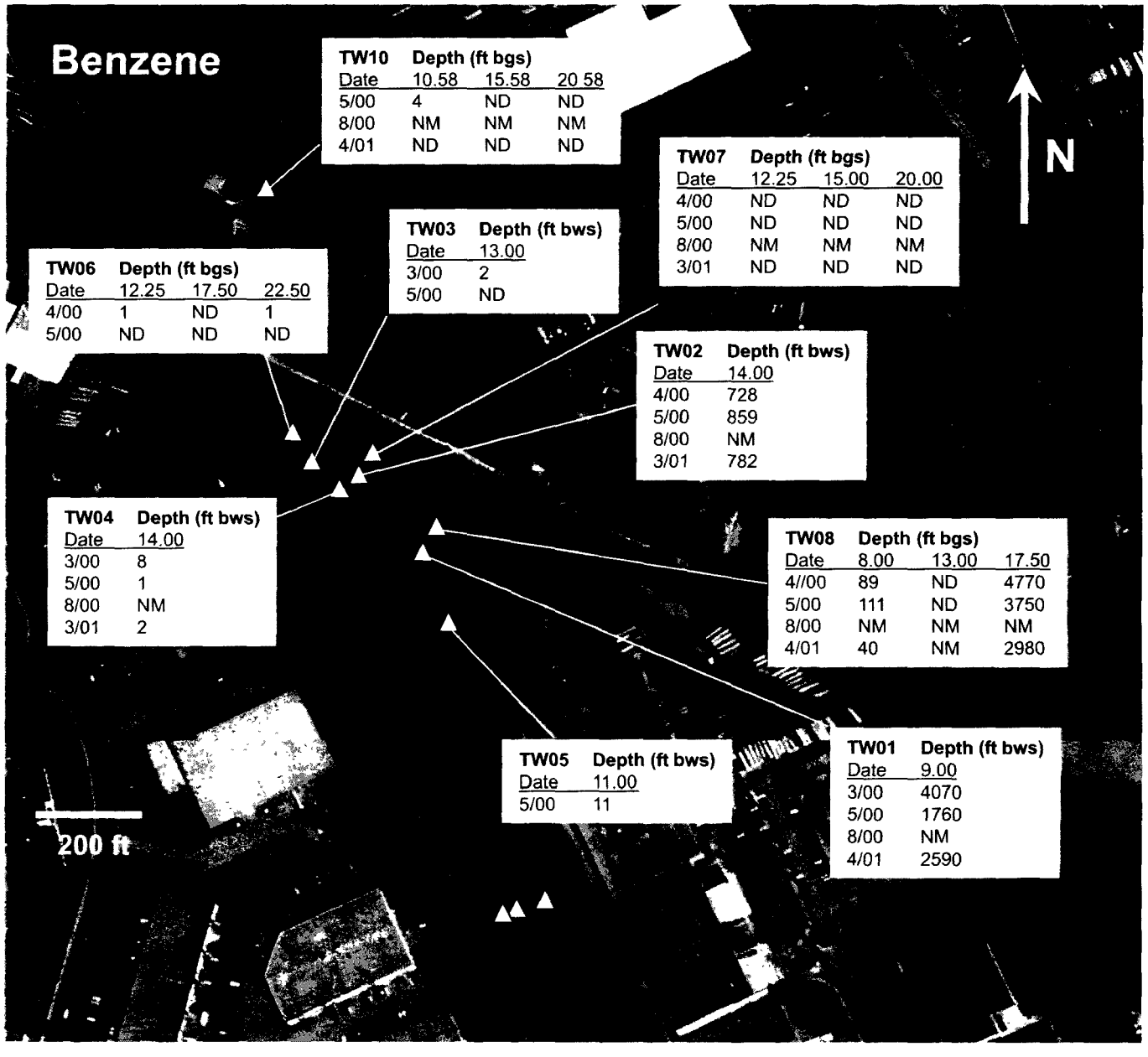


Figure 8 *Aerial distribution and time-dependent variability for benzene concentrations (ppb) detected in tubing wells established adjacent to the HBHA Pond. Depths are shown in feet below ground surface (ft bgs) and feet below water surface (ft bws) for tubing wells installed on land and within the HBHA Pond, respectively. Depths for tubing wells TW01, TW02, TW03, TW04, and TW05 were determined at the time of installation. NM = not measured, ND = not detected (<1 ppb). Image derived from May 1995 aerial photograph obtained from MassGIS.*

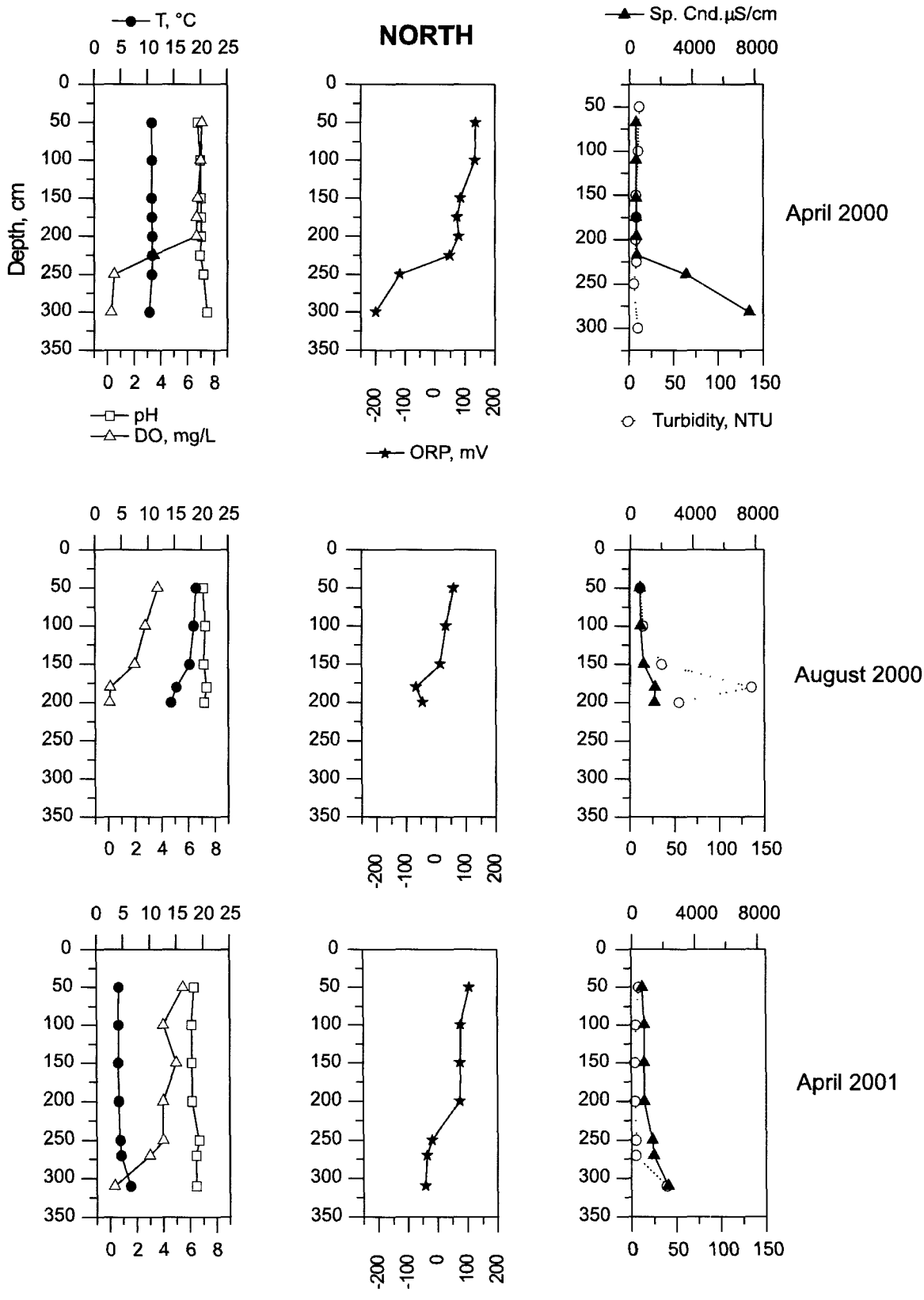


Figure 9 *Vertical patterns in water quality within the northern part of the HBHA Pond on sampling dates in April 2000, August 2000, and April 2001. Symbols: T = temperature, DO = dissolved oxygen, ORP = oxidation-reduction potential, and Sp. Cnd. = specific conductance.*

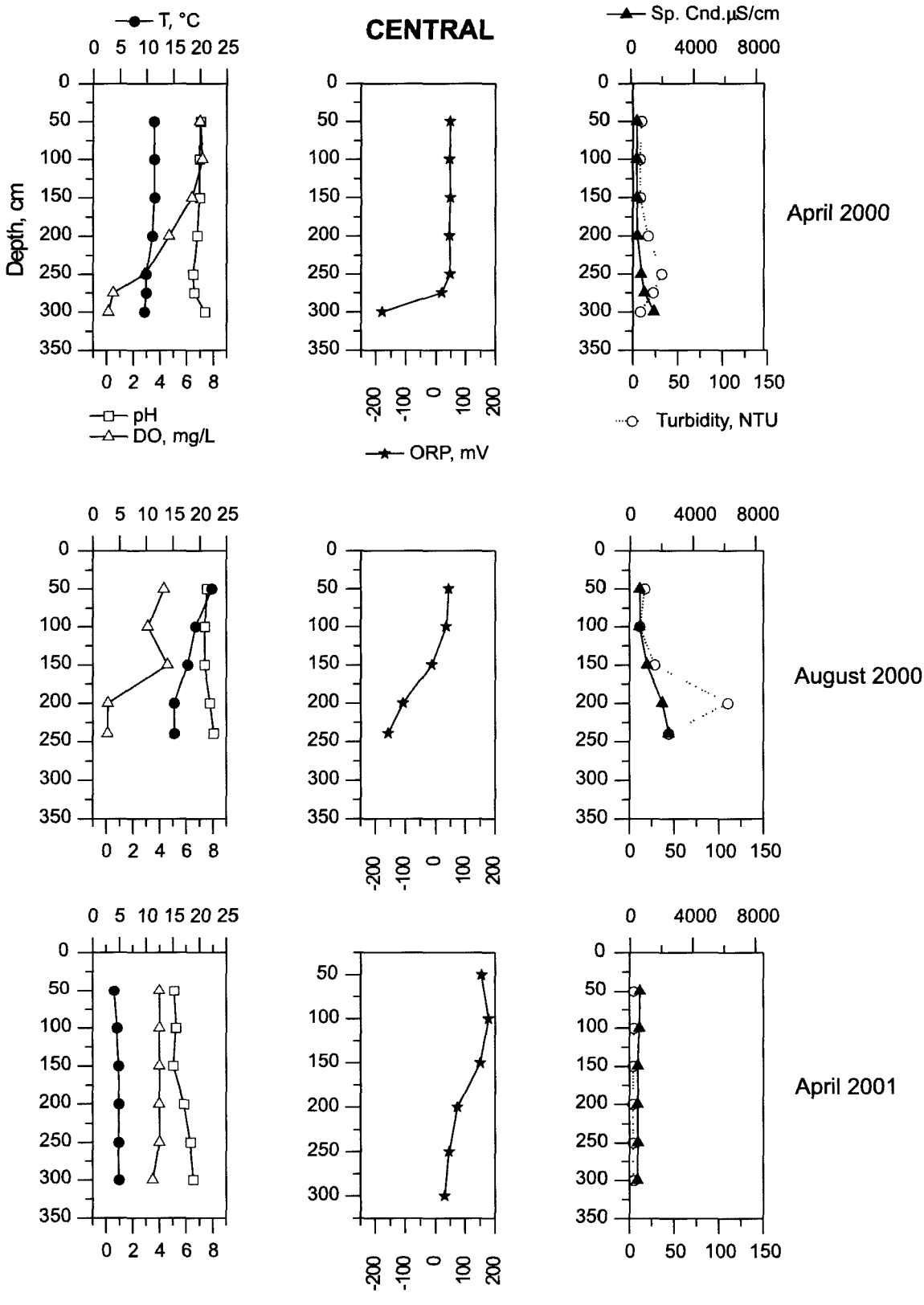


Figure 10 *Vertical patterns in water quality within the central part of the HBHA Pond on sampling dates in April 2000, August 2000, and April 2001. Symbols: T = temperature, DO = dissolved oxygen, ORP = oxidation-reduction potential, and Sp. Cnd. = specific conductance.*

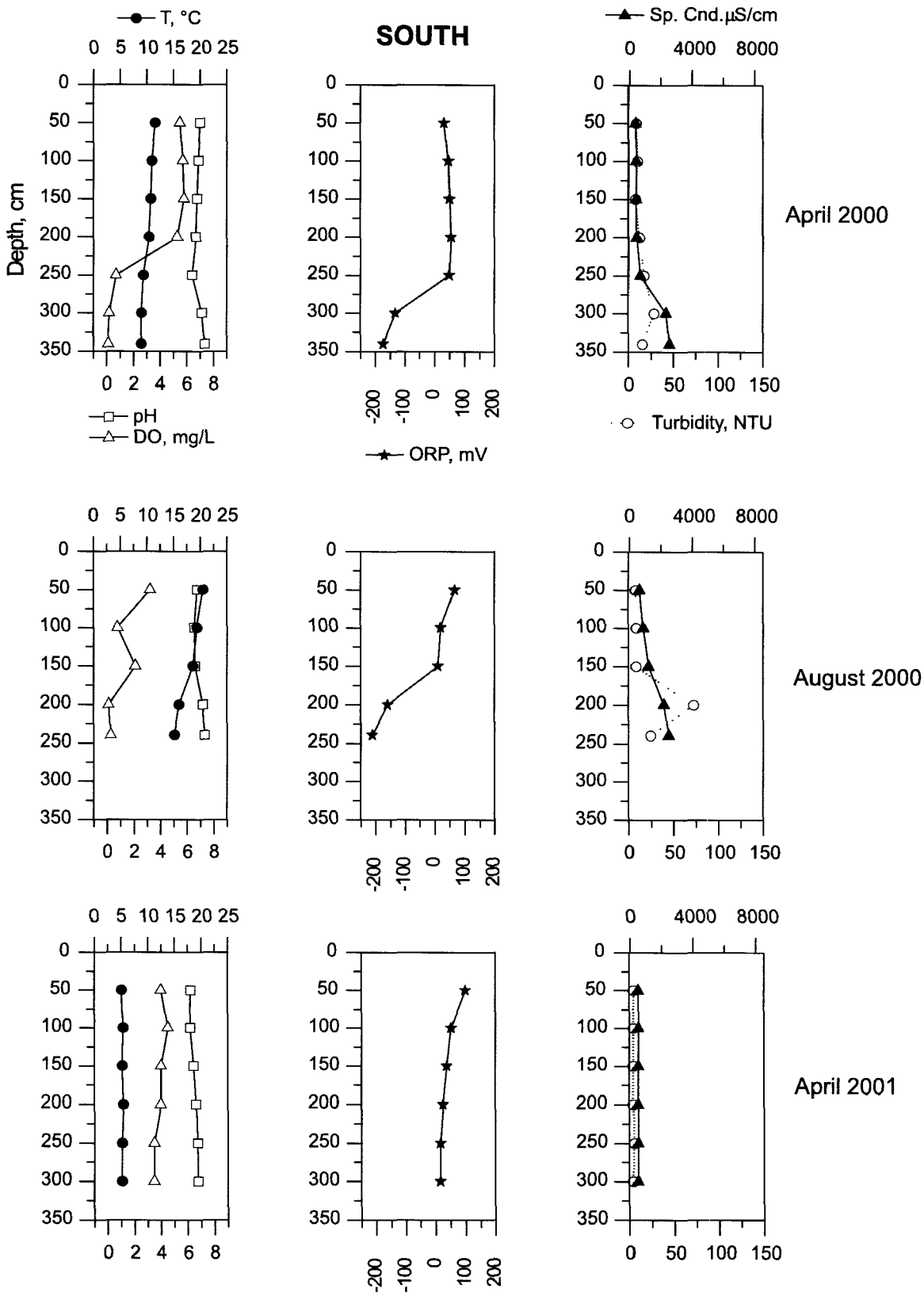


Figure 11 *Vertical patterns in water quality within the southern part of the HBHA Pond on sampling dates in April 2000, August 2000, and April 2001. Symbols: T = temperature, DO = dissolved oxygen, ORP = oxidation-reduction potential, and Sp. Cnd. = specific conductance.*

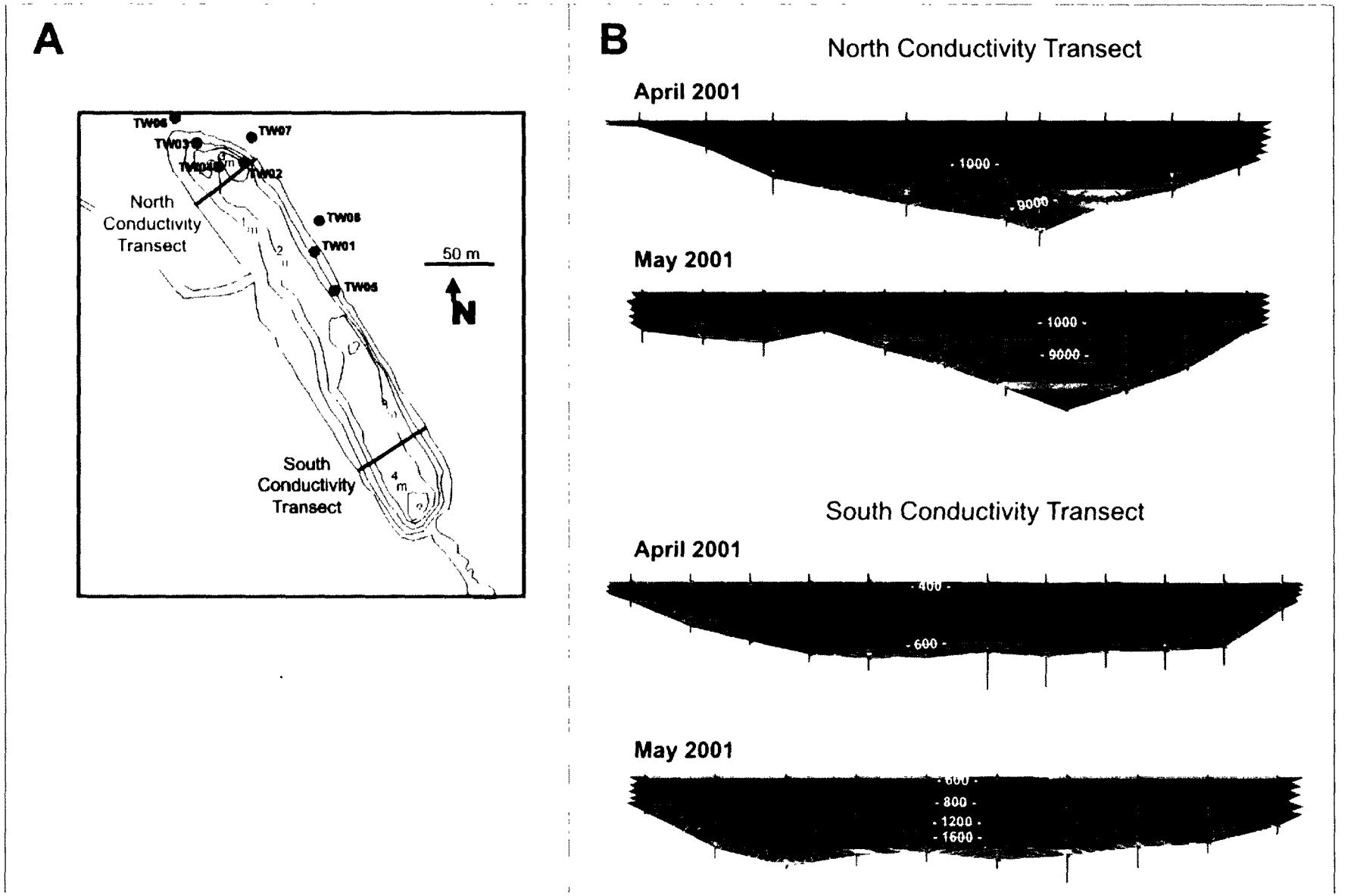


Figure 12 *Evidence of water column mixing within the HBHA Pond as a result of a large surface water flow event. (A) Location of conductivity transects collected within the north and south portions of the HBHA Pond. Contour lines indicate depth to sediment (meters). (B) Specific conductance (μS cm^{-1}) distribution immediately following (April 2001) and approximately one month (May 2001) after the large surface water flow event at the end of March 2001 (See Winchester flow data in Figure 5C.).*

Media-Specific Contaminant Distributions

Ground Water

The general distributions of major ion and contaminant metal concentrations in ground water are depicted in Figures 13 and 14. Patterns in the concentrations of alkalinity, sulfate, and ammonia-nitrogen between well pairs that span the GW/SW transition zone point to the stimulation of microbial activity within this region of the aquifer (specifically well pairs TW07-TW02 and TW08-TW01). There is a systematic decrease in the concentration of sulfate within ground water in moving from a location immediately upgradient to underneath the HBHA Pond (Figure 13B). This decrease is accompanied by concurrent increases in alkalinity and ammonia-nitrogen for these well pairs (Figure 13A and 13C). These trends appear to be confined to a region along the northeastern portion of the HBHA Pond. This region of the pond also corresponds to the location of the BTEX plume (Figure 13D).

Patterns in inorganic contaminant concentrations within the shallow aquifer appear more complex. The highest concentrations of zinc observed within the upgradient aquifer occur along the northern margin of the HBHA Pond (Figure 14). For arsenic, hot spots within ground water occur along the northern margin and also the north-eastern side of the HBHA Pond in a similar region as the BTEX plume. The co-occurrence of elevated arsenic, zinc, and sulfate along the northern portion of the HBHA Pond points to upgradient oxidative weathering of sulfides as a possible source. This is consistent with historical records that document the operation of a sulfuric acid production facility within the Industri-Plex Superfund Site boundary (Aurilio et al., 1995). A common process used in the production of sulfuric acid involved burning pyrites to generate sulfur dioxide gas. The waste products from this process were disposed on site and pose a long-term source of iron, sulfate, and associated inorganic contaminants in shallow ground water (Spanish pyrites with up to 1% arsenic by weight were often utilized). The region of elevated arsenic along the north-eastern side of the HBHA Pond may be due to an additional buried source or the development of chemical conditions conducive to maintaining arsenic in a dissolved state (e.g., iron reduction). There is an apparent source of sulfate at depth at location TW08-3 that may contribute to the elevated concentration of this dissolved component at location TW01. However, sulfate concentrations are significantly lower at shallow depths within this part of the aquifer (See Site 5, TW08-1, and Site 6.).

In general, the highest concentrations of inorganic contaminants discharging from ground water appear to be confined to the north-northeastern shoreline of the HBHA Pond. While inorganic contaminant concentrations appear to be lower in the region of the BTEX plume, it is clear that this portion of the aquifer is exerting an influence on the chemistry within the northern region of the HBHA Pond. The extent of this influence will be examined in greater detail in the following section.

Surface Water

Patterns in surface water chemistry have been reviewed by Ford (2005) for the HBHA Pond. Briefly, the chemistry within the pond is controlled by the relative proportions of surface water and ground-water flows. Due to the physical configuration of the HBHA Pond and the differences in dissolved solids concentrations between the main surface water inflow (Halls Brook) and the ground-water plume, the pond generally remains stratified. This stratification, or chemocline, acts to limit vertical diffusion of dissolved constituents entering the system via ground-water discharge at depth. The barrier to vertical transport within the water column plays an important role in maintaining the redox cycling of iron and co-precipitated arsenic (and metals). In general, ferrous iron entering the system via ground-water discharge is precipitated within the oxic (shallow) portion of the water column, leading to sequestration of dissolved arsenic. The iron (hydr)oxides (poorly crystalline ferrihydrite, Ford et al., 2005) settle to the sediment layer and are subsequently dissolved in the reducing conditions that are established by the microbial degradation of natural and contaminant organic compounds that accumulate within the HBHA Pond. The mineralogical characteristics of the iron (hydr)oxide precipitates and their rate of formation (data not shown) are comparable to those of natural, poorly crystalline ferrihydrite formed in terrestrial systems (Schwertmann, and Fischer, 1973; Davison and Seed, 1983; Schwertmann and Murad, 1988; Perret et al., 2000)

However, this near-permanent stratification can be interrupted by a sufficient surface water flow event. Such an event occurred during the study period (end of March 2001) resulting in complete mixing within the water column at the central and southern portions of the HBHA Pond (i.e., below Halls Brook discharge). The northern portion of the pond remained partially stratified (chemocline suppressed in depth), since this is the primary location of discharge for the contaminant plume. As shown by Ford (2005), the stratification is re-established along with the steady-state redox chemistry that controls iron and arsenic cycling. Based on the ground-water characterization program during this study, it became apparent that two plumes discharge into the north-northeastern portion of the HBHA Pond. The northern plume is the primary source of arsenic and iron into the system. In contrast, the primary input of BTEX compounds is located along the northeastern margin of the pond. The input of sulfate is more widely distributed across these two areas of plume discharge (Figures 11 and 12). Assessment of the temporal variations of the HBHA Pond water chemistry as a function of depth confirms that two separate plumes intersect to discharge into the north-northeastern portion of the HBHA

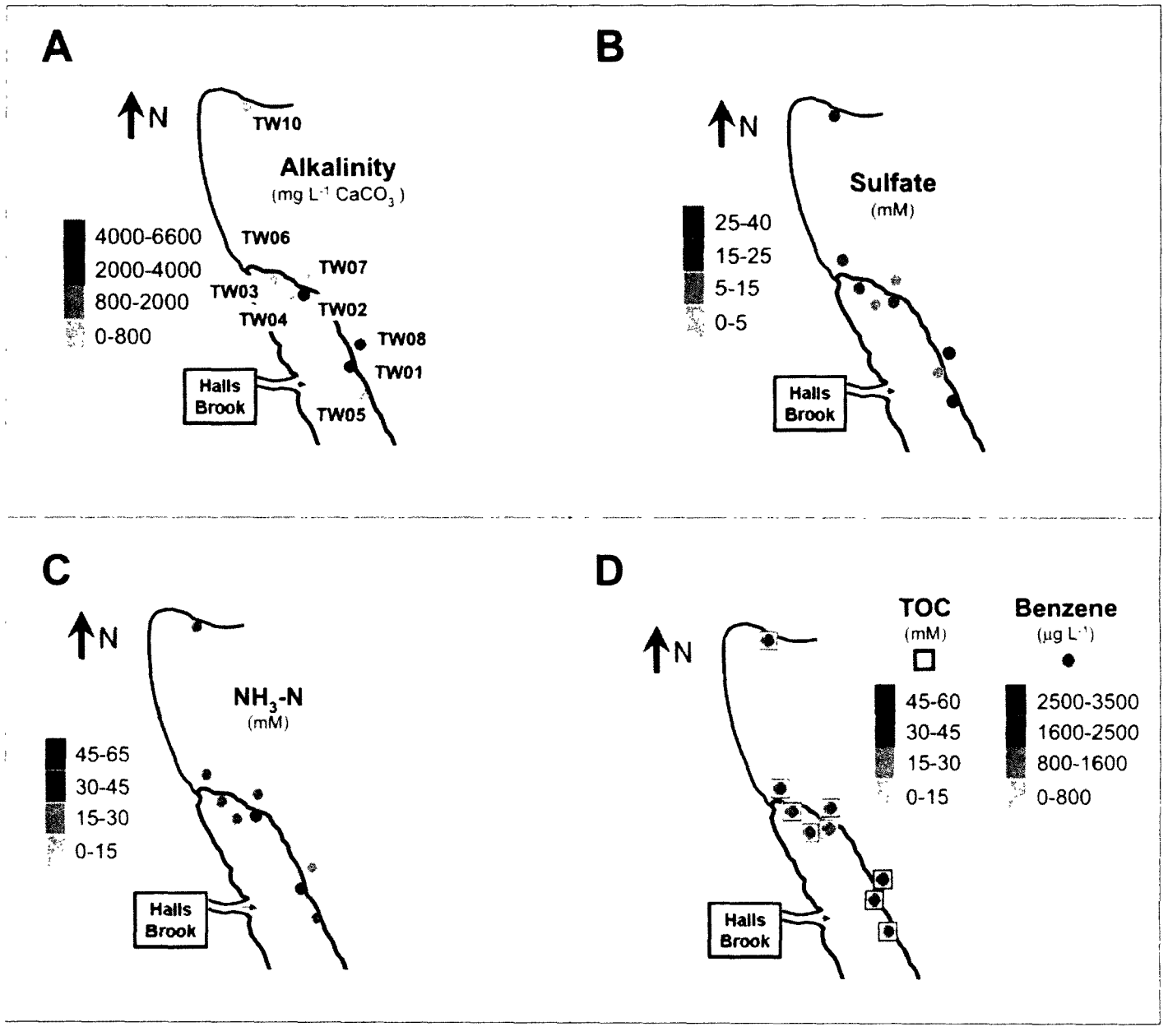


Figure 13 *The concentration distribution of (A) alkalinity, (B) sulfate, (C) ammonia-nitrogen, and (D) total organic carbon (TOC) and benzene in ground water. The plotted concentrations represent an average of all temporal measurements for all depths at each sampling location for the period of study.*

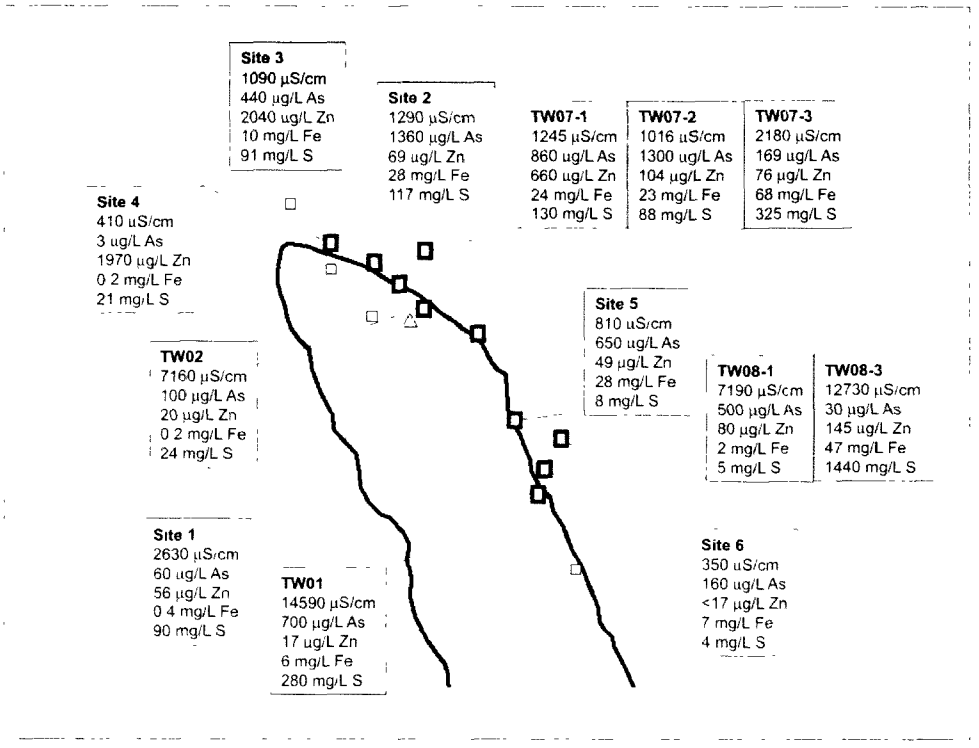


Figure 14 *The distribution of dissolved As, Zn, Fe, and total S in shallow ground water adjacent to the northern and eastern margins of the HBHA Pond. Highlighted regions show locations of elevated arsenic (red) and zinc (orange). Water samples were collected during the September 2004 field trip. Locations with 'Site' designation were temporary sampling points using a push-point sampler. Only data for samples collected near the water table are shown for locations TW07.*

Pond. Water chemistry data are shown in Figure 15 to illustrate the relationships between surface water chemistry and discharging ground water in this portion of the pond. Samples were collected at various times following the large surface water flow event (March, 2001) at several vertical locations within the water column and the adjacent shallow aquifer.

Comparison of the concentrations of dissolved constituents shown in Figure 15 for ground water and surface water reveals three general component groupings. The first group includes NH_3-N, alkalinity, and sodium (also TOC, data not shown). For these components, there does not appear to be a relationship between the concentrations observed within the deeper portion of the HBHA Pond water column at the NML sampling station and the adjacent ground-water wells (TW07 series and TW02). This disparity can most likely be attributed to a separate ground-water source originating from the eastern margin of the HBHA Pond between the TW07 and TW08 well locations. The concentration of these components may also be influenced by microbial processes occurring within pond sediments. The second component grouping includes sulfate and zinc in that there are general similarities in depth-dependent concentrations within the HBHA Pond at location NML and adjacent upgradient ground water. It should also be noted that there is little fluctuation in zinc concentrations at this location within the water column immediately above the sediment-water interface. Thus, dissolved zinc that is derived from ground-water discharge along the northern margin of the HBHA Pond is efficiently sequestered within sediments. The third component grouping includes arsenic and iron, which appear to originate primarily from a northern ground-water source (TW07 and further upgradient). However, concentrations of arsenic and iron within the deeper portion of the HBHA Pond water column exceed those observed in adjacent upgradient ground water (TW07). Since other adjacent ground-water locations (TW08, TW01) showed much lower arsenic concentrations than those observed in the deeper portion of the HBHA Pond water column, this implies that an additional flux of arsenic is derived from shallow sediments. This may be due to the reducing conditions established by microbial iron- and sulfate-reduction at the bottom of the HBHA Pond. Thus, while the primary source of arsenic discharging into the HBHA Pond appears to derive from the north, clearly ground-water inputs from the eastern BTEX plume influences the overall chemistry of the surface water within the northern portion of the pond. This is an important observation, since the BTEX plume (and associated degradable hydrocarbons) serves to stimulate microbial processes that likely influence iron and sulfur redox chemistry within the HBHA Pond.

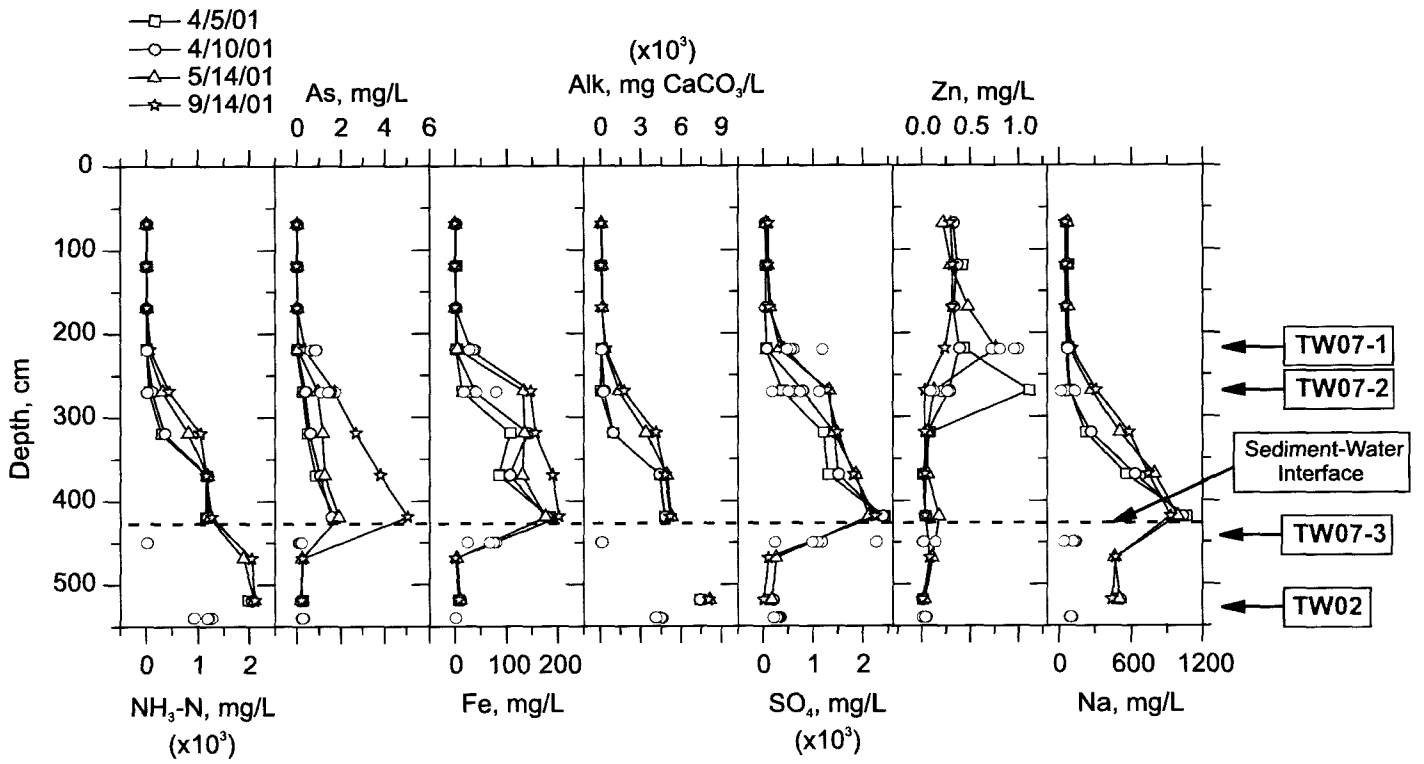


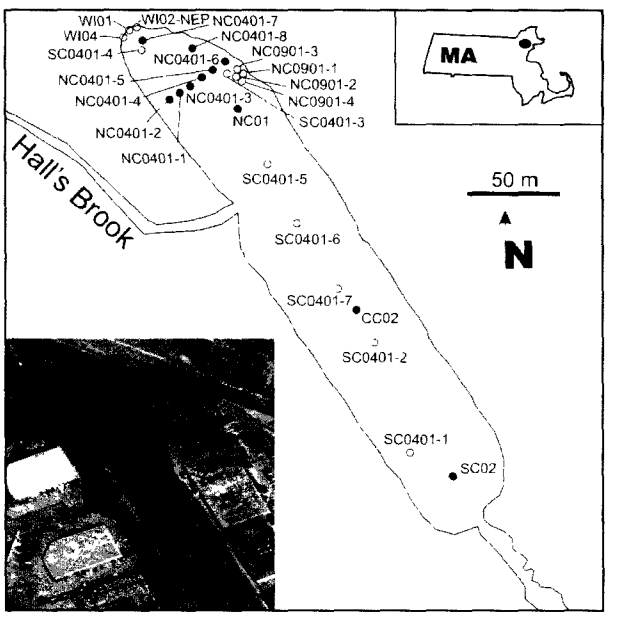
Figure 15 *Temporal trends in water chemistry for the NML sampling station and adjacent ground-water monitoring locations (TW07 and TW02). NML data are shown as open black symbols connected with lines for multiple sampling dates during the period of April 5, 2001, to September 14, 2001; adjacent ground-water data for locations TW07-1, TW07-2, TW07-3, and TW02 are shown as open red symbols for multiple sampling dates during the period of April 6, 2000, to September 11, 2001. Arsenic data for the NML sampling station are from Ford (2005).*

Sediments

Spatially-resolved concentration distributions for arsenic, lead, zinc, chromium, iron, sulfur, and organic carbon in the sediments of the HBHA Pond are shown in Figures 16-19. Raw concentration data are also tabulated in Appendix B. The highest concentrations of arsenic, chromium, and zinc were observed near the location of plume discharge and further downgradient within the HBHA Pond. In contrast, the highest lead concentrations are proximate to the location of the Atlantic Avenue Drainway discharge (Figure 2), which may be attributed to erosion or runoff from areas within the Industri-Plex Superfund Site. Because sediment concentration maxima for arsenic, chromium, and zinc coincide with regions where contaminated ground water discharges into the pond, it is reasonable to suspect that ground water transport coupled with metal deposition near the ground water-surface water interface is a primary mechanism controlling metal concentrations in the pond sediments. This pattern is particularly evident for sulfur, arsenic, and zinc where the highest concentrations of these elements appear to be associated with the area of plume discharge in the north-northeastern region of the HBHA Pond. Analysis of sediment cores showed that the highest concentrations of arsenic, lead, and zinc were associated with sediments that have been deposited following construction of the HBHA Pond (Appendix B). The underlying sandy sediments possess concentrations of carbon, iron, and sulfur that are lower by an order-of-magnitude or more.

A comparatively more even concentration distribution is observed for organic carbon (Figure 19). This pattern is likely the result of multiple sources of carbon to the pond, including ground water discharge, carbon input from Halls Brook, and seasonal deposition of plant materials and woody debris. High concentrations of organic carbon appear to be clustered in areas of low relief at the bottom of the pond suggesting that sedimentary deposition processes play an important role in regulating concentrations of organic carbon. With the exception of the locations of visible ground-water seeps along the north-northeastern margin of the HBHA Pond, iron is also distributed uniformly in shallow sediments throughout the pond (Figure 18, typically 8-12 wt%). The lack of iron concentration gradients in the pond sediments may be tied

to bottom-water redox conditions that are characteristically iron-reducing. That is, iron is highly soluble and mobile in deep bottom-waters of the HBHA Pond; consequently, there are no focused loci of iron accumulation. The highest sediment concentrations of iron are found in red-colored, shallow sediments (<1 m) over which waters are typically oxidizing (>2 mg/L dissolved O_2). Under oxidizing conditions, iron is highly insoluble, and iron would be expected to accumulate in the surface sediments, especially in areas that receive discharge of reducing, ferrous iron-laden water.



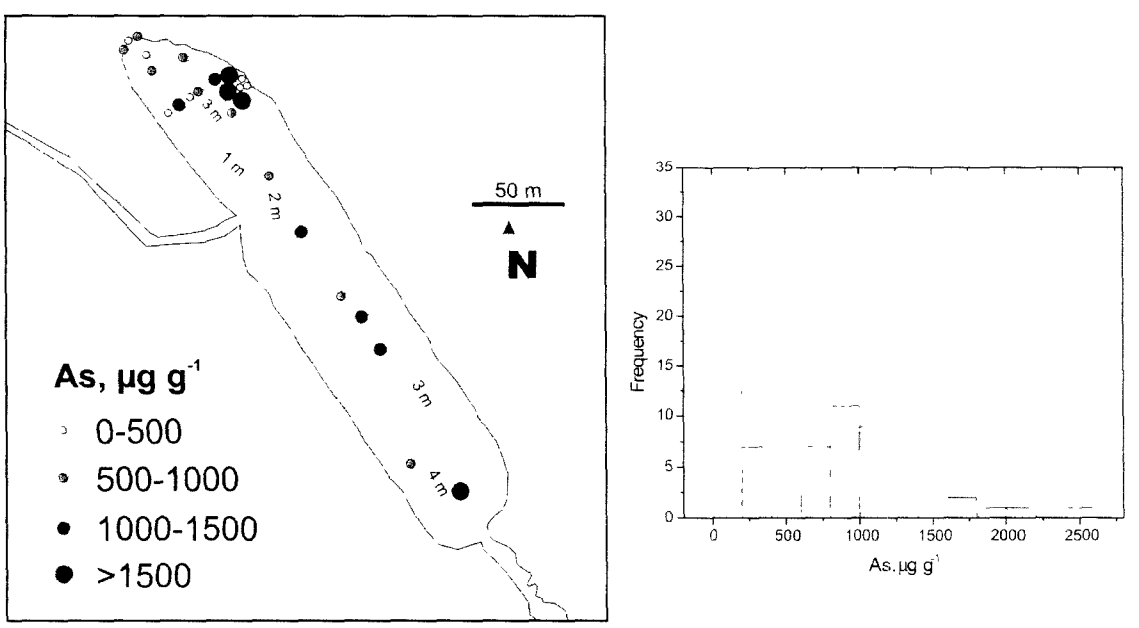


Figure 16 *The distribution of arsenic (As) in sediments collected from the HBHA Pond. The top panel shows the location of sediment samples for which compositional data are reported. The aerial distribution of arsenic is based on grab samples and the top 2-cm interval of core samples; contour lines delineate depth to sediment (meters). The frequency plot includes all grab samples and all sediment core depth intervals; data are compiled in Appendix B.*

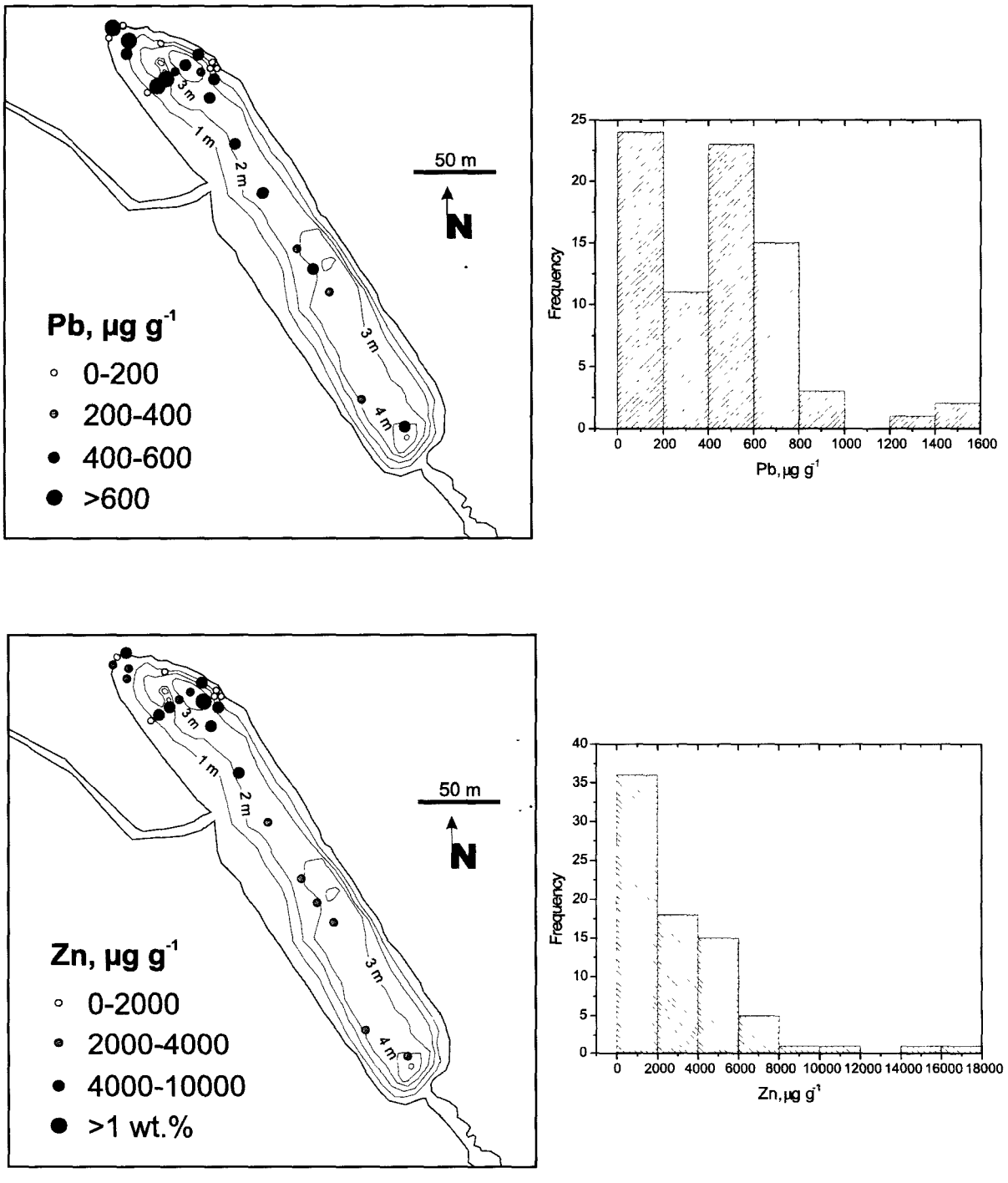


Figure 17 *The distribution of lead (Pb) and zinc (Zn) in sediments collected from the HBHA Pond. The aerial distributions of lead and zinc are based on grab samples and the top 2-cm interval of core samples; contour lines delineate depth to sediment (meters). The frequency plot includes all grab samples and all sediment core depth intervals; data are compiled in Appendix B.*

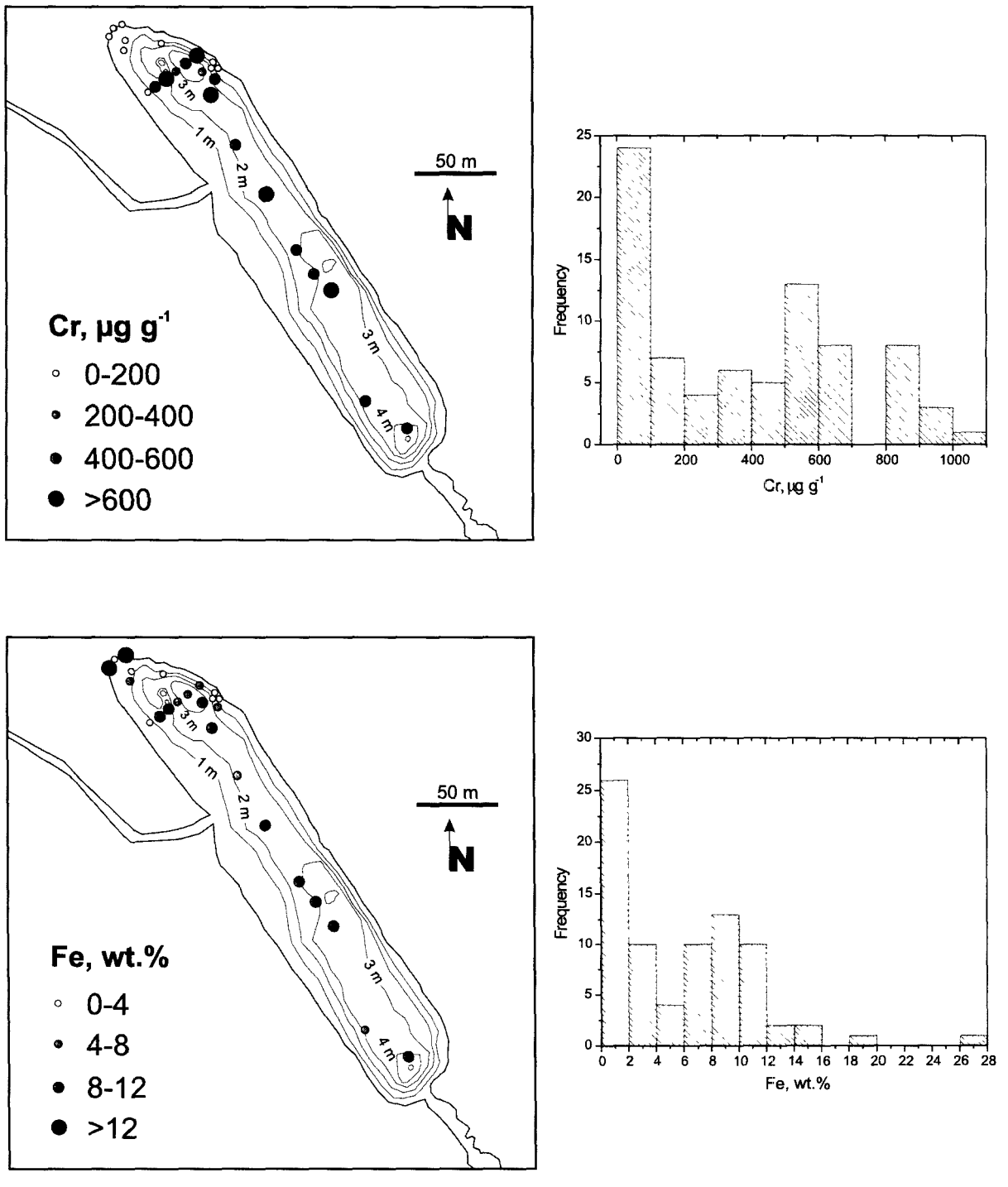


Figure 18 *The distribution of chromium (Cr) and iron (Fe) in sediments collected from the HBHA Pond. The aerial distributions of chromium and iron are based on grab samples and the top 2-cm interval of core samples; contour lines delineate depth to sediment (meters). The frequency plot includes all grab samples and all sediment core depth intervals; data are compiled in Appendix B.*

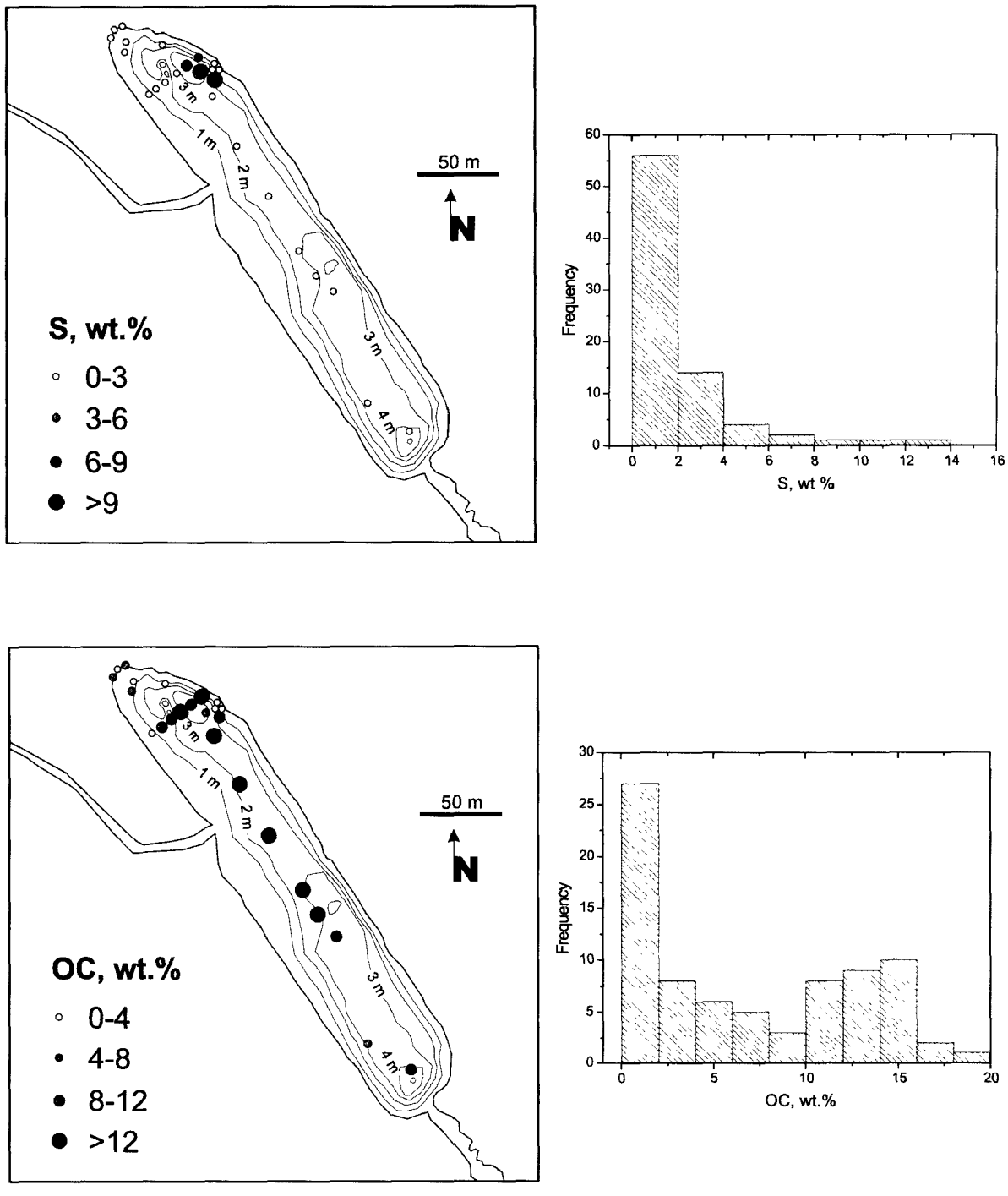


Figure 19 *The distribution of sulfur (S) and organic carbon (OC) in sediments collected from the HBHA Pond. The aerial distributions of sulfur and organic carbon are based on grab samples and the top 2-cm interval of core samples; contour lines delineate depth to sediment (meters). The frequency plot includes all grab samples and all sediment core depth intervals; data are compiled in Appendix B.*

Chemical Speciation of Metals in Sediments

Sediment Extractions

The objective of the chemical extraction tests was to develop a sense of the degree to which arsenic, lead, and zinc were partitioned to sediments in a relatively labile form. It was assumed that the fraction of contaminants released by mild extractant solutions (i.e., $MgCl_2$, phosphate, or Na_2CO_3) or extractant solutions designed to solubilized poorly crystalline iron oxides or sulfides would represent the most labile pool. From this perspective, $MgCl_2$ was chosen to extract lead and zinc present in a readily exchangeable fraction (Tessier et al., 1979); whereas, solutions of phosphate or Na_2CO_3 were chosen to extract arsenic adsorbed on mineral surfaces (Jackson and Miller, 2000). Solutions of ascorbate or hydrochloric acid were chosen to dissolve poorly crystalline iron oxides and sulfides (Kostka and Luther, 1994; Ford et al., 1999). Extraction with HCl was also studied due to its use for the acid volatile sulfide-simultaneously extracted metals (AVS-SEM) procedure commonly employed to determine metal speciation and potential bioavailability in sediments (Wilkin and Ford, 2002).

An implicit assumption in the following analysis was the existence of a direct association between extracted iron oxides and sulfides and co-extracted arsenic, lead, and zinc. The reliability of this assumption was tested via independent assessment of the solid phase speciation of these elements using X-ray absorption spectroscopy (discussed in a later section). It should also be noted that the various extraction solutions were applied in parallel. Thus, contaminants solubilized in either the ascorbate or HCl extractions could potentially have been derived from a variety of partitioning environments such as ion exchange sites and/or more stable environments such as the internal structures of coprecipitates (e.g., zinc incorporated in the structure of an iron oxide) or pure phase precipitates (e.g., zinc sulfide). The slight differences in pH or the concentration of the primary component in the extraction solutions employed for surficial (oxic) versus buried (suboxic) sediments was due to different personnel handling the two sediment classes. It was assumed that these differences were sufficiently insignificant to prevent comparison of extraction trends for the two sediment classes. It should also be noted that selectivity and completeness of the HCl and ascorbate extractions were not calibrated against sediments spiked with reference minerals. Rather, reliance was placed on published data where these procedures have been employed.

Surficial Sediments

Sediment samples were collected from the north-northwestern margin of the HBHA Pond in the vicinity of visible ground-water seeps. The sediments collected from this location were reddish-orange and consistent with the precipitation of poorly crystalline iron oxides due to the rapid oxidation and precipitation of ferrous iron derived from ground-water discharge. A series of chemical extraction tests were carried out on 5 sediment samples from this location (<2 mm size fraction). The solutions used to extract these sediments varied in their aggressiveness for the extraction of contaminants and dissolution of iron oxides or iron sulfides. Results of the chemical extraction tests are presented in Table 1 as percent recoveries of the total amount of arsenic, lead, zinc, and iron in the sediment samples. Total concentrations of these metals in the test sediments are presented in Appendix B. The chemical extraction tests included a spectrum of reagents from relatively mild 1 M magnesium chloride to more aggressive 0.5 M hydrochloric acid.

Test results indicated that arsenic, lead, and zinc were not readily solubilized from the sediments using a 1 M solution of $MgCl_2$. Typically, <1% of the total amount of sediment arsenic, lead, or zinc was leached using the magnesium chloride solution (Table 1); although, a greater fraction of zinc was extracted by this reagent (mean 15.0 %, max. 25.9%). This easily extracted fraction of zinc may be attributed to magnesium competition with zinc for ion exchange sites. Solutions containing phosphate were also examined to assess the degree to which arsenic could be desorbed from the sediment without significant solid phase dissolution. The fraction of extractable arsenic increased to as much as 15.9% in the presence of phosphate at pH 4, but less arsenic was extracted in the presence of phosphate at pH 7. The increase in extractable arsenic relative to the $MgCl_2$ solution can be attributed to the strong competition from phosphate for adsorption sites on sediment minerals (Jackson and Miller, 2000). A significant fraction of Zn (up to 27.4%) was also extracted in the presence of the pH 4 phosphate solution. This result may be attributed to competition with sodium for ion exchange sites and/or desorption of zinc from surface complexation sites due to the low pH (McBride, 1994). An insignificant fraction of lead was extracted from the oxic sediments in the presence of the $MgCl_2$ or phosphate solutions. In general, the highest fractions of arsenic, lead, and zinc were extracted in parallel with significant dissolution of iron-bearing minerals in these sediments. Mineralogical characterization of the clay-sized fraction from these sediments indicated that ferrihydrite was a dominant iron oxide phase. Ferrihydrite is readily solubilized via reductive- or acid-dissolution processes in ascorbate or HCl solutions (Ford et al., 1999; Larsen and Postma, 2001). The lower fraction of extracted lead for the ascorbate versus the HCl extraction (and zinc to a lesser extent) may be due, in part, to precipitation of a carbonate phase during the procedure.

Buried Sediments

A series of selected chemical extraction tests were carried out on 14 buried sediment samples collected from the bottom of the HBHA Pond. These tests were conducted to provide insight into contaminant speciation and the conditions that could favor metal release from the sediments. Results of the chemical extraction tests are presented in Table 2 as percent recoveries of the total amount of arsenic, lead, zinc, and iron in the sediment samples. Total concentrations of these metals in the test sediments are presented in Appendix B. The chemical extraction tests included a spectrum of reagents from relatively mild 0.5 M magnesium chloride to more aggressive 1 M hydrochloric acid. Test results indicated that arsenic and other selected metals analyzed were not readily solubilized from the sediments using 0.5 M magnesium chloride; typically <6% of the total amount of sediment arsenic or metal was leached using the magnesium chloride solution (Table 2). These results indicate that arsenic, lead, zinc, and iron are tightly bound to the solid matrix of the sediments. As expected, alkaline extraction solutions (0.1 M sodium carbonate) were ineffective in solubilizing lead, zinc, and iron; whereas, arsenic was partially recovered using the sodium carbonate solution (Table 2). Similar to the surficial sediments, significant fractions of arsenic and iron were extracted by the ascorbate solution, while extracted fractions of lead and zinc were below detection in this solution. Significant fractions of arsenic, lead, zinc, and iron were extracted in HCl for "unoxidized" and "oxidized" buried sediments. These results suggest the importance of contaminant partitioning to poorly crystalline iron (hydr)oxides and/or acid volatile sulfides. Mineralogical characterization of surficial sediments (discussed below) and a representative sample of buried sediments from the HBHA Pond (Wilkin and Ford, 2002) confirm that both mineral types could potentially be present in sediments deposited within the HBHA Pond.

Apparent differences for the extracted fractions of arsenic and lead between "oxidized" and "unoxidized" sediments treated with HCl suggest a potential artifact associated with the predominant mineralogy in the treated sediment. As shown by Wilkin and Ford (2002), acid volatile sulfides (in particular, iron monosulfides) may be present as a significant component of buried sediments. Typically, one would expect formation of poorly crystalline ferrihydrite as the endproduct of rapid oxidation of iron monosulfides. The high extractable fractions of arsenic, lead, zinc, and iron in these "oxidized" sediments are consistent with an association with either a 'native' poorly crystalline iron (hydr)oxide as well as a similar phase produced upon oxidation of iron monosulfide. Thus, the observed artifact can be attributed to some chemical process that limits the solubility of arsenic and lead in HCl for "unoxidized" sediments.

The ratios of extracted arsenic, lead, zinc, and iron for "unoxidized" and "oxidized" buried sediments are plotted in Figure 20 as a function of total sulfur content. In the absence of analytical artifacts, one would anticipate a value close to unity for this ratio in sediments dominated by acid volatile sulfides ("unoxidized") and/or poorly crystalline iron (hydr)oxides ("oxidized"), since both mineral phases are extracted in hydrochloric acid. Results plotted for arsenic indicate that this metal is less extractable for the "unoxidized" sediment, i.e., extracted ratio << unity. However, as shown by Wilkin and Ford (2002) this behavior can be attributed to an analytical artifact of the acid extraction commonly employed in the acid-volatile sulfide-simultaneously extracted metals (AVS-SEM) procedure rather than to any inherent difference in extractability. Specifically, hydrogen sulfide that is released during acid extraction reacts with co-extracted arsenic to form an orpiment-like phase at acidic pH, which is confirmed through calculation of orpiment solubility at the extraction pH (Wilkin and Ford, 2002). It appears there may be a related concern for Pb, which again displayed a decreased extractability for the "unoxidized" buried sediment with an increase in sulfide content. The extractability ratios clustered around unity for Fe and Zn in these sediment samples are consistent with the high solubility of iron and zinc monosulfides at acid pH. Extract ratios that exceed unity value at low sulfur concentrations may result from the conditions used to oxidize sediments. Exposure to air in a drying oven at 60°C was employed to oxidize sulfides. The elevated drying temperature may have resulted in the production of an iron oxide phase(s) that was resistant to extraction using hydrochloric acid (e.g., Stanjek and Weidler, 1992). This would result in extraction ratios greater than unity, since iron and zinc associated with an acid-resistant iron oxide phase would be less extractable. This process would be less likely for sediments with exceptionally high sulfide concentrations, since the formation of a more extractable ferric sulfate phase(s) would be favored.

Due to the anticipated importance of poorly crystalline iron (hydr)oxides and iron sulfides in HBHA Pond sediments, ascorbate and hydrochloric acid extraction solutions were employed to assist in differentiating the relative proportion of these minerals. Peltier et al. (2005) have shown that extraction tests designed to target easily reducible iron (hydr)oxides via reductive dissolution at acidic pH also extract a significant fraction of acid volatile sulfides. However, this potential artifact was avoided by employing reductive dissolution with ascorbate buffered at a near-neutral pH (Kostka and Luther, 1994). As a point of reference, the results of ascorbate extractions of both surficial and "unoxidized" buried sediments for arsenic and iron are shown in Figure 21. Except for sample WI01, arsenic was completely extracted in the presence of ascorbate for all surficial sediments, which corresponded with an extractable iron fraction of more than 80%. The lower amount of extractable arsenic and iron in sediment WI01 may be attributed to the crystallinity of the dominant iron oxide in this sample. As shown in Figure 22, hematite is the dominant iron oxide in the <2 μm size fraction from this sediment. X-ray diffraction data for the <2 μm size fraction of sediment samples WI01-NEP and WI02-NEP show an increased relative proportion of poorly crystalline 6-line ferrihydrite, consistent with the observed change in

the fraction of ascorbate-extractable iron. As shown by Kostka and Luther (1994), hematite is dissolved to a lesser extent than ferrihydrite by ascorbate under the conditions employed. The increase in extractable iron for samples WI01, WI01-NEP, and WI02-NEP is consistent with the increased relative proportion of a poorly crystalline 6-line ferrihydrite in this series of samples. The low extractability of arsenic concurrent with the significant fraction of hematite in sample WI01 suggests the incorporation of arsenic in hematite during nucleation and growth of this mineral as suggested by experimental studies by Ford (2002). However, this observation remains uncertain without a specific knowledge of the diagenetic history leading to hematite formation in this sediment.

The fraction of ascorbate-extractable arsenic varied significantly for the set of buried sediments that was analyzed. Based on the results shown in Figure 21A, there were two distinct sediment groups in which arsenic was either >90% extractable (6 samples) or <40% extractable (6 samples) with a set of transition sediments between these two limits (5 samples). Examination of the fraction of ascorbate-extractable arsenic as a function of the total sulfur content of buried sediments indicates a general correlation between these two parameters (Figure 21C). It should be noted that a similar correlation (although weaker) apparently exists between ascorbate-extractable iron and total sulfur content for buried sediments (Figure 21D). Insignificant extraction of iron sulfides is anticipated for ascorbate extractions (Kostka and Luther, 1994), suggesting that arsenic may be partitioned to iron sulfides for buried sediments with low ascorbate-extractable arsenic. Sediments in which the iron mineralogy is dominated by iron oxides are anticipated to have similar extractable iron fractions in the presence of ascorbate and HCl. This hypothesis is supported by results presented in Figure 21E. All surficial sediments have an ascorbate:HCl extractable ratio for iron ≥ 1 compared to buried sediments with ratios of ≤ 0.5. Ratios greater than unity for surficial sediments can be attributed to extraction, in the presence of ascorbate, of iron oxides that are more crystalline than ferrihydrite (Dos Santos Afonso et al., 1990; Larsen and Postma, 2001). These results point toward the presence of acid volatile iron sulfides in all of the buried sediments. In general, it appears that the iron mineralogy for buried sediments is increasingly dominated by acid volatile iron sulfides with increasing sulfur content.

Comparison to observed trends in apparent lead and zinc partitioning in surficial and buried sediments suggests differences in the partitioning environment of these contaminants relative to arsenic (Tables 1 and 2). The ascorbate-extractable fractions of lead and zinc were below analytical detection for "unoxidized" buried sediments (Table 2). The observation that a majority of lead and zinc (more than 80% and 90% of lead and zinc, respectively) were extracted in "oxidized" buried sediments suggests that a significant fraction of these contaminants are partitioned to acid volatile sulfides. As for the surficial sediments, the presence of a high concentration of bicarbonate may cause precipitation of lead/zinc carbonates during the ascorbate extraction. In addition, re-adsorption of lead/zinc to the surface of unextracted minerals may also have resulted due to the absence of citrate in the procedure applied for buried sediments. Citrate would act as a complexant to help maintain extracted metals in solution. Overall, the results from sediment extractions employing ascorbate and HCl were less definitive for delineation of lead and zinc speciation. This limitation was addressed for a limited set of sediment samples using X-ray absorption spectroscopy to directly determine the in-situ speciation of arsenic, lead, and zinc.

Table 1 Percent of Total Element Released by Selected Wet Chemical Extraction Tests. Range and Mean Value are Reported for Replicate Analyses of 5 Sediment Samples Collected from the North-Northeastern Margin of the HBHA Pond

Solution	As	Pb	Zn	Fe	Association
1 M $MgCl_2$	<1% mean 0.2%	0.2 to 1.0% mean 0.5%	7.7 to 25.9% mean 15.0%	<1% mean 0.01%	Water-soluble; labile; easily desorbed (pH 7)
0.005 M NaH_2PO_4	8.3 to 15.9% mean 11.6%	<1% mean †	5.8 to 27.4% mean 16.2%	<1% mean 0.3%	Water-soluble; strongly adsorbed (pH 4)
0.005 M NaH_2PO_4	2.2 to 5.1% mean 3.3%	<1% mean †	<1% mean 0.2%	<1% mean 0.04%	Water-soluble; strongly adsorbed (pH 7)
Ascorbate 0.2 M Na-citrate 0.6 M $NaHCO_3$ 0.4 M Ascorbic acid	39.2 to 127.0% mean 101.8%	4.5 to 33.2% mean 17.6%	20.0 to 80.3% mean 57.6%	27.6 to 115.9% mean 88.0%	Soluble with a mild reductant (pH 8)
0.5 M HCl	16.7 to 66.9% mean 32.0%	17.2 to 95.7% mean 61.0%	27.1 to 95.3% mean 71.4%	16.4 to 97.0% mean 70.2%	Acid-soluble (pH<2)

Notes: *Samples used in extraction tests: WI01, WI01-NEP, WI02, WI02-NEP, WI04. † indicates element was undetected or below quantitative limits in the extraction solution.*

Table 2 Percent of Total Element Released by Selected Wet Chemical Extraction Tests. Range and Mean Value are Reported for 14 Sediment Samples Collected from the HBHA Pond

Solution	As	Pb	Zn	Fe	Association
0.5 M $MgCl_2$	1 to 26.5% mean 5.8%	<1% mean †	0.1 to 1.9% mean 0.6%	0.3 to 11.0% mean 4.3%	Water-soluble; labile; easily desorbed (pH 6.8)
0.1 M Na_2CO_3	10.9 to 73.5% mean 25.9%	<1% mean †	<1% mean †	<1% mean 0.3%	Base-soluble; complexed with organic carbon (pH 10.9)
0.02 M Ascorbic acid 0.6 M $NaHCO_3$	16.1 to 108% mean 65.7%	<1% mean †	<1% mean †	6.1 to 51.0% mean 23.2%	Soluble with a mild reductant (pH 7.0)
1 M HCl "oxidized" sediment	71 to 106% mean 91.7%	80.0 to 113.1% mean 99.1%	90.3 to 109.4% mean 100.8%	56.8 to 107% mean 86.7%	Acid-soluble; leaching characteristic of air-exposed sediment at pH<2
1 M HCl "unoxidized" sediment	<1 to 20.9% mean 13.2%	3.6 to 105.8% mean 63.5%	62.2 to 105% mean 98.2%	83.0 to 107% mean 98.5%	Acid-soluble; leaching characteristic of unaltered sediment at pH<2

Notes: *Samples used in extraction tests: SC0401-1, SC0401-2, SC0401-3, SC0401-5, SC0401-6, SC0401-7, NC0901-1, NC0901-2, NC0901-3, NC0901-4a, NC0901-4b, NC0901-4c, NC0401-1 (0-2cm), NC0401-1 (2-4cm), NC0401-6 (0-2cm), NC0401-6 (2-4cm). "Oxidized" sediments extracted in HCl were exposed to air to oxidize sulfide to sulfate prior to extraction, while "unoxidized" sediments were processed in an inert atmosphere to prevent oxidation of sulfides. † indicates element was undetected or below quantitative limits in the extraction solution.*

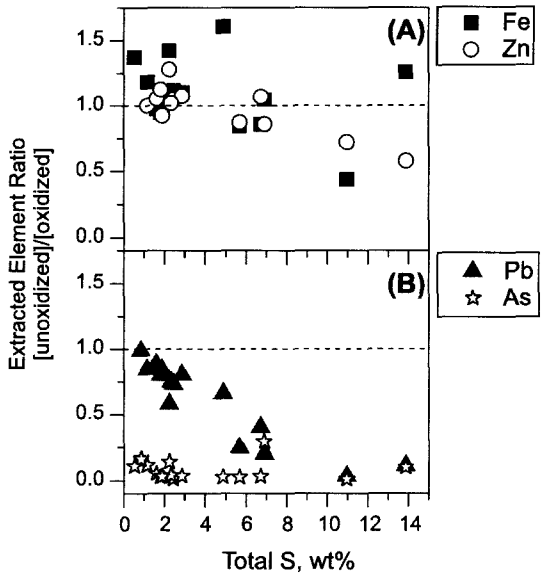


Figure 20 *The ratio of As, Fe, Pb, and Zn extracted by HCl for unoxidized and oxidized sediments collected from suboxic zones within the HBHA Pond.*

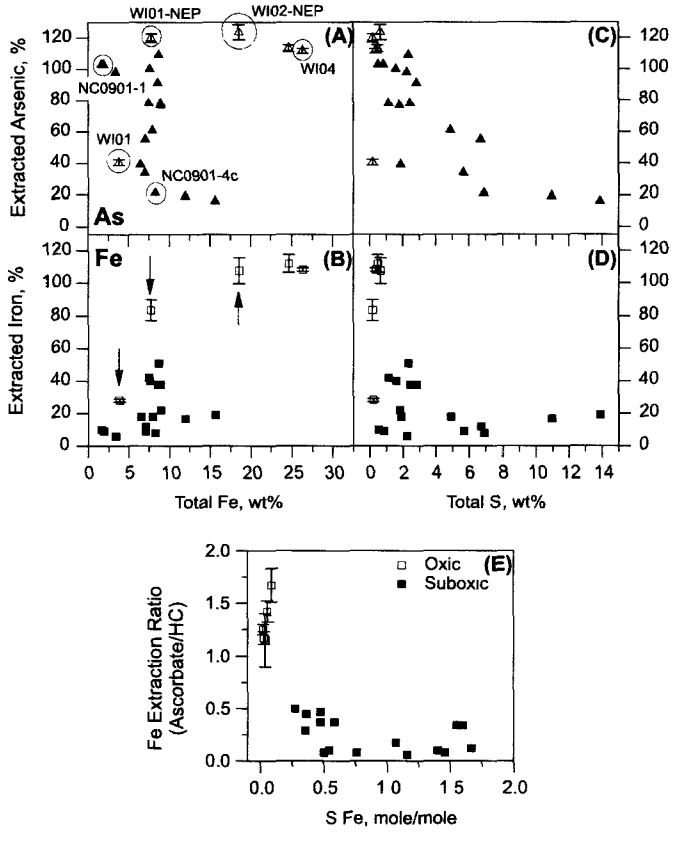


Figure 21 *(A-D) Comparison of the amount of As and Fe extracted by an ascorbate solution as a function of total Fe and S content in sediments (oxic = open symbols, suboxic = filled symbols). (E) Changes in the ratio of ascorbate-to-HCl extractable Fe as a function of the molar ratio of S and Fe in sediments. X-ray diffraction data are shown below for sediment samples WI01, WI01-NEP, and WI02-NEP (Figure 20). X-ray absorption spectroscopic data are shown below for arsenic in sediment samples WI01-NEP, WI04, NC0901-1, and NC0901-4c (Figure 23).*

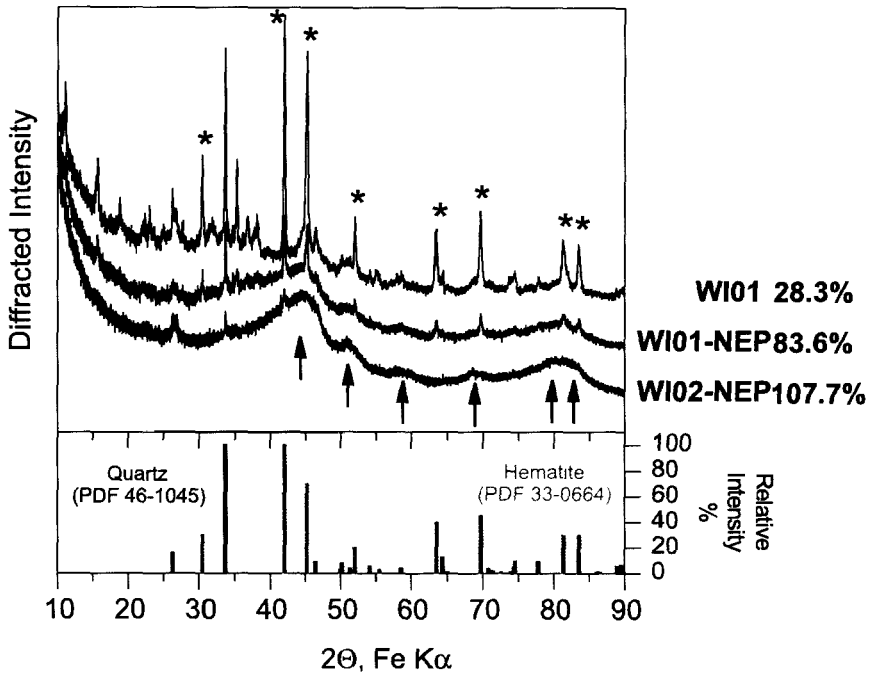


Figure 22 *X-ray diffraction data showing the relative proportion of hematite and ferrihydrite in the <2 μm size fraction isolated from surficial sediment samples WI01, WI01-NEP, and WI02-NEP collected near the north-north-western margin of the HBHA Pond. The starred peaks in the pattern for sample WI01 correspond with the dominant peaks in reference hematite (PDF 33-0664). Mean percent iron extracted by ascorbate in duplicate samples is shown to the right of the sample labels. The diffraction pattern for sample WI02-NEP is dominated by a poorly crystalline 6-line ferrihydrite (see peaks marked with arrows).*

Element Speciation by X-ray Absorption Spectroscopy

To provide a constraint on the interpretation of the extraction results, the in-situ speciation of arsenic, lead, and zinc were determined for a representative set of samples using X-ray absorption spectroscopy. The results of contaminant speciation analyses employing X-ray absorption spectroscopy are documented in Figures 23-25. Specifically, linear combination fitting (LCF) of the X-ray absorption near edge (XANES) region of the spectra was used to delineate element speciation in sediments. Reference spectra collected for model solid phase compounds were used in the fitting procedure in order to estimate the relative fraction of representative contaminant-mineral associations in each analyzed sediment sample. In aggregate, these results attest to the importance of the redox gradients within the HBHA Pond and attest to the apparent degree of disequilibrium that exists within the sediments.

The results from a selection of samples characterized for arsenic speciation are shown in Figure 23, and the aerial distribution of arsenic phase associations within the HBHA Pond are shown in Figure 26. Analysis of these samples indicates that the fate of arsenic is directly tied to the iron minerals that dominate within oxic and suboxic portions of the HBHA Pond. Arsenic speciation is dominated by adsorption/coprecipitation of As(III) or As(V) with iron (hydr)oxides that precipitate in shallow ground-water seeps near the margin of the HBHA Pond (WI01-NEP, WI04). The speciation of arsenic transitions to As(III) partitioned to iron monosulfides within the deepest buried sediments (NC0901-4C) with a fraction of As(III) remaining bound to iron (hydr)oxides or iron carbonate at shallower depths within the HBHA Pond (NC0901-1). It should be noted that arsenic associated with orpiment (As_2S_3) represented an insignificant fraction (<10%) within buried sediments. The position of the arsenic absorption edge in all sediment samples that were evaluated was significantly higher than that observed for mineral specimens and laboratory-prepared As_2S_3 (data not shown). The arsenic speciation results for these samples are broadly consistent with the extraction results shown in Figure 21A. These results are consistent with the extraction data previously discussed where the bulk of the sediment-associated arsenic was extracted using reagents that targeted poorly crystalline iron (hydr)oxides and iron sulfides (Tables 1 and 2). The relative fraction of arsenic bound to oxygen increases for sediments with higher iron (hydr)oxide content (Fe_{Asc}/Fe_{HCl} ratio near unity), while the fraction of arsenic bound to sulfur increases with higher iron sulfide content (low Fe_{Asc}/Fe_{HCl} ratio). Therefore, the stability of solid phase arsenic in these sediments will partly be dictated by the stability of these metastable minerals.

The results from a selection of samples characterized for lead speciation are shown in Figure 24 (all data fits in Appendix B), and the aerial distribution of lead phase associations within the HBHA Pond are shown in Figure 26. Analysis of these samples indicates that lead speciation is dominated by partitioning to iron (hydr)oxide minerals. This pattern holds even in sediments collected from the bottom of the HBHA Pond where there is evidence for iron- and sulfate-reduction (Figures 13 and 15) and formation of iron sulfides (Figure 21E; low Fe_{Asc}/Fe_{HCl} ratios). A fraction of lead is partitioned to a sulfidic phase within buried sediments, but in most cases, this represents a minor fraction of the species of lead identified based on the LCF-XANES approach. This observation in combination with Fe_{Asc}/Fe_{HCl} extraction ratios >25% for half of the buried sediment samples shown in Figure 21E clearly indicates that iron (hydr)oxides formed within oxic portions of the HBHA Pond survive the reducing conditions established at the bottom of the pond. The persistence of iron (hydr)oxides in zones of iron- and sulfate-reduction in sediments has been observed by others (Kostka and Luther, 1994). Since both poorly crystalline iron (hydr)oxides and iron sulfides are extracted by HCl, this suggests potential limitations to the use of tests such as the AVS-SEM procedure to define element speciation.

Finally, the results from a selection of samples characterized for zinc speciation are shown in Figure 25 (all data fits in Appendix B) and the aerial distribution of zinc phase associations within the HBHA Pond is shown in Figure 26. The results of this analysis contrast with those for lead in that zinc sulfides play a more dominant role in the speciation of this metal in buried sediments. Zinc partitioned to an iron (hydr)oxide phase is still observed as a significant component within all sediments indicating that the survival of this mineral fraction still plays a role in zinc speciation within the suboxic zone of the HBHA Pond. The decrease in the abundance of the sediment species for zinc relative to lead is consistent with the greater stability of the lead sorption complex on iron (hydr)oxide surfaces (Stumm, 1992). In general, the importance of sulfide minerals to element speciation within buried sediments appears to follow the order As > Zn > Pb.

A sediment incubation study was conducted to observe the changes in metal speciation that may occur as iron (hydr)oxides formed in the oxic zone are deposited in the suboxic zone within the HBHA Pond. In this study, surficial sediments from the northern margin of the HBHA Pond were incubated with their native pore water in closed vessels within the laboratory at room temperature. No attempt was made to control the biogeochemical conditions within the vessel during incubation for a period of 2.5 years. The silt (<53 μm) and clay (<2 μm) fractions of the fresh and incubated sediments were isolated by sieving and centrifugation to facilitate mineralogical characterization of the most reactive mineral fraction. Significant alterations of the iron mineralogy were observed as a result of incubation. X-ray diffraction data collected on the clay fraction of a representative sediment sample showed that a poorly-crystalline 6-line ferrihydrite was dominant in the fresh sediment (Figure 27A). However, this mineral was transformed to a mixture of goethite and siderite during the incubation period. Zinc speciation data were collected for the silt-sized fraction of the fresh and incubated sample to determine the concurrent changes in contaminant speciation that accompanied the observed transformations in bulk mineralogy (Figure 27B; arsenic and lead data not collected). Analysis of these data using the LCF-XANES approach demonstrated significant changes in zinc speciation during sediment incubation. The speciation of zinc was dominated by a combination of a hydroxide-like precipitate and adsorption/coprecitation with an iron (hydr)oxide phase in the fresh sample. During incubation, a zinc sulfide phase formed at the expense of the zinc-iron (hydr)oxide phase. The results of the XRD and LCF-XANES analyses demonstrate that iron-reducing and sulfate-reducing conditions developed during the period of incubation, potentially driven by the growth of native microbial communities in the closed environment. Unfortunately, data on the chemical conditions during aging and evidence for microbial reactions were not collected during this experiment. However, the results of this experiment are consistent with the observed change in zinc speciation in transitioning from surficial (oxic) to buried (suboxic) sediments within the HBHA Pond. Specifically, iron- and sulfate-reducing processes play a critical role in determining contaminant speciation in sediments deposited within the HBHA Pond.

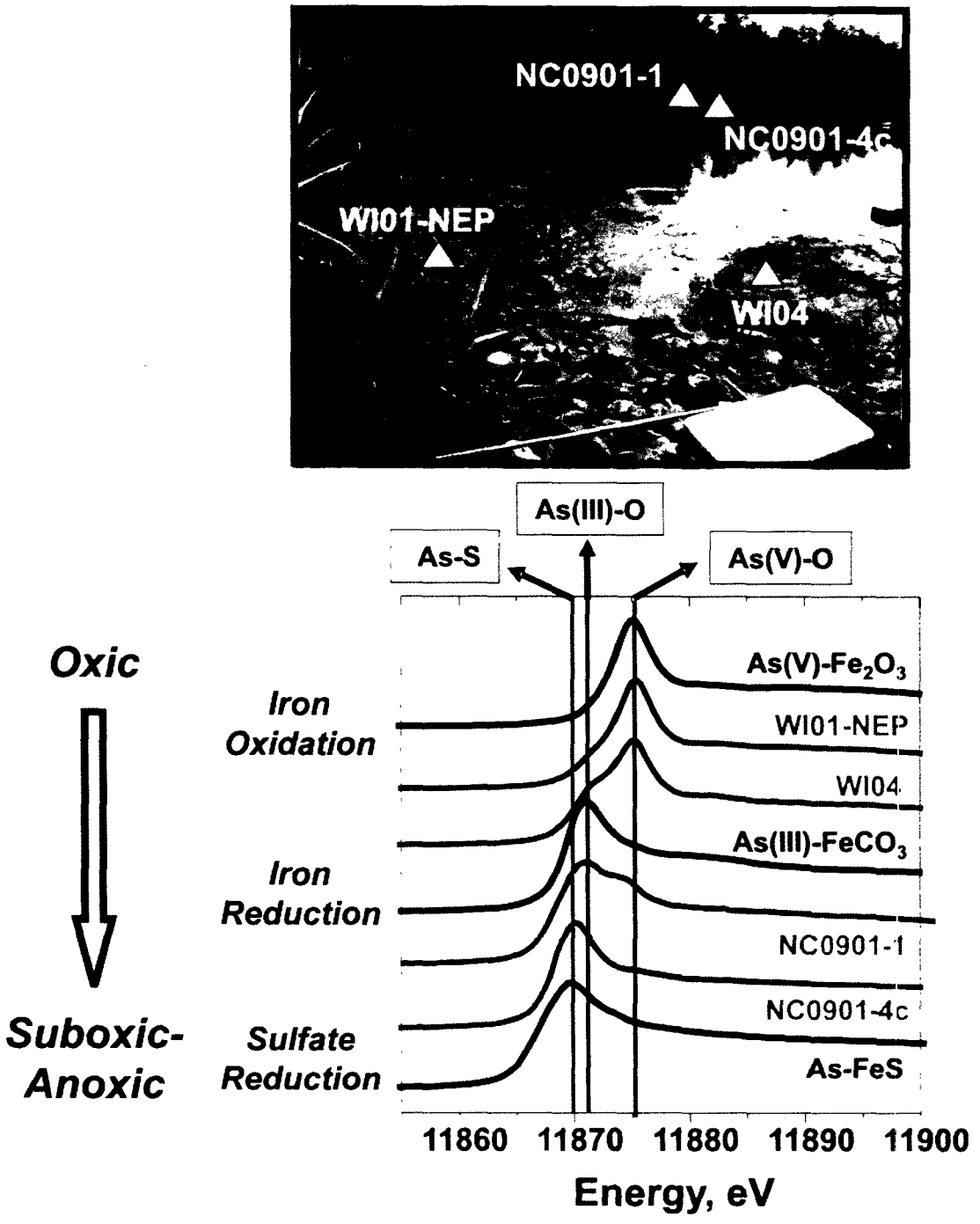


Figure 23 *Locations of a selection of sediments collected from oxic and suboxic zones within the HBHA Pond. XANES data are shown for sediments that span the observed redox gradient within the system relative to representative reference compounds.*

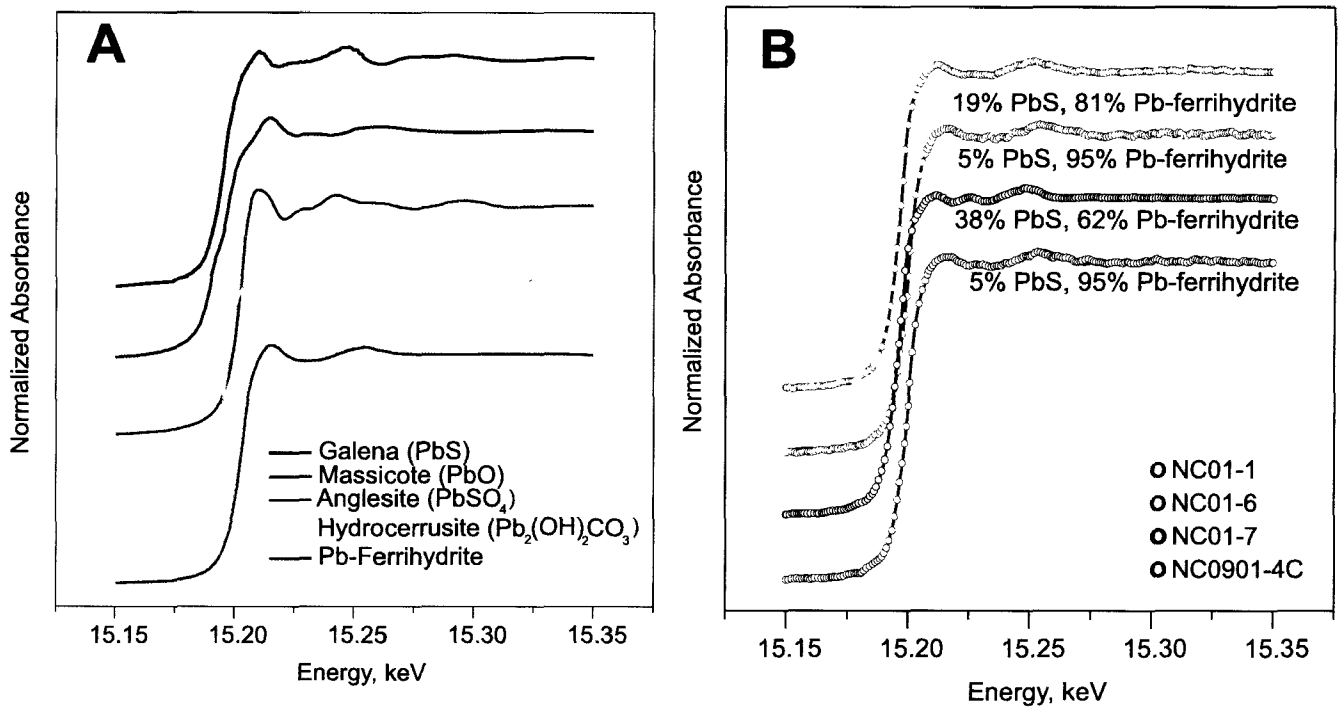


Figure 24 *XANES data for (A) a series of reference compounds and (B) a selection of sediments collected within the HBHA Pond. The relative percentage of Pb species is shown in Panel B based on the results of LCF-XANES data analysis.*

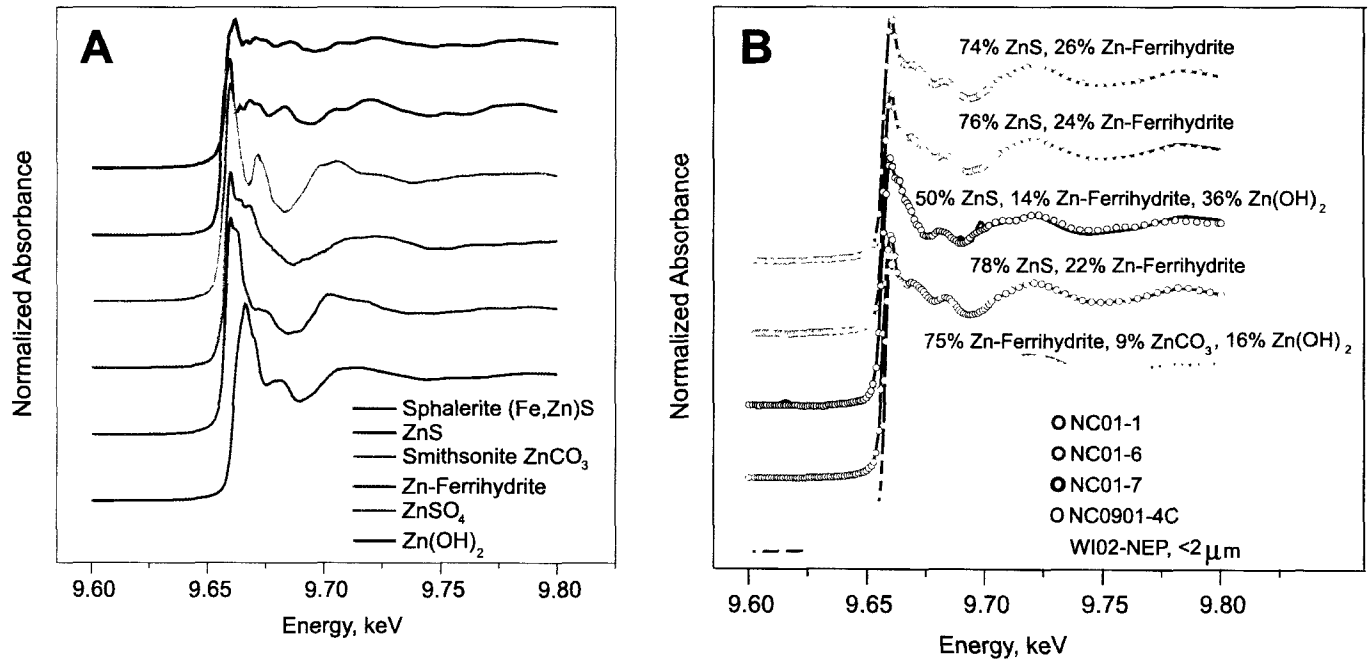


Figure 25 *XANES data for (A) a series of reference compounds and (B) a selection of sediments collected within the HBHA Pond. The relative percentage of Zn species is shown in Panel B based on the results of LCF-XANES data analysis.*

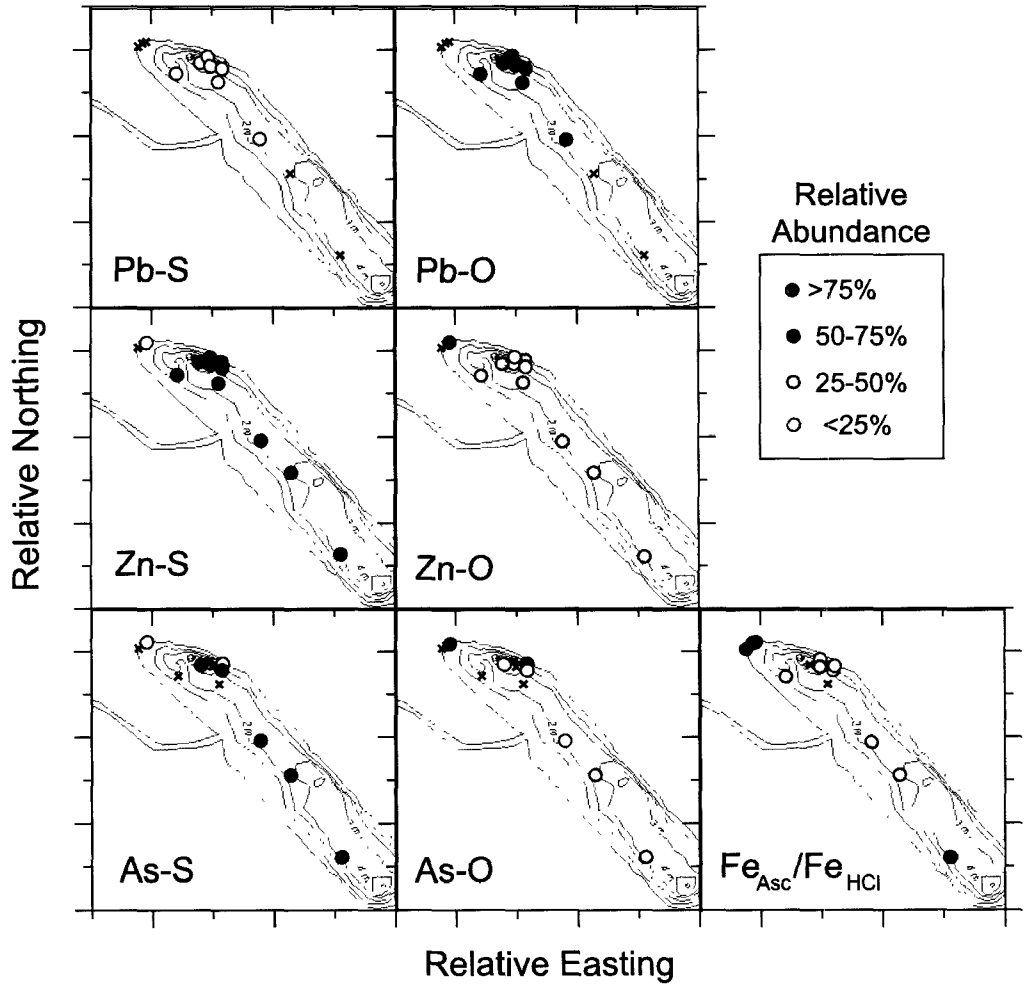


Figure 26 *Aerial distribution of contaminant sediment speciation within the HBHA Pond based on LCF-XANES analysis; contour lines delineate depth to sediment (meters). Fe_{Asc}/Fe_{HCl} is a measure of the relative fraction of iron (hydr)oxide minerals. An 'x' denotes a location for which data is not available.*

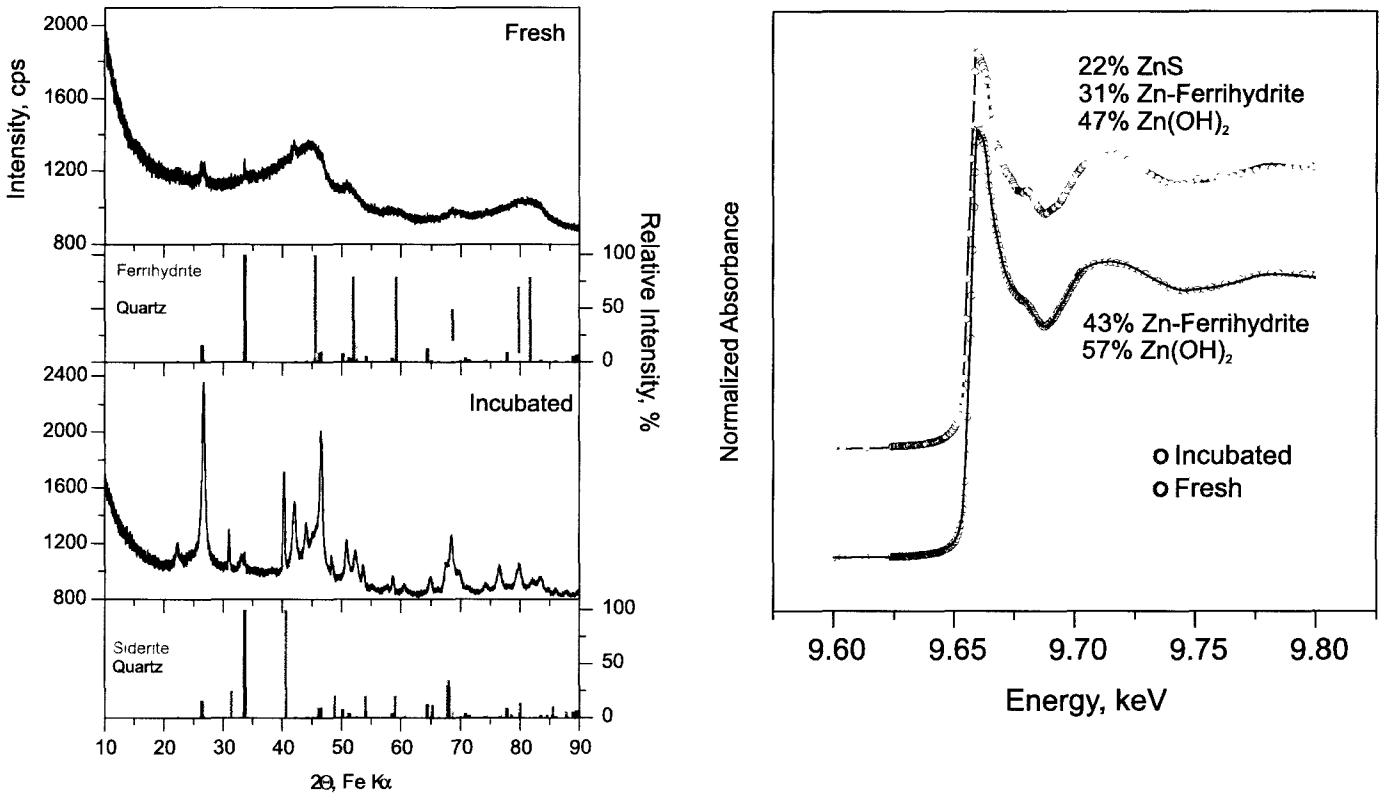


Figure 27 *Characterization of the mineralogy of the clay-sized sediment fraction and zinc speciation in the silt-sized fraction of surficial sediment sample WI02-NEP before and after incubation for a period of 2.5 years. (A) XRD data for the <2 μm fraction of the fresh and incubated sediment along with identification of the predominant mineral components. (B) Raw XANES data (lines) and LCF-XANES fit results (data symbols) for the 2-53 μm fraction of the same sediment samples*

Scanning Electron Microscopy

Scanning electron microscopy (SEM) with energy dispersive spectroscopy (EDS) was employed to derive information on mineral textures in HBHA Pond sediments along with elemental associations within sediment particles. The SEM-EDS results support the importance of iron-bearing minerals in HBHA Pond sediments (Table 3). The EDS spectra for a selection of analyses for these samples are shown in Figure 28. It should be noted that the Lα emission line was used for detection and semiquantitation of arsenic. In general, the concentration of arsenic in individual particles was below instrumental detection by EDS. This is consistent with the apparent continuous redistribution of arsenic between iron (hydr)oxides and iron sulfides. This process would tend to disperse arsenic more uniformly, in contrast to arsenic being present in detrital phases eroded from surrounding contaminated soils and deposited into sediments within the HBHA Pond. Back-scattered electron images shown in Figures 29 and 30 indicate that the iron minerals present in sediments are fine-grained. This is likely a result of the intensive redox cycling of iron that takes place across redox gradients established within the HBHA Pond system. Observation of a pyrite framboid in what is presumably an oxic (surficial) sediment sample also points to the extent of redox disequilibria within these sediments. The extent and variability of non-equilibrium conditions that exist within the HBHA Pond sediment system are unknown, but it is clear that site characterization efforts must be cognizant of this issue in order to circumvent potential analytical artifacts that could prevent accurate interpretation of contaminant speciation and potential mobility/bioavailability

Table 3 Atomic Percentages of Elements in 5 Samples Determined by SEM-EDS. Sample PS-3 is Composed of 2-line Ferrihydrite; Poorly Crystalline 6-line Ferrihydrite is the Dominant Iron (Hydr)oxide in Samples WI02-NEP and WI01-NEP. Atomic Percentages for Fe and O are Shown in Parentheses under the PS-3 Column for the Ferrihydrite Structure as Proposed by Towe and Bradley (1967)

Element (emission shell)	WI02-NEPA <2 μm "oxic sediment"	WI02-NEPA <2 μm "pyrite framboid"	WI02-NEPB 2 μm < d < 53 μm "oxic sediment"	PS-3 "water column sample"	PS-3 Compositional data from acid digestion	SC0401-3 "anoxic sediment"
S (K)	ND	49.63% ± 1.08%	ND	ND	2.54 wt%	7.98% ± 0.32%
Fe (K)	11.16% ± 0.52%	50.37% ± 1.08%	19.63% ± 0.80%	61.92% ± 0.64% (64.58%)	34.28 wt%	12.08% ± 0.48%
Si (K)	1.84% ± 0.20%	ND	7.78% ± 0.46%	3.26% ± 0.29%	0.87 wt%	1.48% ± 0.16%
O (K)	37.94% ± 1.31%	ND	25.75% ± 1.54%	30.25% ± 0.57% (33.33%)	--	20.44% ± 1.13%
Ca (K)	ND	ND	0.56 ± 0.17%	1.83% ± 0.13%	1.21 wt%	*0.44% ± 0.11%
K (K)	*0.36% ± 0.12%	ND	ND	ND	0.16 wt%	ND
Zn (K)	ND	ND	ND	ND	0.11 wt%	1.38% ± 0.36%
Al (K)	* 0.49% ± 0.17%	ND	0.92% ± 0.19%	0.89% ± 0.16%	0.21 wt%	1.52% ± 0.17%
As (L)	ND	ND	ND	0.85% ± 0.26%	0.44 wt%	ND
Cu (K)	ND	ND	ND	ND	--	ND
Na (K)	ND	ND	*0.47% ± 0.21%	ND	--	ND
magnification	2000x	4300x	3000x	10000x	--	2000x

Notes: *ND = Not Detected*
Below Limit of Quantitation (BLQ)

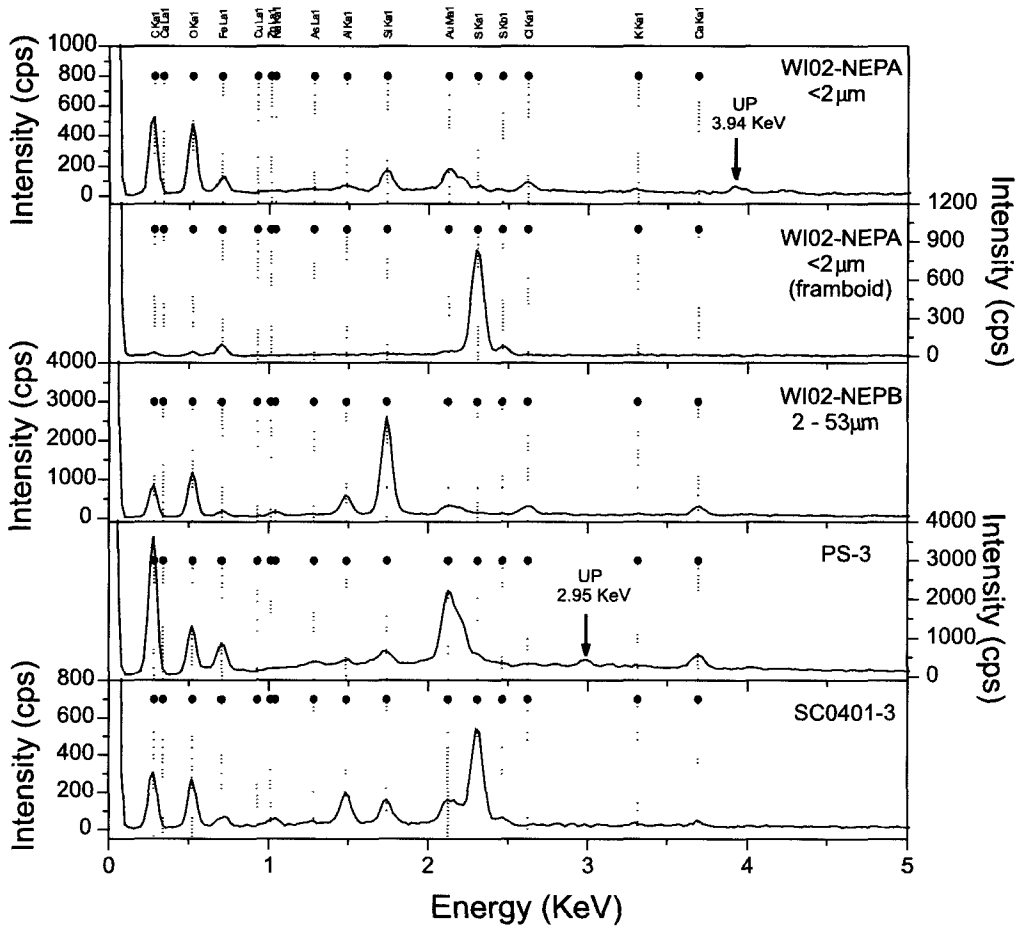


Figure 28 *Representative compositional spectra for samples imaged using SEM-EDS; UP = unidentified peak.*

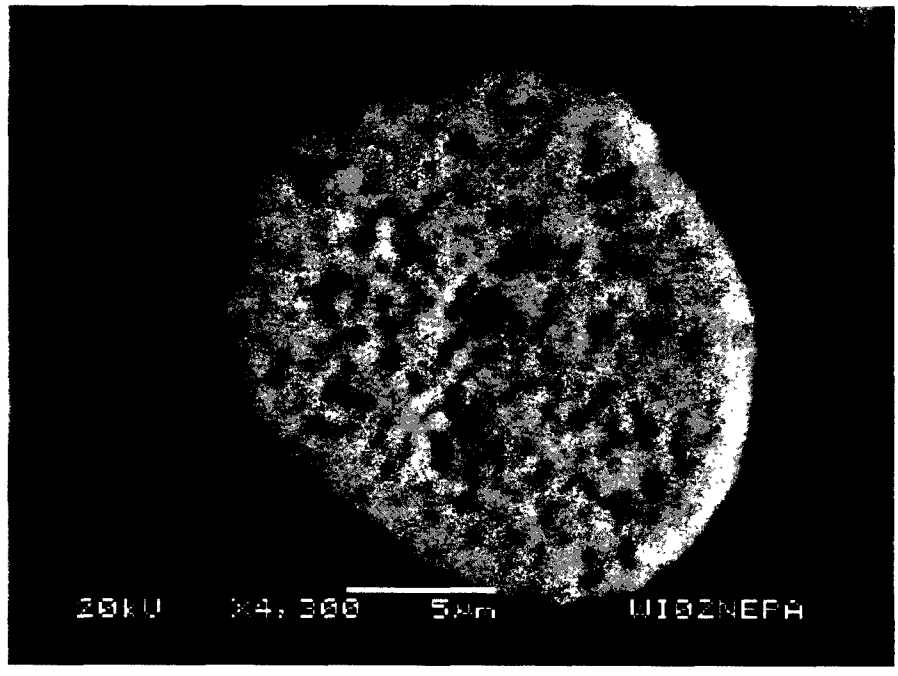


Figure 29 *Image of a pyrite framboid observed in a surficial (oxic) sediment (WI02-NEP, clay-sized fraction).*

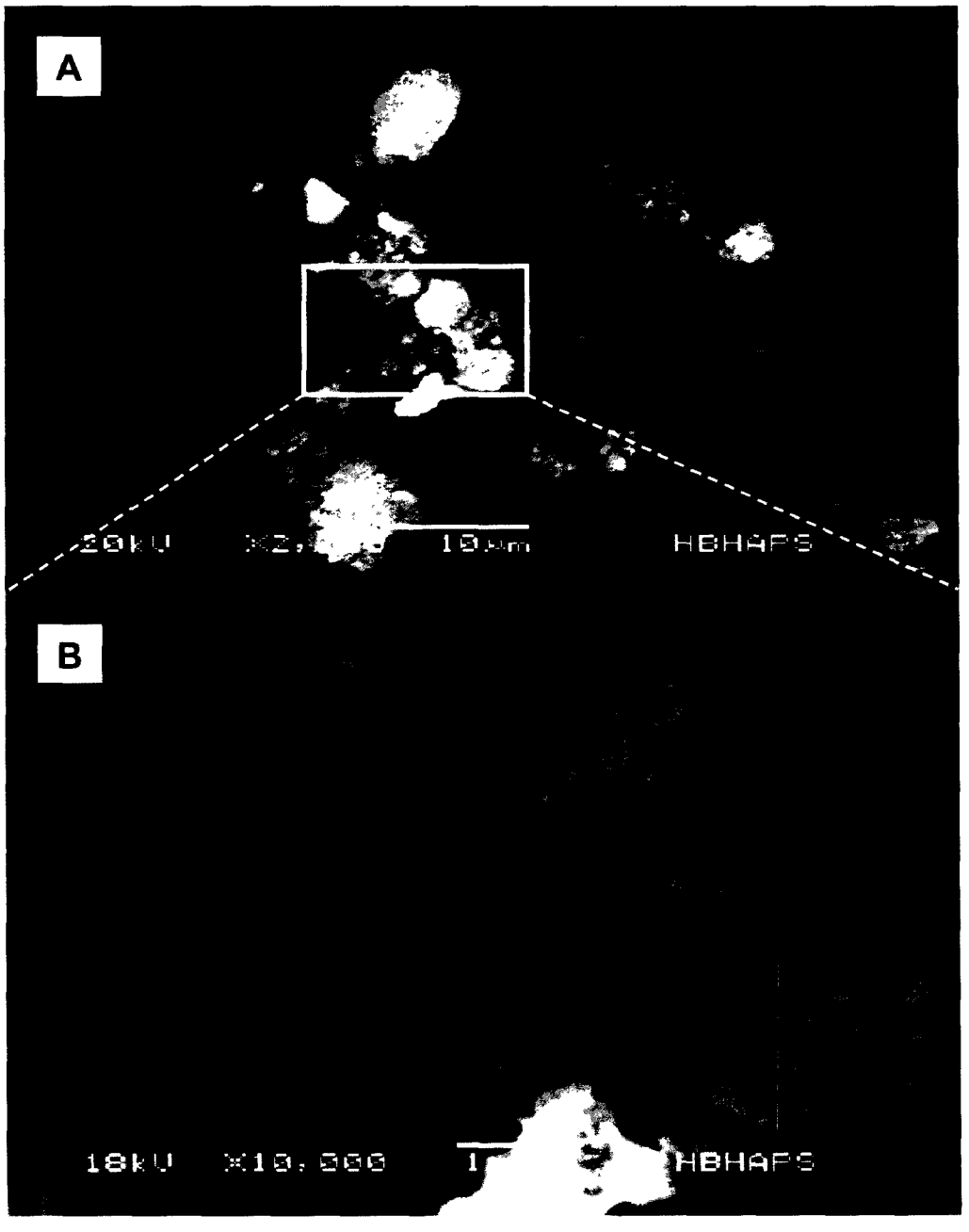


Figure 30 *Images of iron (hydr)oxide precipitates collected near the chemocline within the water column of the HBHA Pond (PS-3).*

Chapter 4

Stability of Contaminants in HBHA Pond Sediments

Assessment of ground-water data collected during this study and historic data collected within the study site indicate that the primary point of discharge for contaminated ground water is into the HBHA Pond. Long-term monitoring at the HBHA Pond surface water discharge indicates that dissolved arsenic is typically below a concentration of 100 ppb. This suggests that arsenic and metals discharged via site-derived ground water are partially sequestered within the HBHA Pond. The apparent geochemical processes controlling the solid-solution partitioning of arsenic, lead, and zinc are illustrated in Figure 31. In general, arsenic solid-solution partitioning is linked to precipitation-dissolution cycles that control the distribution of iron between dissolved and oxidic/sulfidic mineral phases. Arsenic remains in a relatively labile chemical state, although the physicochemical characteristics of the HBHA Pond result in significant sequestration within the pond boundary. The cycling of lead and zinc within the HBHA Pond water column is less clear due to the lack of clear chemical patterns in dissolved concentrations for these contaminants. However, the solid-solution partitioning of lead and zinc in sediments also appears to be linked to the production of iron (hydr)oxides and sulfides. These contaminants are also sequestered within the boundaries of the HBHA Pond, primarily in association with sediments. As noted previously (Figure 14 and 17), zinc derived from ground-water discharge is efficiently sequestered in sediments. The observed release of arsenic from shallow sediments confirms the partial instability of iron (hydr)oxides deposited on the bottom of the HBHA Pond (Ford, 2005). Dissolved concentrations of arsenic are a maximum within the hypolimion near the sediment-water interface where iron (hydr)oxide dissolution prevails with a limited capacity for production of iron sulfides (until sediment burial and more intense sulfate reduction). This observation is consistent with projections made by Hounslow (1980), where regions of iron reduction coupled with insufficient sulfate reduction are anticipated to result in the most labile/mobile forms of arsenic. The circumneutral pH near the sediment-water interface also contributes to selective sequestration of zinc versus arsenic in sulfate-reducing zones due to the higher solubility of iron and arsenic sulfides (Wilkin and Ford, 2002). Ultimately, although the HBHA Pond retains a significant fraction of arsenic and metals derived from ground-water discharge, it could still supply a continual flux of arsenic and metals to downgradient wetlands and the Aberjona River via discharge of dissolved contaminant species or suspended solids.

The critical factors maintaining arsenic, lead, and zinc at depth within the HBHA Pond hypolimnion are 1) the presence of a fairly stable chemocline and 2) the high capacity for metal sorption to iron (hydr)oxides and/or iron sulfides formed at the oxic-anoxic transition zone (Taillefert et al., 2000; Ford, 2002; Taillefert and Gaillard, 2002). The capacity for arsenic and metal sequestration from the HBHA Pond water column is dependent on a continual supply of ferrous iron into the system, while the continual production of iron sulfides is dependent on maintenance of sulfate reduction processes within the hypolimnion. The arsenic (and potentially lead and zinc) sequestration capacity will decline concurrent with a decline in ferrous iron from the upgradient aquifer. Since performance of the HBHA Pond for arsenic removal is also dependent on continued stratification of the water column, assessment of the long-term sedimentation capacity is also an important factor. Water column monitoring data from this study suggest that the chemocline is typically located approximately 100-200 cm above the sediment-water interface depending on the season. While there are no data to assess sediment accumulation rates for the HBHA Pond, it is not anticipated that sediment in-filling would cause disruption of the chemocline. Regardless, projections of potential sediment erosion or turnover within the HBHA Pond will depend on knowledge of modifications to the pond geometry over time. Buried sediments within the HBHA Pond have accumulated significant concentrations of metals such as lead and zinc. Mineralogical characterization and contaminant speciation indicate that both iron (hydr)oxides and iron sulfides play a significant role in this process within the hypolimnion and buried sediments. The relative distribution of these two mineral classes will depend on the extent of sulfate-reduction and the rates of dissolution of the iron (hydr)oxides deposited onto buried sediments (Wersin et al., 1991; Poulton et al., 2004). The stability of these sediments will depend on the maintenance of iron- and sulfate-reducing conditions at depth within the HBHA Pond. Current and historical ground-water data suggest that these processes will continue into the future, but consideration should be given to the impact of water column turnover and the potential long-term depletion of the reducing capacity within the aquifer as the BTEX plume diminishes over time (e.g., Saulnier and Mucci, 2000).

Since the location and mass of arsenic (and iron) within contaminated soils upgradient from the HBHA Pond are poorly defined, it is difficult to assess the long-term capacity of the HBHA Pond. Given this level of uncertainty, it is recommended that a long-term monitoring strategy be implemented that continuously tracks arsenic and redox chemistry within the aquifer and the HBHA Pond. This appears to be less of a concern for lead and zinc, since elevated concentrations of these metals were rarely observed within the HBHA Pond water column. A proposed strategy is outlined below. Recommendations for site monitoring and potential remediation apply only to discharge of contaminated ground water into the HBHA Pond and are not intended to address potential contaminant migration in surface water and ground water downgradient from the HBHA Pond.

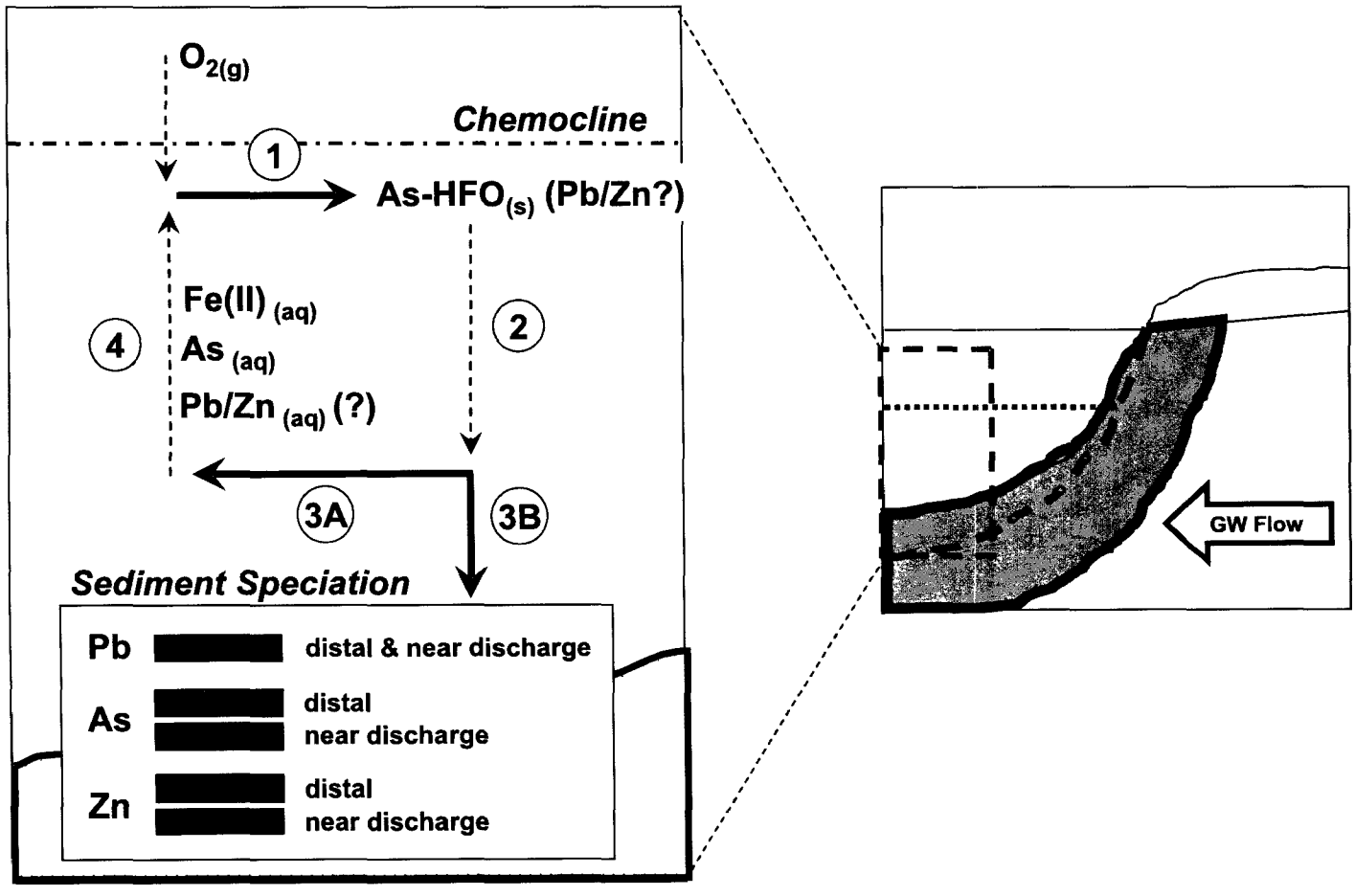


Figure 31 *Illustration of the apparent geochemical processes controlling solid-solution partitioning of arsenic, lead, and zinc within the HBHA Pond: 1) Fe(II) oxidation near chemocline upon encountering dissolved oxygen and coprecipitation of As with iron (hydr)oxides, 2) settling of precipitated iron (hydr)oxides, 3A) reductive dissolution of a fraction of settling iron (hydr)oxides generating dissolved Fe(II) and arsenic, 3B) deposition and diagenisis of a fraction of precipitated iron (hydr)oxides – partial conversion to iron sulfides, and 4) vertical transport of dissolved Fe(II) and As up to the chemocline. The speciation of arsenic, lead, and zinc in sediments located near and distal to the primary zone of contaminated ground-water discharge is shown (red = oxide association; black = sulfide association).*

Monitoring Long-Term Behavior (or Performance) of HBHA Pond

It is evident that the HBHA Pond currently serves to remove a fraction of the metal burden from ground water originating from the Industri-Plex Superfund Site. However, the ability of the HBHA Pond to function in this capacity over the long term will be controlled by 1) continued maintenance of the chemical stratification within the water column and 2) continued supply of iron and sulfate from site ground water for the production of iron (hydr)oxides and sulfides.

As shown via the HBHA Pond water column sampling during April 2001, high surface water flow events can perturb the chemical stratification (Ford, 2005). While the chemocline was re-established within the HBHA Pond, there are insufficient monitoring data to track the impact of these transient flow events on the long-term performance of the HBHA Pond for metal sequestration. Forecasting the impact of surface flow events is critical due to site development, which can modify patterns in surface runoff into the HBHA Pond. It is recommended that a long-term monitoring program incorporate input and output flow measurements for the HBHA Pond in order to establish whether the major flow event occurring at the end of March 2001 was anomalous or is likely to occur on a more frequent basis. Note that continued discharge from Halls Brook should be maintained, since this continuous source of fresh water helps maintain chemical stratification within the HBHA Pond. As demonstrated by depth-resolved measurements, the highest concentration of dissolved As occurs at the bottom of the HBHA Pond and is relatively invariant throughout the year. This mass of dissolved As will be distributed throughout the water column during turnover, leading to increased mass flux of As at the shallow outlet. This is a critical factor, since the HBHA Pond is a potential long-term source of arsenic transport to the Aberjona River. Based on the observed perturbation to the performance of the HBHA Pond during the March 2001 surface flow event, it is recommended that control structures be installed to better regulate surface water inputs into the HBHA Pond. Structures to divert excess flows during precipitation/snow melt events of similar magnitude to that observed during March - April 2001 will facilitate maintenance of the chemocline within the HBHA Pond, which appears critical to the precipitation and settling characteristics of the iron cycle within the water column.

It is recommended that a more comprehensive site monitoring strategy be implemented in the near-term to better track performance of the HBHA Pond system and detect possible failure. The current focus of monitoring efforts outside of this study has entailed extensive evaluation of surface water inputs and discharge out of the HBHA Pond. In order to properly assess performance of the HBHA Pond to sequester arsenic and metal contaminants, it is recommended that a permanent ground-water monitoring network be established within the aquifer upgradient and downgradient from the HBHA Pond. The network should be sufficient to document the extent of the arsenic contaminant plume and its elimination down gradient to the HBHA Pond. Contaminants of concern and the general redox chemistry of ground water should be monitored concurrent with surface water sampling events. In general, quarterly sampling will provide sufficient frequency to monitor the dynamics of the ground-water plume and the HBHA system, but it is recommended that additional efforts be made to assess system response to storm events. Assessment of seasonal patterns in contaminant mobility and sequestration within the HBHA Pond is required to establish the long-term viability of the metal sequestration reactions active within the HBHA Pond to mitigate mobilization of arsenic and metals.

There is evidence that the chemical stratification within the HBHA Pond can be interrupted during large flow events. Ford (2005) has documented the loss of chemical stratification in the central and southern portions of the HBHA Pond following a large flow event during March 2001. The flow-induced mixing resulted in distribution of the entire budget of hypolimnetic arsenic throughout the water column in these portions of the pond and ultimately resulted in a temporary increase in arsenic export from the HBHA Pond. Evaluation of contemporary and historical water flow records at a hydrologic monitoring station approximately 2.5 miles south of the HBHA Pond (USGS 01102005) indicates that an event of this magnitude could potentially occur on a 3-4 year cycle. These results suggest that efforts to control high-flow events into the HBHA Pond will be important to limiting down gradient transport of arsenic and metals derived from discharge of contaminated ground water. However, the ultimate performance of the HBHA Pond system will be limited by net sedimentation, which will slowly consume the storage capacity for contaminated water and sediments within the deeper portions of the pond.

Relevance to Other Sites

The observations of the dynamics of iron mineralogical cycling and the chemical speciation of arsenic, lead, and zinc from this study site may be relevant to other sites. The differential influence of iron- and sulfate-reduction processes on the solid-solution partitioning of inorganic contaminants observed in this study is important relative to the design of the characterization plan for other sites with complex metal and metalloid contaminant mixtures. The overall stability of sediment-associated contaminants as well as the technologies that may be employed for their remediation will depend on the types of mineral associations controlling contaminant solid-phase speciation. The results of the work described in this document indicate that, of the three inorganic contaminants that were studied, arsenic posed the greatest concern due to its higher potential mobility. This may apply to other sites where inorganic contaminants are a primary concern. The extent to which this could be defined for the HBHA Pond was dependent on development of a comprehensive knowledge of the influence of iron- and sulfate-reduction on the solid-phase partitioning of arsenic within the system

boundaries. This study demonstrated a general correspondence between observed patterns in the aqueous distribution of arsenic, lead, and zinc relative to the predominant solid-phase speciation patterns for these contaminants based on chemical extractions and spectroscopic analyses. In general, this work supports the applicability of using chemical extractions to help define contaminant speciation. However, results for the specific contaminants indicate that care should be taken during the design of an extraction protocol relative to observed site conditions. Ultimately, the reliability and utility of extraction protocols to define inorganic contaminant speciation will be predicated on concurrently developed knowledge of the mineralogical composition of the tested solids.

References

Aggett, J., and M.R. Kriegman. The extent of formation of arsenic(III) in sediment interstitial waters and its release to hypolimnetic waters in Lake Ohakuri *Water Resources* 22: 407-411 (1998).

Aggett, J., and G.A. O'Brien. Detailed model for the mobility of arsenic in lacustrine sediments based on measurements in Lake Ohakuri. *Environmental Science and Technology* 19: 321-238 (1985).

Ahmann, D., L.R. Krumholz, H.F. Hemond, D.R. Lovely, and F.M.M. Morel. Microbial mobilization of arsenic from sediments of the Aberjona watershed. *Environmental Science and Technology* 31: 2923-2930 (1997).

Atkin, B.P. and C. Somerfield. The determination of total sulfur in geological materials by coulometric titration. *Chemical Geology* 111: 131-134 (1994).

Aurilio, A.C., R.P. Mason, and H.F. Hemond. Speciation and fate of arsenic in three lakes of the Aberjona watershed. *Environmental Science and Technology* 28: 577-585 (1994).

Aurilio, A.C., J.L. Durant, H.F. Hemond, and M.L. Knox. Sources and distribution of arsenic in the Aberjona watershed, eastern Massachusetts. *Water Air Soil Pollution* 78: 1-18 (1995).

Balistrieri, L.S., J.W. Murray, and B. Paul. The geochemical cycling of trace elements in a biogenic meromictic lake. *Geochimica et Cosmochimica Acta* 58: 3993-4008 (1994).

Bartlett, R.J. and R.R. James, *Chromium in the Natural and Human Environment,* New York: John Wiley & Sons, 1988.

Beauchemin, S., D. Hesterberg, and M. Beauchemin. Principal component analysis approach for modeling sulfur K-XANES spectra of humic acids. *American Journal of Soil Science Society* 66: 83-91 (2002).

Biksey, T.M., and E.D. Gross. The hyporheic zone: linking groundwater and surface water – understanding the paradigm. *Remediation* 12: 55-62 (2001).

Davis, A., J.H. Kempton, A. Nicholson, and B.Yare. Groundwater transport of arsenic and chromium at a historical tannery, Woburn, Massachusetts, U.S.A. *Applied Geochemistry* 9: 569-582 (1994).

Davis, A., C. Sellstone, S. Clough, R. Barrick, and B. Yare. Bioaccumulation of arsenic, chromium and lead in fish: constraints imposed by sediment geochemistry. *Applied Geochemistry* 11: 409-423 (1996).

Davison, W. and G. Seed. The kinetics of the oxidation of ferrous iron in synthetic and natural waters. *Geochimica et Cosmochimica Acta* 47: 67-79 (1983).

Davison, W., C. Woof, and E. Rigg. The dynamics of iron and manganese in a seasonally anoxic lake; direct measurement of fluxes using sediment traps. *Limnol. Oceanography* 27: 987-1003 (1982).

Dos Santos Afonso, M., P.J. Morando, M.A. Blesa, S. Banwart, and W. Stumm. The reductive dissolution of iron oxides by ascorbate: The role of carboxylate anions in accelerating reductive dissolution. *Journal of Colloid and Interface Science* 138: 74-82 (1990).

Durant, J.L., J.J. Zemach, and H.F. Hemond. The history of leather industry waste contamination in the Aberjona watershed: A mass balance approach. *Civil Engineering Practice* 5: 41-66 (1990).

Ferdelman, T.G. "The distribution of sulfur, iron, manganese, copper, and uranium in a salt marsh sediment core as determined by sequential extraction methods." Masters Thesis, University of Delaware, 1988.

Ford, R.G. Rates of hydrous ferric oxide crystallization and the influence on coprecipitated arsenate. *Environmental Science and Technology* 36: 2459-2463 (2002).

Ford, R.G. *The impact of ground water-surface water interactions on contaminant transport with application to an arsenic contaminated site,* EPA/600/S-05/002. Cincinnati, OH: U.S. Environmental Protection Agency, 2005.

Ford, R.G., K.M. Kemner, and P.M. Bertsch. Influence of sorbate-sorbent interactions on the crystallization kinetics of nickel- and lead-ferrihydrite coprecipitates. *Geochimica et Cosmochimica Acta* 63: 39-48 (1999).

Ford, R.G., R.T. Wilkin, and G. Hernandez. Arsenic cycling within the water column of a small lake receiving contaminated ground-water discharge. *Chemical Geology* (accepted) (2005).

Gomez-Ariza, J.L.,D. Sanchez-Rodas, I. Giraldez, and E. Morales. A comparison between ICP-MS and AFS detection for arsenic speciation in environmental samples. *Talanta* 51: 257-268 (2000).

Hach. "Iron, ferrous." In *Water Analysis Handbook*, Loveland, CO: Hach Co., 1992a, 343-346.

Hach. "Iron, total." In *Water Analysis Handbook*, Loveland, CO: Hach Co., 1992b, 353-357.

Hounslow, A.W. Ground-water geochemistry: arsenic in landfills. *Ground Water* 18: 331-333 (1980).

Huffman, E.W.D. Performance of a new carbon dioxide coulometer. *Microchemical Journal* 22: 567-573 (1977).

Jackson, B.P., and W.P. Miller. Effectiveness of phosphate and hydroxide for desorption of arsenic and selenium species from iron oxides. *Soil Science Society of America Journal* 64: 1616-1622 (2000).

JCPDS. *Mineral Powder Diffraction File Databook; Sets 1-42,* International Centre for Diffraction Data: Swarthmore, PA, 1993.

Kneebone, P.E., P.A. O'Day, N. Jones, and J.G. Hering. Deposition and fate of arsenic in iron- and arsenic-enriched reservoir sediments. *Environmental Science and Technology* 36: 381-386 (2002).

Kostka, J.E., and G.W. Luther III. Partitioning and speciation of solid phase iron in saltmarsh sediments. *Geochimica et Cosmochima Acta* 56: 1701-1710 (1994).

Larsen, O., and D. Postma. Kinetics of reductive bulk dissolution of lepidocrocite, ferrihydrite, and goethite. *Geochimica et Cosmochimica Acta* 65: 1367-1379 (2001).

Martin, A.J., and T.F. Pederson. Seasonal and interannual mobility of arsenic in a lake impacted by metal mining. *Environmental Science and Technology* 36: 1516-1523 (2002).

McBride, M.B. *Environmental Chemistry of Soils*, New York: Oxford University Press, 1994.

McCleskey, R.B., D.K. Nordstrom, and A.S. Maest. Preservation of water samples for arsenic(III/V) determinations: an evaluation of the literature and new analytical results. *Applied Geochemistry* 19: 995-1009 (2004).

Peltier, E., A.L. Dahl, and J.-F. Gaillard. Metal speciation in anoxic sediments: When sulfides can be construed as oxides. *Environmental Science and Technology* 39: 311-316 (2005).

Perret, D., J.-F. Gaillard, J. Dominik, and O. Atteia. The diversity of natural hydrous iron oxides. *Environmental Science and Technology* 34: 3540-3546 (2000).

Poulton, S.W., M.D. Krom, and R. Raiswell. A revised scheme for the reactivity of iron (oxyhydr)oxide minerals towards dissolved sulfide. *Geochimica et Cosmochimica Acta* 68: 3703-3715 (2004).

Puls, R.W., and C.J. Paul. Low-flow purging and sampling of ground-water monitoring wells with dedicated systems. *Ground Water Monitoring and Remediation* 15: 116-123 (1995).

Rehr, J.J., and A.L. Ankudinov. Progress and challenges in the theory and interpretation of X-ray spectra. *Journal of Synchrotron Radiation* 8: 61-65 (2001).

Rehr, J.J., and A.L. Ankudinov. New developments in the theory and interpretation of X-ray spectra based on fast parallel calculations. *Journal of Synchrotron Radiation* 10: 43-45 (2003).

Ressler, T. WinXAS: A program for X-ray absorption spectroscopy data analysis under MS-Windows. *Journal of Synchrotron Radiation* 5: 118-122 (1998).

Roberts, D.R., A.C. Scheinost, and D.L. Sparks. Zinc speciation in a smelter-contaminated soil profile using bulk and microspectroscopic techniques. *Environmental Science and Technology* 36: 1742-1750 (2002).

Saulnier, I., and A. Mucci. Trace metal remobilization following the resuspension of estuarine sediments: Saguenay Fjord, Canada. *Applied Geochemistry* 15: 191-210 (2000).

Scheckel, K.G., and J.A. Ryan. Spectroscopic speciation and quantification of Pb in phosphate amended soils. *Journal of Environmental Quality* 33: 1288-1295 (2004).

Scheinost, A.C., R. Kretzschmar, and S. Pfister. Combining selective sequential extractions, X-ray absorption spectroscopy, and principal component analysis for quantitative zinc speciation in soil. *Environmental Science and Technology* 36: 5021-5028 (2002).

Schwertmann, U., and W.R. Fischer. Natural "amorphous" ferric hydroxide. *Geoderma* 10: 237-247 (1973).

Schwertmann, U., and E. Murad. The nature of an iron oxide-organic iron association in a peaty environment. *Clay Minerals* 23: 291-299 (1988).

Senn, D.A., and H.F. Hemond. Nitrate controls on iron and arsenic in an urban lake. *Science* 296: 2373-2376 (2002).

Seyler, P., and J.-M. Martin. Biogeochemical processes affecting arsenic species distribution in a permanently stratified lake. *Environmental Science and Technology* 23: 1258-1263 (1989).

Sholkovitz, E.R., and D. Copland. The chemistry of suspended matter in Esthwaite Water, a biologically productive lake with seasonally anoxic hypolimnion. *Geochimica et Cosmochimica Acta* 46: 393-410 (1982).

Sohrin, Y., M. Matsui, M. Kawashima, M. Hojo, and H. Hasegawa. Arsenic biogeochemistry affected by eutrophication in Lake Biwa, Japan. *Environmental Science and Technology* 31: 2712-2720 (1997).

Spliethoff, H.M., R.P. Mason, and H.F. Hemond. Interannual variability in the speciation and mobility of arsenic in a dimictic lake. *Environmental Science and Technology* 29: 2157-2161 (1995).

Standard Methods for the Examination of Water and Wastewater. Section 4140 B Capillary Ion Electrophoresis with Indirect UV Detection, 20th Edition, pp. 1-4 to 1-13 (1999).

Stanjek, H., and P.G. Weidler. The effect of dry heating on the chemistry, surface area, and oxalate solubility of synthetic 2-line and 6-line ferrihydrites. *Clay Miner* 27: 397-412 (1992).

Stumm, W. *Chemistry of the Solid-Water Interface*, New York: John Wiley & Sons, Inc., 1992.

Taillefert, M., C.-P. Lienemann, J.-F. Gaillard, and D. Perret. Speciation, reactivity, and cycling of Fe and Pb in a meromictic lake. *Geochimica et Cosmochimica Acta* 64: 169-183 (2000).

Taillefert, M., and J.-F. Gaillard. Reactive transport modeling of trace elements in the water column of a stratified lake: iron cycling and metal scavenging. *Journal of Hydrology* 256: 16-34 (2002).

Tessier, A., P.G.C. Campbell, and M. Bison. Sequential extraction procedure for the speciation of particulate trace metals. *Analytical Chemistry* 51: 844-851 (1979).

Tomassoni, G. "A federal statutory/regulatory/policy perspective on remedial decision-making with respect to groundwater/surface-water interaction." In *Proceedings of the Ground-Water/Surface-Water Interactions Workshop*, Denver, CO, 1999.

Towe, K.M., and W.F. Bradley. Mineralogical constitution of colloidal "hydrous ferric oxides." *Journal of Colloid and Interface Science* 24: 384-392 (1967).

U.S. Environmental Protection Agency. *Methods for chemical analysis of water and wastes.* EPA/600/4-79/020. Washington, DC, 1983.

Welch, A.H., and M.S. Lico. Factors controlling As and U in shallow ground water, southern Carson Desert, Nevada. *Applied Geochemistry* 13: 521-539 (1998).

Wersin, P., P. Hohener, R. Giovanoli, and W. Stumm. Early diagenetic influences on iron transformations in a fresh-water lake sediment. *Chemical Geology* 90: 233-252 (1991).

Wick, L.Y., and P.M. Gschwend. Source and chemodynamic behavior of diphenyl sulfone and ortho- and para-hydroxybiphenyl in a small lake receiving discharges from an adjacent superfund site. *Environmental Science and Technology* 32: 1319-1328 (1998a).

Wick, L.Y., and P.M. Gschwend. By-products of a former phenol manufacturing site in a small lake adjacent to a Superfund site in the Aberjona watershed. *Environmental Health Perspectives* 106: 1069-1074 (1998b).

Wick, L.Y., K. McNeill, M. Rojo, E. Medilanski, and P.M. Gschwend. Fate of benzene in a stratified lake receiving contaminated groundwater discharges from a superfund site. *Environmental Science and Technology* 34: 4354-4362 (2000).

Wilkin, R.T., and R.G. Ford. Use of hydrochloric acid for determining solid-phase arsenic partitioning in sulfidic sediments. *Environmental Science and Technology* 36: 4921-4927 (2002).

Winter, T.C., J.W. Harvey, O.L. Franke, and W.M. Alley. Ground water and surface water: a single resource. *U.S. Geological Survey Circular* 1139: 77 pp (1998).

Appendix A
Analytical Performance for Laboratory Methods

Table A.1. Analytical Methods, Detection Limits, Precision, and Accuracy for Measurement of Aqueous Chemistry

Parameter	Method	Detection Limit	Precision	Accuracy
Benzene, Toluene	Purge-and-Trap Gas Chromatography	0.29 µg/L, benzene 0.22 µg/L, toluene	±15% based on duplicate analyses of unknowns	±20% based on spike recovery for unknowns
TOC, DOC	Wet Oxidation/Infrared Detection EPA Method 415.2	0.02 mg C/L	±10% based on duplicate analyses of unknowns	±20% based on spike recovery for unknowns
Fe^{2+}	Colorimetric, 1,10-phenanthroline	0.01 mg/L	±10% based on duplicate analyses of unknowns	±20% based on spike recovery for unknowns
Arsenic, Iron, Sodium, Lead, Sulfur, Zinc	ICP-OES	0.033 mg/L, As 0.035 mg/L, Fe 0.479 mg/L, Na 0.015 mg/L, Pb 0.137 mg/L, S 0.014 mg/L, Zn	±10% based on duplicate analyses of unknowns	±20% based on spike recovery for unknowns
NO_3-N	EPA Method 353.2	0.004 mg N/L	±10% based on duplicate analyses of unknowns	±20% based on spike recovery for unknowns
NH_3-N	EPA Method 350.1	0.03 mg N/L	±10% based on duplicate analyses of unknowns	±20% based on spike recovery for unknowns
SO_4	Capillary electrophoresis	0.1 mg/L	±10% based on duplicate analyses of unknowns	±20% based on spike recovery for unknowns

n.d. not determined

Table A.2. Analytical Methods, Detection Limits, Precision, and Accuracy for Measurement of Solid Phase Chemistry

Parameter	Method	Detection Limit	Precision	Accuracy
Total Carbon	Coulometry/ combustion	0.01 wt% C for a 100-mg sample	±3.2% based on 32 analyses of $CaCO_3$	±2.8% using $CaCO_3$ (12.0 wt% C)
Total Sulfur	Coulometry/ combustion	0.005 wt% S for a 100-mg sample	±5.1% based on 35 analyses of NIST 1646a	±2.5% using NIST 1646a (0.35 wt% S)
Arsenic, Chromium, Iron, Lead, Zinc	ICP-OES/microwave assisted digestion/ chemical extraction	1 to 10 ppm for 100-mg sample (depending on element) and 20 mL extraction volume	±5 to 15% based on duplicate or triplicate analyses of unknowns	Variable, depending on element and reference material As (±3 to 12%)

n.d. not determined; standard reference materials used: NIST 1646a Estuary sediment, NIST 2710 Montana soil, NIST 2780 Hard rock mine waste, CCRMP Lake sediment-1

Appendix B
Sediment Composition Data

Table B.1. Concentrations of Selected Elements in Halls Brook Holding Area Pond Core NC01

Core Sample	Depth cm	Fe wt%	S wt%	TOC wt%	As µg/gm	Pb µg/gm	Cr µg/gm	Zn µg/gm
NC01-1	1.4	9.91	2.20	15.24	836	593	839	5920
NC01-2	2.8	9.65	1.80	15.58	857	610	970	5560
NC01-3	4.2	9.54	2.20	14.27	828	613	1060	5710
NC01-4	5.6	9.38	2.11	14.61	839	628	815	5130
NC01-5	7.0	9.38	2.10	13.32	834	607	856	5290
NC01-6	8.4	10.20	1.77	14.52	952	668	940	6060
NC01-7	10.0	10.10	0.05	5.95	639	606	691	3990
NC01-8	18.3	2.21	0.04	0.27	150	507	501	2850
NC01-9	26.6	1.51	0.04	0.17	101	106	87.4	609
NC01-10	34.9	0.37	0.03	0.03	10	34	13.8	71

Notes: Core collected 4/03/2000. Fe, As, Pb, Cr, and Zn determined by ICP-OES after microwave-assisted extraction in 10% nitric acid. TOC=total carbon minus inorganic carbon, determined using an UIC, Inc. carbon coulometer. S determined by coulometery (UIC, Inc.).

Table B.2. Concentrations of Selected Elements in Halls Brook Holding Area Pond Core CC02

Core Sample	Depth cm	Fe wt%	S wt%	TOC wt%	As µg/ gm	Pb µg/ gm	Cr µg/gm	Zn µg/gm
CC02-1	2.1	9.89	1.36	15.37	1120	429	593	3500
CC02-2	4.1	11.01	1.38	17.06	1101	425	573	3499
CC02-3	6.3	11.40	1.34	14.58	1020	514	830	4170
CC02-4	8.4	11.80	1.43	14.64	1050	528	901	4380
CC02-5	10.5	12.36	1.73	14.26	914	521	826	4420
CC02-6	12.6	14.55	1.31	13.09	945	633	830	4884
CC02-7	14.7	10.10	1.41	11.71	639	606	691	3990
CC02-8	16.8	7.21	1.00	9.81	455	507	501	2850
CC02-9	21.1	1.51	0.20	1.91	101	106	87.4	609
CC02-10	25.4	0.37	0.04	0.33	10.3	34.0	13.8	71
CC02-11	31.9	0.74	0.23	0.33	18.5	49.5	31.5	373
CC02-12	38.4	0.61	0.05	0.29	6.49	9.8	15.5	121
CC02-13	45.9	0.62	0.05	0.12	2.00	4.7	8.9	45
CC02-14	53.4	0.75	0.04	0.05	6.22	3.0	7.4	24

Notes: *Core collected 4/03/2000. Fe, As, Pb, Cr, and Zn determined by ICP-OES after microwave-assisted extraction in 10% nitric acid. TOC=total carbon minus inorganic carbon, determined using an UIC, Inc. carbon coulometer. S determined by coulometery (UIC, Inc.).*

Table B.3. Concentrations of Selected Elements in Halls Brook Holding Area Pond Core SC02

Core Sample	Depth cm	Fe wt%	S wt%	TOC wt%	As µg/gm	Pb µg/gm	Cr µg/gm	Zn µg/gm
SC02-1	3.0	10.20	2.54	10.33	1570	403	529	2780
SC02-2	6.0	11.94	2.25	11.32	1439	455	594	3612
SC02-3	9.0	10.30	2.18	9.51	1510	412	557	3060
SC02-4	12.0	3.40	1.37	5.04	232	315	328	1790
SC02-5	15.0	2.72	0.57	6.46	200	452	462	1860
SC02-6	18.0	1.28	0.17	1.87	66	226	219	357
SC02-7	21.0	0.07	0.03	0.13	10	202	187	255

Notes: *Core collected 4/03/2000. Fe, As, Pb, Cr, and Zn determined by ICP-OES after microwave-assisted extraction in 10% nitric acid. TOC=total carbon minus inorganic carbon, determined using an UIC, Inc. carbon coulometer. S determined by coulometery (UIC, Inc.).*

Table B.4. Concentrations of Selected Elements in Halls Brook Holding Area Pond Grab Sediment Samples

Sediment Sample	Depth cm	Fe wt%	S Wt%	TOC wt%	As µg/gm	Pb µg/gm	Cr µg/gm	Zn µg/gm
WI01	<10	3.80	0.20	3.10	494	794	197	583
WI01-NEP	<10	7.70	0.18	3.00	830	572	122	767
WI02	<10	24.60	0.47	4.75	715	203	106	3034
WI02-NEP	<10	18.50	0.65	5.24	630	262	162	4589
WI04	<10	26.30	0.35	5.26	840	115	49	1517
SC0401-1	<10	7.46	1.14	5.24	682	274	511	2550
SC0401-2	<10	8.94	2.44	10.26	1150	392	698	3790
SC0401-3	<10	11.90	10.95	6.69	1680	398	250	17500
SC0401-4	<10	5.03	0.37	4.53	539	494	148	3920
SC0401-5	<10	7.59	1.59	14.18	676	526	593	3440
SC0401-6	<10	8.56	2.85	18.61	1070	481	694	3190
SC0401-7	<10	8.65	2.32	17.34	973	360	549	2590
NC0901-1	<10	1.90	0.83	1.50	207	92	65	836
NC0901-2	<10	3.37	2.24	2.29	356	144	107	1580
NC0901-3	<10	1.65	0.51	0.25	117	20	23.6	682
NC0901-4a	<20	7.00	6.71	13.32	1430	464	431	4300
NC0901-4b	<20	7.04	5.68	12.98	1490	461	437	4780
NC0901-4c	<20	8.23	6.89	12.86	1690	649	478	7480
NC0901-4d	<20	9.66	9.91	11.09	2050	548	606	9810

Notes: 'WI' sediments collected on 8/24/2000; 'SC0401' sediments collected on 4/03/2001; and 'NC0901' samples collected in September 2001. Fe, As, Pb, Cr, and Zn determined by ICP-OES after microwave-assisted extraction in 10% nitric acid. TOC=total carbon minus inorganic carbon, determined using an UIC, Inc. carbon coulometer. S determined by coulometery (UIC, Inc.).

Table B.5. Concentrations of Selected Elements in Halls Brook Holding Area Pond Cores

Core Sample	Depth cm	Fe wt%	S wt%	TOC wt%	As µg/gm	Pb µg/gm	Cr µg/gm	Zn µg/gm
NC0401-1	1.0	8.87	1.80	11.92	1020	763	549	4270
NC0401-1	3.0	6.47	1.87	12.28	850	755	893	6320
NC0401-1	5.0	1.84	0.31	3.92	183	1550	421	1240
NC0401-1	7.0	0.57	0.10	1.39	68	837	31	77
NC0401-2	1.5	0.35	0.09	1.01	19	1070	11	67
NC0401-2	4.5	0.91	0.41	2.84	154	350	140	1120
NC0401-3	1.0	8.78	1.61	8.82	284	923	640	7170
NC0401-3	3.0	6.61	1.65	7.91	330	957	500	4390
NC0401-3	6.0	2.34	0.18	2.42	126	1430	300	505
NC0401-3	10.0	1.71	0.10	1.56	88	734	221	334
NC0401-3	14.0	0.68	0.05	0.92	6	38	17	46
NC0401-4	1.0	5.94	2.89	13.27	694	369	389	2270
NC0401-4	3.0	7.05	2.17	13.32	1020	506	811	4090
NC0401-4	6.0	0.82	0.16	0.46	20	18	17	104
NC0401-4	9.5	0.44	0.06	0.02	2	2	6	24
NC0401-4	12.5	0.40	0.03	0.03	2	0.5	6	18
NC0401-5	1.0	7.85	5.42	11.62	1060	459	508	3080
NC0401-5	3.0	12.00	4.54	10.21	1960	557	632	10300
NC0401-5	5.0	3.85	0.49	0.69	342	244	120	1900
NC0401-5	7.5	5.70	0.43	2.57	405	681	149	1210
NC0401-5	11.5	1.25	0.04	0.05	21	27	22	185
NC0401-6	1.0	7.87	4.86	12.66	1550	452	617	5520
NC0401-6	3.0	15.60	13.86	7.02	2570	404	359	15500
NC0401-6	5.0	3.85	1.60	0.14	65	27	22	273
NC0401-6	7.0	2.12	0.49	0.26	78	62	37	301
NC0401-6	11.0	1.20	0.12	0.23	32	50	27	162
NC0401-6	13.5	0.32	0.02	0.06	2	6	5	29
NC0401-7	3.0	1.63	0.21	3.18	158	1210	278	2100
NC0401-7	9.0	1.01	0.09	3.08	107	784	368	275
NC0401-8	4.0	0.57	<0.01	0.07	<2	4	8	15

Notes: *NC0401 cores collected in April 2001. Fe, As, Pb, Cr, and Zn determined by ICP-OES after microwave-assisted extraction in 10% nitric acid. TOC=total carbon minus inorganic carbon, determined using an UIC, Inc. carbon coulometer. S determined by coulometery (UIC, Inc.).*

Table B.6. Results from LCF-XANES Fits of the Pb XANES Data Collected for Sediments from Suboxic and Oxic Zones within the HBHA Pond

	Weighted Percent Contribution					
	Galena	**s**	**Pb-Sorbed Ferrihydrite**	**s**	**F-Test**	**Residual**
NC01-1	19.4	1.11	80.6	1.10	1	0.774
NC01-3	12.7	1.09	87.3	1.09	1	0.807
NC01-6	5.0	0.21	95.0	0.21	1	0.875
NC01-7	37.8	0.32	62.3	0.32	1	0.622
NC0401-1 0-2	11.6	1.24	88.4	1.23	1	0.851
NC0401-1 2-4	4.1	0.28	95.9	0.28	1	0.543
NC0401-5 0-2	16.1	0.86	83.9	0.86	1	0.856
NC0401-5 2-4	3.2	0.25	96.8	0.26	1	0.822
NC0401-6 0-2	4.9	0.21	95.2	0.21	1	0.823
NC0901-4B	3.6	0.26	96.4	0.26	1	0.744
NC0901-4C	5.3	0.11	94.7	0.11	1	0.784
NTW4	20.3	1.74	79.7	1.73	1	0.747
SC0401-3	4.2	0.32	95.8	0.32	1	0.872
SC0401-6	4.1	0.15	95.9	0.15	1	0.808

s = standard deviation

Table B.7. Results from LCF-XANES Fits of the Zn XANES Data Collected for Sediments from Suboxic and Oxic Zones within the HBHA Pond

	Weighted Percent Contribution									
	Sphalerite	**s**	**Zn-Sorbed Ferrihydrite**	**s**	**Smith-sonite**	**s**	**$Zn(OH)_2$**	**s**	**F-Test**	**Residual**
NC01-1	73.8	0.09	26.2	0.09	--	--	--	--	1	1.82
NC01-3	70.5	0.09	29.5	0.09	--	--	--	--	1	1.42
NC01-6	75.7	0.10	24.3	0.09	--	--	--	--	1	1.65
NC01-7	49.5	0.11	13.6	0.17	--	--	36.9		1	2.64
NC0401-1 0-2	55.0	0.11	45.0	0.10	--	--	--	--	1	2.22
NC0401-1 2-4	73.6	0.09	26.4	0.09	--	--	--	--	1	1.50
NC0401-5 0-2	67.2	0.09	32.8	0.09	--	--	--	--	1	1.81
NC0401-5 2-4	73.4	0.11	26.6	0.10	--	--	--	--	1	1.72
NC0401-6 0-2	79.6	0.11	20.4	0.09	--	--	--	--	1	1.28
NC0401-6 2-4	72.9	0.09	27.2	0.09	--	--	--	--	1	1.45
NC0901-1	65.3	0.09	34.7	0.09	--	--	--	--	1	1.51
NC0901-4B	80.6	0.10	19.5	0.03	--	--	--	--	1	1.41
NC0901-4C	78.3	0.09	21.7	0.09	--	--	--	--	1	1.58
NTW4	75.1	0.09	24.9	0.09	--	--	--	--	1	1.71
SC0401-1	68.5	0.09	31.5	0.09	--	--	--	--	1	1.88
SC0401-3	84.6	0.09	15.4	0.09	--	--	--	--	1	1.29
SC0401-6	70.7	0.09	29.3	0.09	--	--	--	--	1	2.26
SC0401-7	69.1	0.09	30.9	0.09	--	--	--	--	1	1.89
WI02-N1-53D2	--	--	42.8	0.40	--	--	57.2	0.40	1	1.59
WI02-N2-53D2	21.7	0.40	30.8	0.60	--	--	47.4	0.50	1	1.81
WI02-N2B 2um	--	--	24.9	0.39	12.4	0.29	62.8	0.49	1	2.38
WI02-NINE	--	--	75.0	0.50	9.0	0.50	15.9	0.6	1	1.68

s = standard deviation

Appendix C
Description of Methods for Data Collection and Analysis to Determine Element Speciation Employing X-ray Absorption Spectroscopy

Introduction

X-ray Absorption Spectroscopy (XAS) refers to a technique that employs analysis of X-ray Absorption Fine-Structure (XAFS) to determine structural and chemical speciation of elements in various matrices. At characteristic energies for a given element, absorption of an x-ray results in ejection of a core level electron. The ejected photo-electron may subsequently be scattered from neighboring atoms and interfere with itself resulting in modulation of the energy of the photo-electron and, therefore, the absorption event (http://cars9.uchicago.edu/xafs/xas_fun/xas_fundamentals.pdf). In practice, XAFS involves probing and analyzing the modulation of the x-ray absorption probability of an atom due to the chemical and physical state of the atom. XAFS spectra are especially sensitive to the formal oxidation state, coordination chemistry, and the interatomic distances, coordination number, and species of the atoms in the surrounding proximity of the selected element of interest. As a result, XAFS provides a practical and straight-forward way to determine the chemical state and local atomic structure for a selected atomic species. XAFS can be used in a wide variety of systems and bulk physical environments.

Current practice for collection of XAFS data usually involves the use of a synchrotron as the source of x-rays. The flux of x-rays from a synchrotron facility is sufficiently high to prevent the need to conduct experiments in a vacuum or the removal of water. Thus, an important aspect from an environmental perspective is that XAFS can be used as an *in-situ* spectroscopy allowing for the investigation of samples in their natural state. Another unique aspect of this technique is that it provides a means to collect element-specific data. Since each element absorbs x-rays at unique and discrete energies, it is possible to selectively collect chemical and structural data for a specific element. In addition, XAFS probes the short-range structure of a substance and is, therefore, not limited to analysis of materials possessing long-range structural order, e.g., as required for x-ray diffraction analysis. Thus, XAFS measurements can be used to probe the chemical and structural speciation of noncrystalline material, disordered compounds, and solutions feasible; matrices that are most relevant to environmental systems.

Though XAFS measurements can be operationally simple, interpretation of XAFS data involves a mixture of modern physics and chemistry, and a complete mastery of the data analysis can be somewhat challenging. Though the basic phenomena are well understood, an accurate theoretical treatment is fairly involved, and in some respects, still an area of active research.

X-Ray Absorption Fine Structure Spectroscopy

X-ray Absorption Fine-Structure (XAFS) is the modulation of the x-ray absorption coefficient at energies near and above an x-ray absorption edge. XAFS is also referred to as X-ray Absorption Spectroscopy (XAS) and is subdivided into 2 regimes (Figure C.1):

XANES - X-ray Absorption Near-Edge Spectroscopy

EXAFS - Extended X-ray Absorption Fine-Structure

that contain related, but slightly different, information about the local coordination and chemical state of an element.

X-rays (light with wavelength 0.03 12 Å or energy 1 E 500 keV) are absorbed by all matter through the photoelectric effect: An x-ray is absorbed by an atom, promoting a core-level electron (K, L, or M shell) out of the atom and into the continuum. The atom is left in an excited state with an empty electronic level (a core hole). The electron ejected from the atom is called the photoelectron. When X-rays are absorbed by the photoelectric effect, the excited core-hole will relax back to a "ground state" of the atom. A higher level core electron drops into the core hole, and a fluorescent X-ray or Auger electron is emitted.

X-ray Fluorescence: An x-ray with energy equal to the difference of the core levels is emitted.

Auger Effect: An electron is promoted into the continuum from another core level.

X-ray fluorescence occurs at discrete energies that are characteristic of the absorbing atom and can be used to identify the absorbing atom.

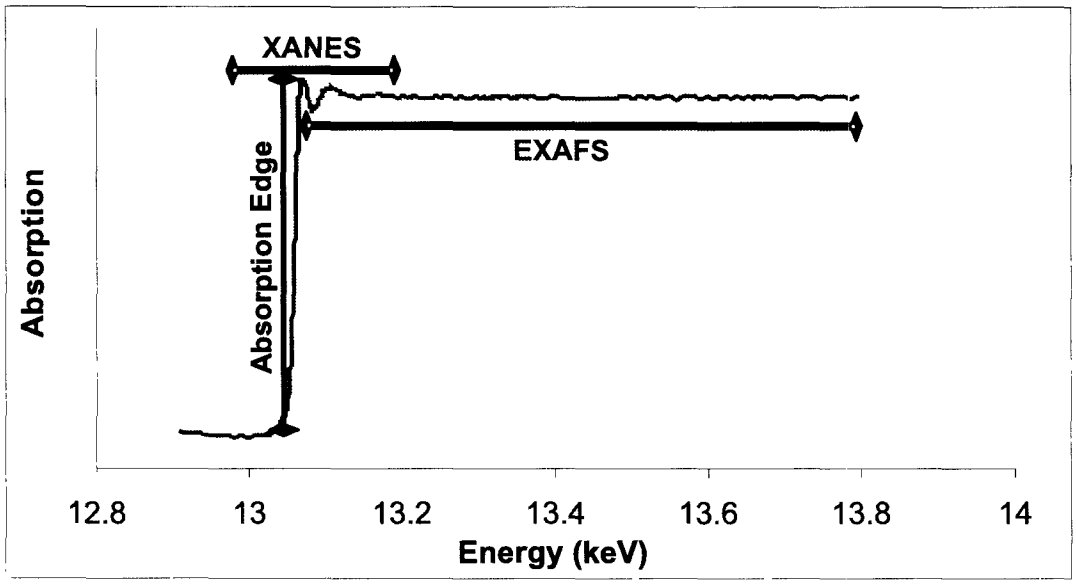


Figure C.1 *Location of XANES and EXAFS regions of an XAS spectrum. The characteristic energy required to excite core level electrons is unique to each element and is known as the absorption edge or edge step.*

The intensity of an X-ray beam as it passes through a material of thickness, t, is given by the absorption coefficient, μ:

$$I = I_0 e^{-\mu t}$$

where I_0 is the X-ray intensity hitting the material, and I is the intensity transmitted through the material. The absorption coefficient depends strongly on X-ray energy, E, and atomic number, Z, and on the density, , and atomic mass, A:

$$\mu \quad (Z^4)/(AE^3)$$

In addition, μ has sharp absorption edges (Figure C.1) corresponding to the characteristic core level energies of the atom. The energies of the K-edge absorption edges go roughly as $E_K \sim Z^2$. All elements with Z>18 have either a K- or L-edge energies between 3 and 35 keV, which can be accessed at many synchrotron sources.

X-ray Absorption Spectroscopy Data Collection

While room-sized accelerators exist for conducting XAS studies, the intensity pales in comparison to accelerators found at synchrotron radiation facilities such as Department of Energy National Laboratories (Figure C.2). Figure C.2 shows the Advanced Photon Source (APS) synchrotron radiation research facility at Argonne National Laboratory in the southeastern suburbs of Chicago, IL. Applying components of Figure C.2B to explain structures in Figure C.2A, the operation of the APS synchrotron facility entails (A) production of electrons in a linear accelerator which are deposited into (B) the booster/injector ring to bring the electron packets near the speed of light. The electron beam is then sent to the storage ring (C) from which beamlines (D) as either insertion devices, ID, or bending magnets, BM, are constructed for experimental research (E). In-line with the research beamlines are monochromaters that tune the electron beam to selected energies via Bragg diffraction and must be capable of energy resolutions of ~ 1 eV at 10 keV.

XAS data collection can be divided into two realms: 1) configuration of beamline equipment and 2) sample preparation. XAS measures the energy dependence of the x-ray absorption coefficient, μ(E), at and above the absorption edge of a selected element. μ(E) can be measured in two experimental configuration setups:

Transmission: The absorption is measured directly by measuring what is transmitted through the sample (Figure C.3):

$$I = I_0 e^{-\mu(E)t}$$

$$\mu(E)t = \ln(I/I_0)$$

Fluorescence: The re-filling of the deep core hole is detected. Typically the fluorescent x-ray is measured (Figure C.4).

$$\mu(E) \sim I_f / I_0$$

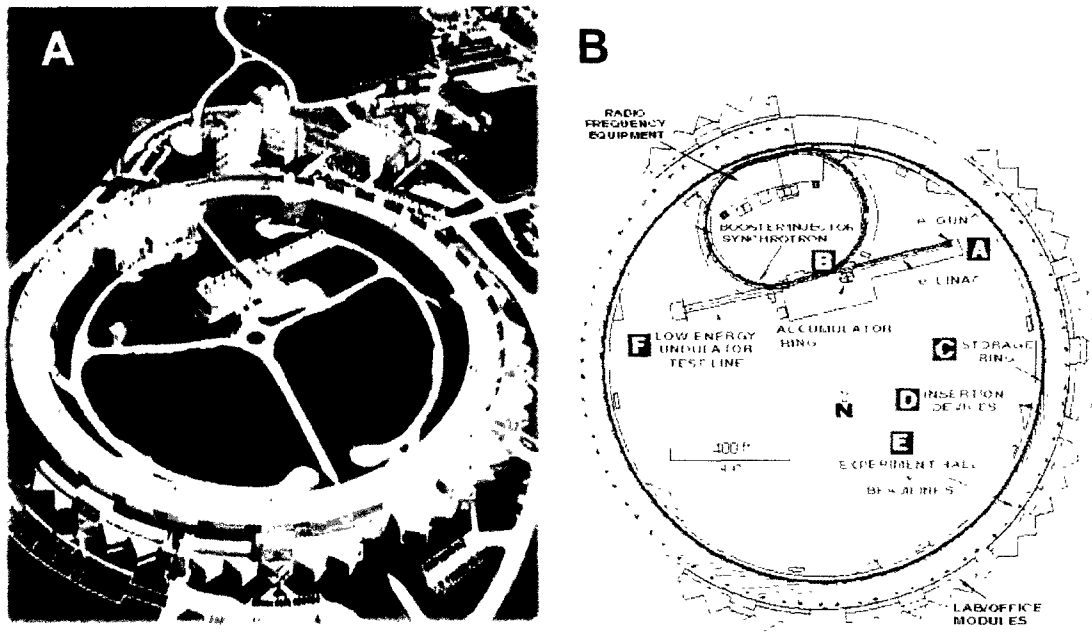


Figure C.2 *Aerial photo and architectural diagram of the Advanced Photon Source at Argonne National Laboratory, Chicago, IL.*

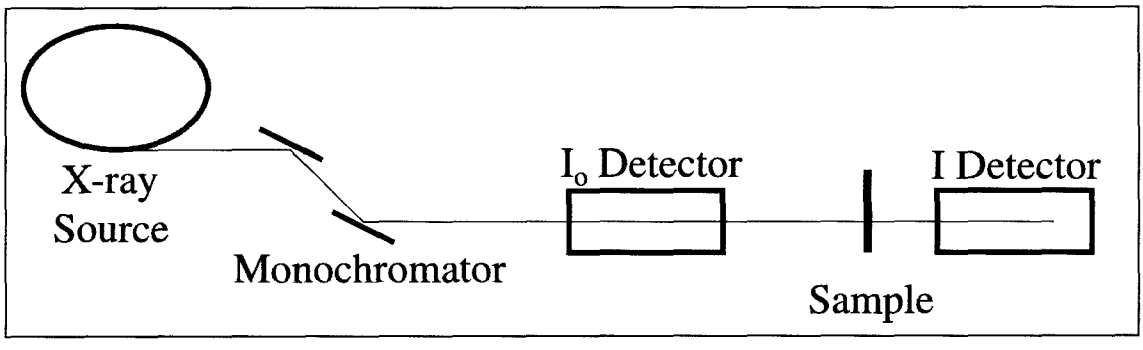


Figure C.3 *Experimental configuration for transmission data collection.*

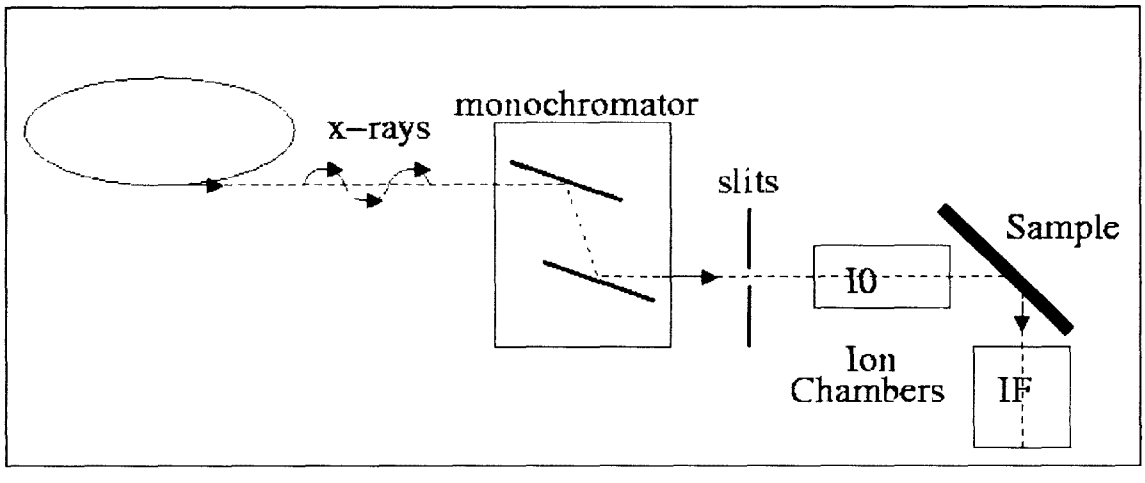


Figure C.4 *Experimental configuration for fluorescence data collection.*

Upon commencing an XAS scan to collect data, one has the option to use step-scan, continuous scan, or dispersive XAFS modes. Typically, step-scan is used so that regions can be defined, and specific time can be allocated at step to ensure adequate counts for statistical purposes.

Typical scan parameters for spectral regions for environmental samples include (Figure C.5):

A. Sample ***pre-edge*** to get background trend
(Range ~ -100 eV to -20 eV, 5 eV sampling)

C. Sample ***edge*** region
(-20 eV to +40 eV, 1 eV)

C. ***EXAFS*** region
Uniform in k-space (to > 12 $Å^{-1}$, sampling 0.05 $Å^{-1}$)
Prefer increased integration time per point at high k

Sample preparation can be as crucial as data collection setup when attempting to collect quality data. Although much imagination can be employed for sample preparation, many considerations must be examined to ensure that the integrity of the sample is maintained. For example, with redox sensitive materials such as arsenic, one must be mindful of possible oxidation of arsenite either from oxygen in the air, as a result of materials in the sample holder, and over exposure of the electron beam. Another important issue to evaluate for sample preparation is the adequacy of the beamline one chooses to conduct the experiments. This can be overcome by first working out the absorption lengths of the material at the relevant energies. One should check for beamlines with the needed energy range and focal properties for the intended samples. If the X-rays can get through the sample with only a few absorption lengths of attenuation, i.e. small, homogeneous particle sizes, one can consider transmission data collection which can be superior to fluorescence measurements. However, the edge step must be large enough for a transmission measurement which is hampered by concentration of the element of interest. Thus, if the sample is dilute or inhomogeneous, fluorescence data collection is better and most often employed.

If the energy is too low, absorption from air and windows can be a problem (a general rule is absorption energy decreases as atomic weight decreases, so lighter elements such as chromium can have artifacts which heavier elements such as arsenic can avoid) but can be overcome by enclosing the sample and detection chambers in a non-ionizing gas environment. Once an accurate understanding of detector limitations is accomplished for sample preparation, sample mounting should be designed with simplicity in mind.

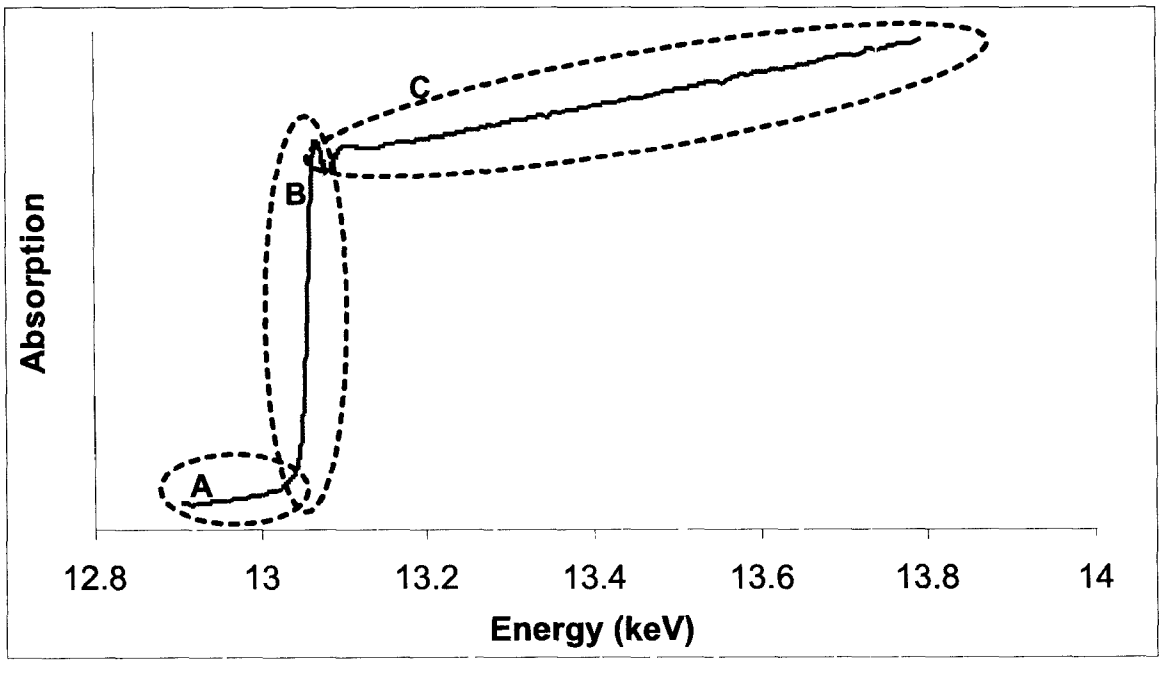


Figure C.5 *Standard raw XAFS spectra illustrating the three regions: (A) pre-edge, (B) edge step, and (C) EXAFS. The XANES portion of the spectra contains all of edge step and small portions of the pre-edge and EXAFS regions (Figure C.1).*

Placement of the sample within an experimental hutch at a synchrotron facility is outlined in Figures C.3 and C.4, for transmission and fluorescence data collection, respectively. In both setups, the sample is placed after the I_o detector which measures the intensity of the beam before interaction with the sample. The only difference between sample mounting for transmission and fluorescence data collection is that the sample must be situated at a 45° angle to the incident electron beam for fluorescence mode (Figure C.4) to allow maximum fluorescence detection to occur and minimize elastic scattering. As such, a fluorescence detector for fluorescence data collection must be placed perpendicular to the electron beam and in line with the sample (Figure C.4). While transmission data can be collected from samples offset of the penetrating beam, data quality is theoretically better by allowing the beam to pass directly through the sample placed perpendicular to the electron beam (Figure C.3) with a suitable detector aligned with the electron beam (Figure C.3) behind the sample.

Sample holders can vary significantly but follow a basic design. Sample holders can be as simple as smearing a solid material on the tacky side of tape and folding the tape back onto itself to secure the sample (Figure C.6). Another common sample holder is a small block of non-reactive material with a depression or hole lathed into the holder to which the sample is added with tape securing the opening (Figure C.7). This type of sample holder allows analysis of solids, slurries, and solutions. The thickness and size of openings can be customized. An adaptation of this sample holder in conjunction with a movable sample stages and automation software yields a basic autosampler (Figure C.8) which permits all types of samples for analysis.



Figure C.6 *Solid sample sandwiched between pieces of Kapton tape.*

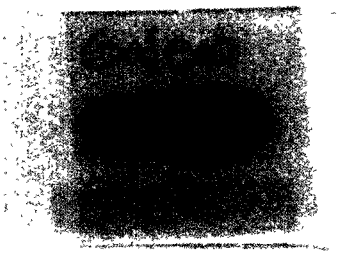


Figure C.7 *Sample backfilled into opening of a Teflon block and secured with tape.*

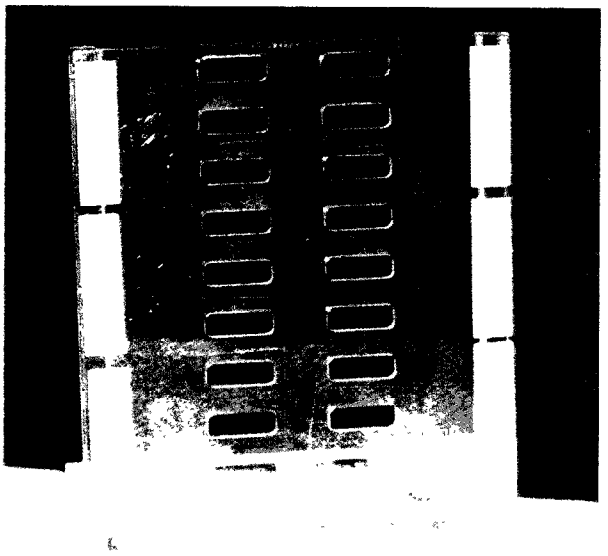


Figure C.8 *Autosampler template for multi-sample analysis.*

Traditional spectroscopic sample holders, such as thin films and thin sections, are often employed as well for specialized projects, but the above mentioned methods are more suitable for typical environmental analyses. However, some of the traditional holders are being examined for the purpose of biological specimens and modified approaches can be used to deal with samples with unusual physical characteristics (Figure C.9).

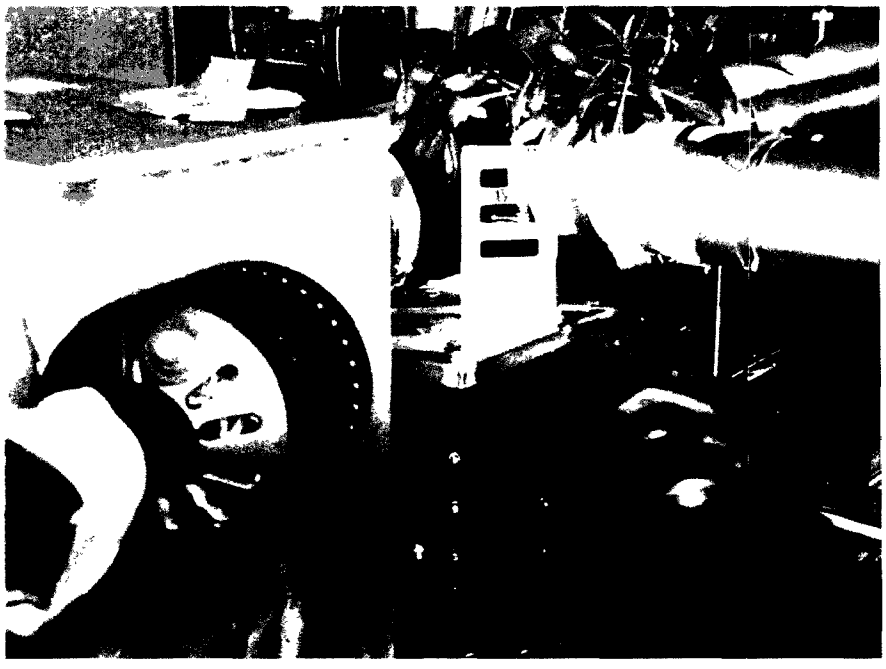


Figure C.9 *Fluorescence data collection of metal hyperaccumulation in plant leaves.*

Extended X-Ray Absorption Fine-Structure Data Analysis

Whether transmission or fluorescence data are collected, the data reduction and analysis are essentially the same. The steps to data analysis are 1) reduce the raw spectra (Figure C.10) to k-space (conversion of energy [eV] to wavelength [inverse distance]), 2) apply a Fourier transform to convert the k-space data into R-space (conversion of wavelength to actual distance), and 3) XAFS data modeling.

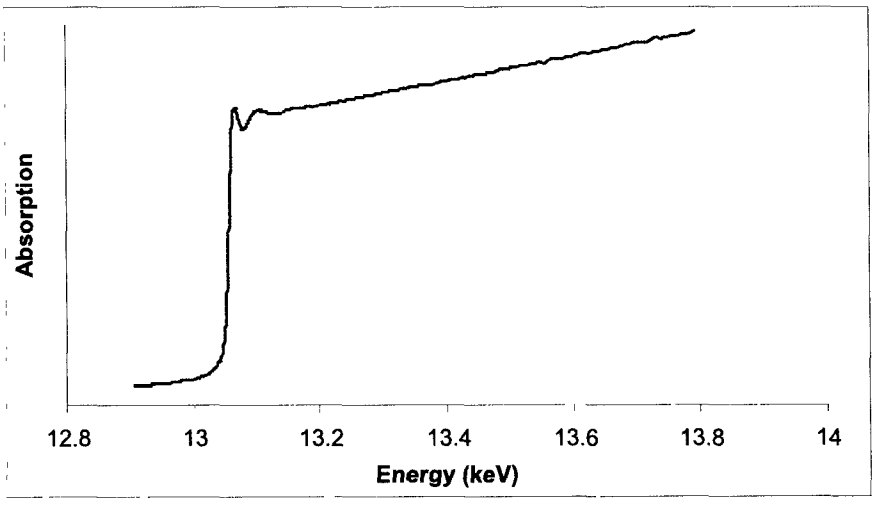


Figure C.10 *Raw fluorescence data Pb sorption on ferrihydrite*

Background correction of a raw spectrum involves assigning a baseline value of zero to the pre-edge region and a normalized unity value of one to the EXAFS region (Figure C.11).

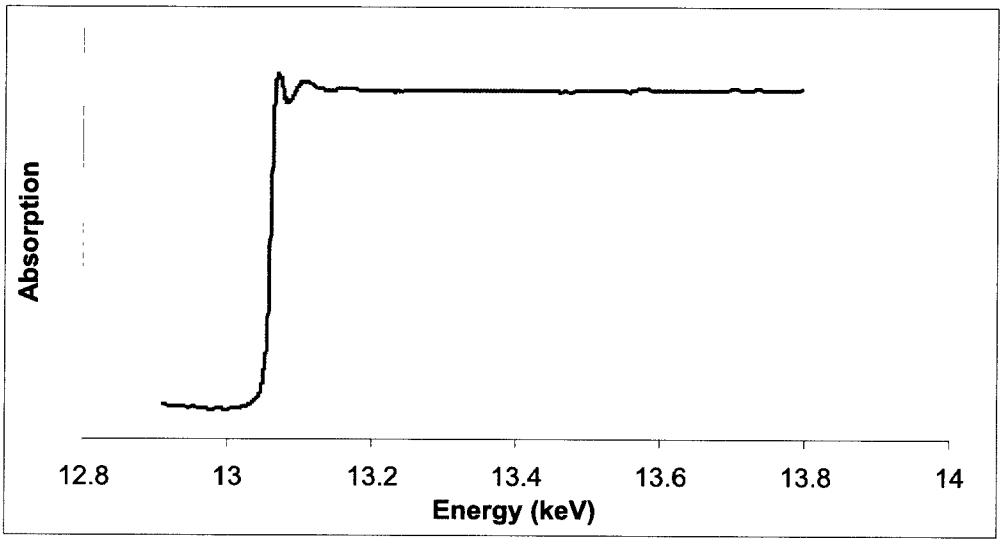


Figure C.11 *Background corrected spectra of Figure C.10.*

The conversion of energy (E) to k-space (Figure C.12) involves first the identification of the threshold energy, E_o, which is the energy maximum of the edge step. Thereafter, one isolates the EXAFS region in terms of the wave behavior of the photoelectron (k) created in the absorption process by the equation:

$$k = \sqrt{\frac{2m(E - E_0)}{\hbar^2}}$$

where E is energy, E_o is the absorption edge energy, is Planck's constant, and m is the electron mass.

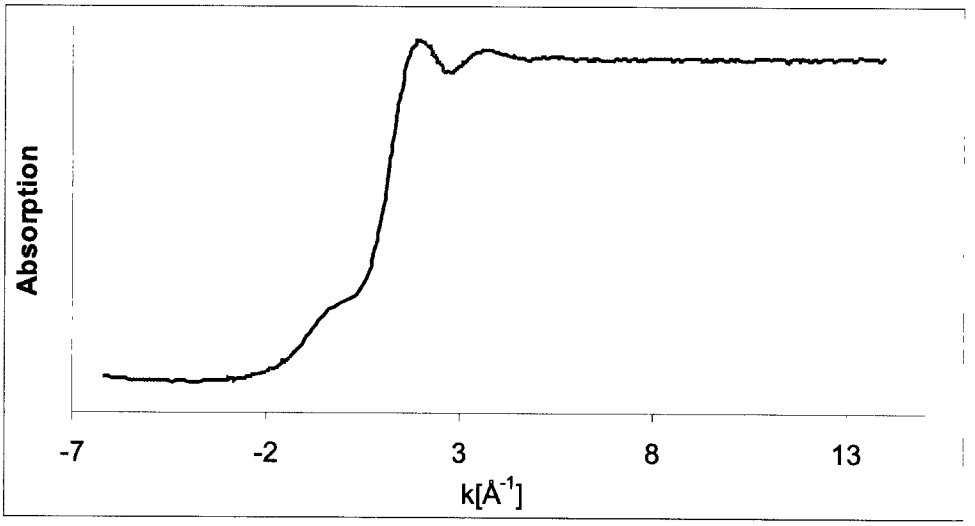


Figure C.12 *k-space conversion of spectra in Figure C.11.*

By selecting and emphasizing (k-weighting) only positive k-space, one generates oscillations as a function of the photoelectron wave number also known as the (chi) (k)-function (Figure C.13). The oscillations in Figure C.13 correspond to different near-neighbor coordination shells which, after Fourier transformation (Figure C.14), can be described by the EXAFS equation:

$$\chi^{(k)} = \sum_j \frac{N_j f_j(k) e^{-2k^2\sigma_j^2}}{kR_j^2} \sin\left[2kR_j + \delta_j(k)\right]$$

Where f(k) and (k) are scattering properties of the atoms neighboring the excited atom, N is the number of neighboring atoms, R is the distance to the neighboring atom, and ^{2} is the disorder in the neighbor distance. Though complex in appearance, the EXAFS equation allows one to determine N, R, and ^{2} if the scattering amplitude, f(k), and phase-shift, (k), are known. Since f(k) and (k) depend on the Z of the neighboring atoms, EXAFS is also sensitive to the atomic species of the neighboring atom.

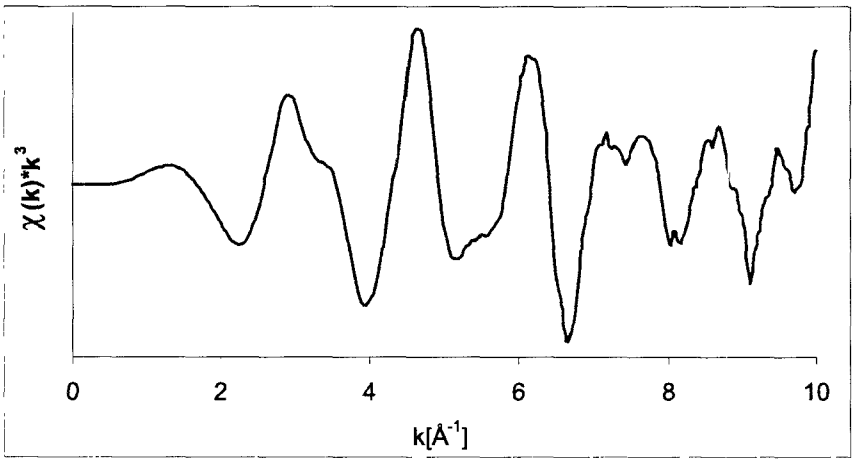


Figure C.13 *The k^3-weighted -function of Figure C.12. The oscillations describe the photoelectron wave number as the photoelectron constructively and destructively interacts with neighboring atoms around PC.*

Now that the energy spectrum in Figure C.11 is converted to k-space (Figure C.13), one can Fourier transform the k-space data in R-space (distance). The Fourier transformation is critical to XAFS analysis and is often the area of confusion for novice data analyzers. Since the photoelectron effect causes backscattering in XAFS data collection, a phase shift causes real values of distance to be offset at least 0.5 Å when determining interatomic bond distances in the data modeling techniques. For example, the protruding peak located at approximately 1.8 Å in Figure C.14 for the Fourier transformed k-space data is actually determined to be 2.53 Å in the modeling procedure to follow.

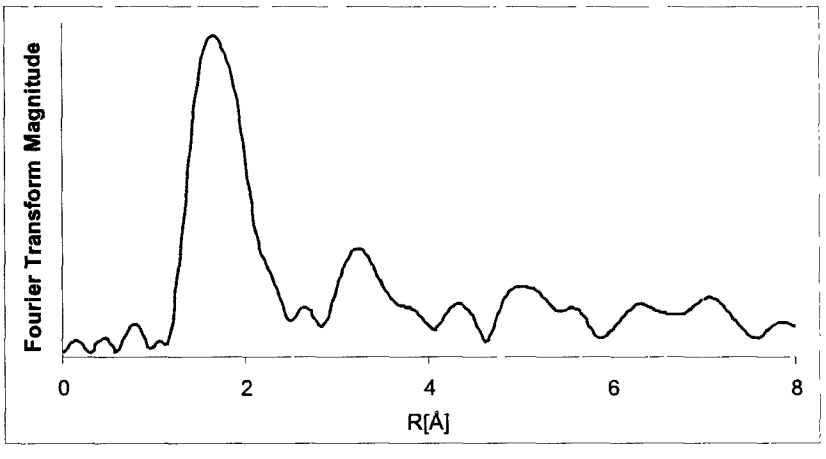


Figure C.14 *Radial distribution (or structure) function of Fourier transformed k-space data for Figure C.13.*

The final step in EXAFS data analysis is modeling which is often the most complex and time consuming aspect of the procedure. The most common method of modeling is to develop a library of fitting paths generated crystallographic parameters. Figure C.15 shows the crystalline unit cell parameters for magnetoplumbite, an iron oxide with small amounts of Pb in the structure. A commercially available software program, ATOMS, is available for this purpose to record what and where the information was derived (title and notes sections), space group identity and unit cell angles (abc) of the phase, the ab-initio calculation sphere in angstroms (rmax), which element to centralize the calculation around (core), and the 3-dimensional positions (xyz) of each element with corresponding tags (Pb1, Fe2, etc).

This ATOMS input file is used to generate possible coordinations of elements within magnetoplumbite as a FEFF file (commercially available software) (Figure C.16). (NOTE: The XAS research user community is rather small, and many software packages are available free of charge from the international experts.) The FEFF program then uses this information to generate, via ab-initio calculations, fitting paths to describe the interatomic bond distances (R) and coordination numbers (N) with neighboring elements.

```
title name:    magnetoplumbite
title formula: PbFe_12O_19
title sites.   Pb1, Fe1 -5, O1-5
title refer1:  Moore et al.(1989) Am. Min. 74, 1186-1194
title refer2:
title schoen.
title notes1   Pb2+, Fe3+ oxidation state
title notes2:  modified from Moore et al's structure
title notes3:  see notes below
space  p 63/m m c
a   = 5.873   c   = 23 007
rmax = 6.00
core = Pb1
atom
Pb    0.66667   0.33333   0 25000  Pb1
Fe    0 00000   0.00000   0.00000  Fe1
Fe    0 00000   0.00000   0.25000  Fe2
Fe    0 33333   0.66667   0.02730  Fe3
Fe    0.33333   0.66667   0.19000  Fe4
Fe    0.16900   -0.16900  -0.10900 Fe5
O     0.00000   0 00000   0 15100  O1
O     0.33333   0.66667   -0.05500 O2
O     0.18400   -0.18400  0.25000  O3
O     0 15500   -0 15500  0.05200  O4
O     0.50400   -0.50400  0.15000  O5
-----
% notes·
% Moore et al put the Pb at (0.72,0.384,1/4), a site with 12j symmetry,
% and have an occupation of 1/6 for this site. This is a large distortion
% of the Pb environment from the "normal" (2/3, 1/3, 1/4) position (with 2d
% symmetry) used here.
% Since fractional occupation is poorly defined in the context of local
% structure, it isn't supported in atoms. So the point of high symmetry is
% needed (otherwise unphysically short Pb-Pb bonds are made).
% similarly, the Fe2 position has been moved from (0,0,0.256) with an
% occupation of 1/2 to (0,0,1/4) with full occupation.
% the Pb-O and Fe-O near-neighbor distances for all 5 Fe sites agree
% fairly well with Moore et al.
```

Figure C.15 *ATOMS input file for magnetoplumbite listing crystallographic information.*

```
TITLE name    magnetoplumbite TITLE formula  PbFe_12O_19 TITLE sites    Pb1, Fe1-5 O1-5
TITLE refer1  Moore et al (1989) Am Min 74 1186-1194 TITLE refer2  TITLE schoen  TITLE notes1
Pb2+, Fe3+ oxidation state  TITLE notes2  modified from Moore et al's structure  TITLE notes3  see
notes below

HOLE 4  1 0  * Pb L3 edge (13035 0 eV), second number is S0^2

*      mphase mpath mfeff mchi
CONTROL  1    1    1    1
PRINT    1    1    1    3

RMAX     6 0

*CRITERIA   curved  plane
*DEBYE      temp    debye-temp
*NLEG       8

POTENTIALS
*   ipot   Z  element
     0   82  Pb
     1   82  Pb
     2   26  Fe
     3    8  O

ATOMS                    * this list contains 84 atoms
*  x          y          z          ipot  tag          distance
   0 00000    0 00000    0 00000    0     Pb1          0 00000
   1 65468    0 00003    2 30070    3     O5_1         2 83394
  -0 82737   -1 43298    2 30070    3     O5_1         2 83394
   1 65468    0 00003   -2 30070    3     O5_1         2 83394
  -0 82737   -1 43298   -2 30070    3     O5_1         2 83394
  -0 82737    1 43304    2 30070    3     O5_2         2 83397
  -0 82737    1 43304   -2 30070    3     O5_2         2 83397
   2 63123   -1 31552    0 00000    3     O3_1         2 94176
  -0 17634   -2 93647    0 00000    3     O3_1         2 94176
   2 63123    1 31558    0 00000    3     O3_2         2 94179
  -2 45494   -1 62092    0 00000    3     O3_2         2 94179
  -2 45494    1 62098    0 00000    3     O3_3         2 94182
  -0 17634    2 93653    0 00000    3     O3_3         2 94182
   1 69537   -2 93647    0 00000    2     Fe2_1        3 39074
  -3 39080    0 00003    0 00000    2     Fe2_2        3 39080
   1 69537    2 93653    0 00000    2     Fe2_2        3 39080
   0 83581   -1 44767    3 24399    2     Fe5_1        3 64935
   0 83581   -1 44767   -3 24399    2     Fe5_1        3 64935
  -1 67167    0 00003    3 24399    2     Fe5_2        3 64937
   0 83581    1 44772    3 24399    2     Fe5_2        3 64937
  -1 67167    0 00003   -3 24399    2     Fe5_2        3 64937
   0 83581    1 44772   -3 24399    2     Fe5_2        3 64937
   3 39074    0 00006    1 38042    2     Fe4_1        3 66097
  -1 69542   -2 93644    1 38042    2     Fe4_1        3 66097
   3 39074    0 00006   -1 38042    2     Fe4_1        3 66097
  -1 69542   -2 93644   -1 38042    2     Fe4_1        3 66097
  -1 69542    2 93656    1 38042    2     Fe4_2        3 66106
  -1 69542    2 93656   -1 38042    2     Fe4_2        3 66106
```

Figure C.16 *FEFF file used to determine fitting paths for EXAFS modeling showing the interaction of a central Pb atom (Pb1) with two different oxygen atoms (O5 and O3) and three different iron atoms (Fe2, Fe5, and Fe4).*

Once theoretical fitting paths are generated, one can return to the radial distribution function (Figure C.14) to conduct the actual fitting protocol. Again, using one of several software packages for this procedure allows one to evaluate real data collected at a synchrotron facility relative to fitting paths from model data. An overlay of the resulting model fit to the actual data shows the goodness of the model parameter fitting and determines the relevant information to understand the overall system in terms of the coordination environment (R and N) (Figure C.17). Figure C.17 shows that Pb is octahedrally coordinated (N=6) with a bond distance of 2.53 Å to oxygen (Pb-O shell: oxygen is the first nearest neighbor) followed by Pb-Fe shell indicating a coordination number of approximately 2 and an interatomic bond distance of 3.67 Å. The Pb-Fe data suggest a bidentate (2 bonds) innersphere (oxygen between the Pb and Fe atoms) sorption complex for Pb sorption on ferrihydrite.

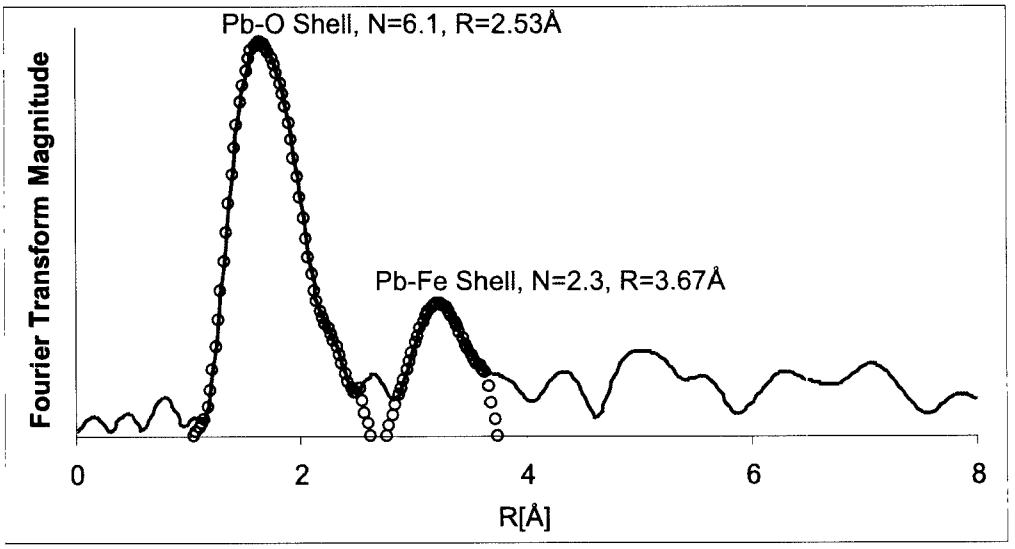


Figure C.17 *Structural data derived from ab-initio calculated fitting paths for Pb sorption on ferrihydrite. The red curve is the sample data reduced from a raw spectrum, and the blue dots represent the fit from the modeled paths. The fitting data can then determine coordination numbers (N) and interatomic bond distances (R).*

X-Ray Absorption Near Edge Spectroscopy Data Analysis

The XANES portion of the spectrum (Figure C.1) is a much larger signal than EXAFS which allows data collection for samples with lower concentrations and less than ideal sample conditions. The XANES portion is typically limited to within the range of -100 eV to 300 eV. These values vary depending on the element of interest and shape of the spectrum. The interpretation of XANES is complicated by the fact that there is not a simple chemical or physical description of the spectrum since XANES is uniquely different for each element; a fingerprint as an analogy. However, there is significant chemical data in the XANES region, notably the formal valence and coordination environment. The valence is identifiable by the position of the maximum edge energy by taking the derivative of the XANES region (Figure C.18). Typically, the energy difference between oxidation (valence) states of a given element can range significantly. For example, identification of arsenite (As^{3+}) and arsenate (As^{5+}) can be easily distinguished (Figure C.19). In the case of aqueous Zn and ZnS in Figure 18, Zn is in the divalent (2+) valence; however, there is a slight shift (1 eV) of the ZnS spectrum to a lower energy versus the Zn-O coordination of aqueous Zn. One can clearly notice distinctly different shapes of the Zn XANES spectra which allow for understanding of the influence of ligand type (first nearest neighbor) (Zn-O and Zn-S) on the coordination environment. For the As species in Figure C.19, oxygen is the nearest neighbor for both, resulting in similar spectra but offset in E due to different oxidation states. Note that the higher oxidation state of arsenate is at a higher E value than arsenite. This is intuitively correct when considering an oxidized atom will exert more effort to hang on to remaining electrons.

While analysis of XANES data can provide information on the oxidation state and the first coordination shell, the structural information is much more limited than what is accessible via EXAFS analysis. However, not all cases require one to know the level of information provided by EXAFS. XANES data analysis is significantly less labor intensive and in some cases can provide the level of information necessary to answer research questions.

Data Analysis of Complex, Heterogeneous Samples

In many instances for environmental samples, the speciation of metals can result in multiple phases. This can make data analysis difficult. For example, EXAFS data analysis is providing information on the average coordination numbers and bond distances for a given shell. When multiple species are present, these parameters are organized into one value that does not represent the complexity of the metal species. The same problem arises when interpreting the coordination environment of metals for XANES data analysis. To overcome this issue, one can apply a statistical fitting procedure that seeks to strip the multiple components of a sample spectrum into individual parts through the assistance of known reference spectra. The two most common methods are linear combination fitting (LCF) and principle component analysis (PCA). LCF analysis of XANES and XAFS spectra (LCF-XANES and LCF-XAFS) is simple to apply to normalized XANES spectrum or the $k^{2 \text{ or } 3}$-weighted -function from EXAFS data reduction. The goal in this procedure is to accu-

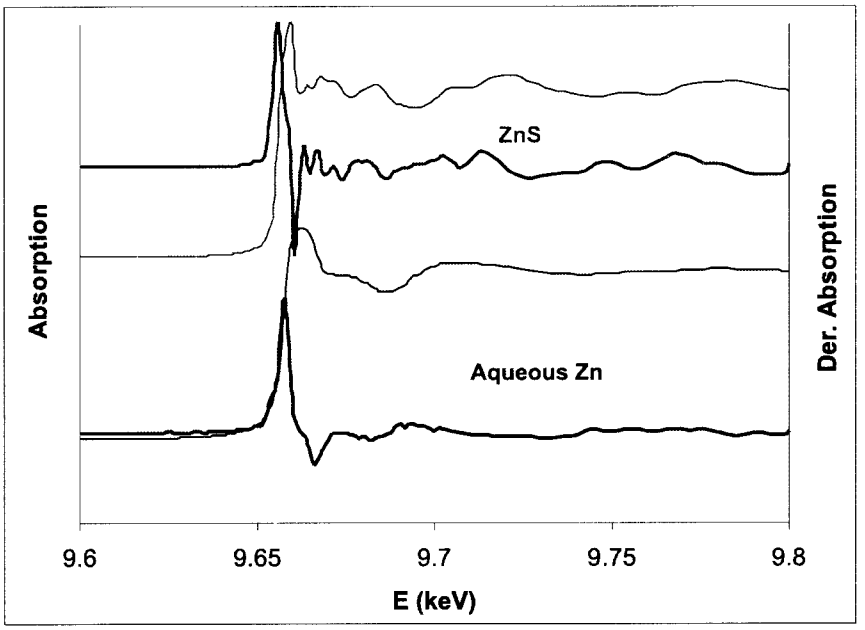


Figure C.18 *XANES spectra (thin line) and derivative of XANES spectra (thick line) for aqueous Zn^{2+} (blue) and ZnS (red).*

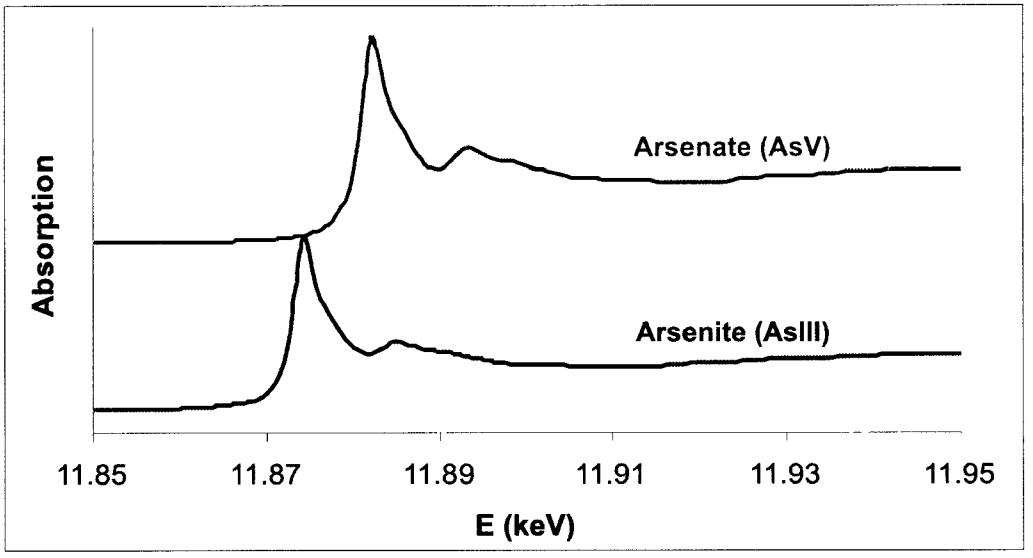


Figure C.19 *XANES spectra for arsenite [As(III) - blue] and arsenate [As(V) - red].*

mulate enough relevant reference spectra that can explain and represent the unknown environmental sample. Through the use of available software, one selects an unknown spectrum to evaluate and multiple known reference spectra to fit against the unknown. By repeating the procedure and removing nonessential reference spectra, one can gain a semi-quantitative analysis of the major metal species present in the unknown sample (Figure C.20). Detailed information as collected in EXAFS analysis is not possible, but identity of multiple species in the sample is accomplished.

For typical environmental samples, the use of finger-printing methods such as LCF-XANES and LCF-XAFS can be a very powerful tool to determine metal speciation when multiple phases are present. This approach proves very effective in monitoring contaminated sites to evaluate changes in metal speciation either through in-situ amendments or monitored natural attenuation.

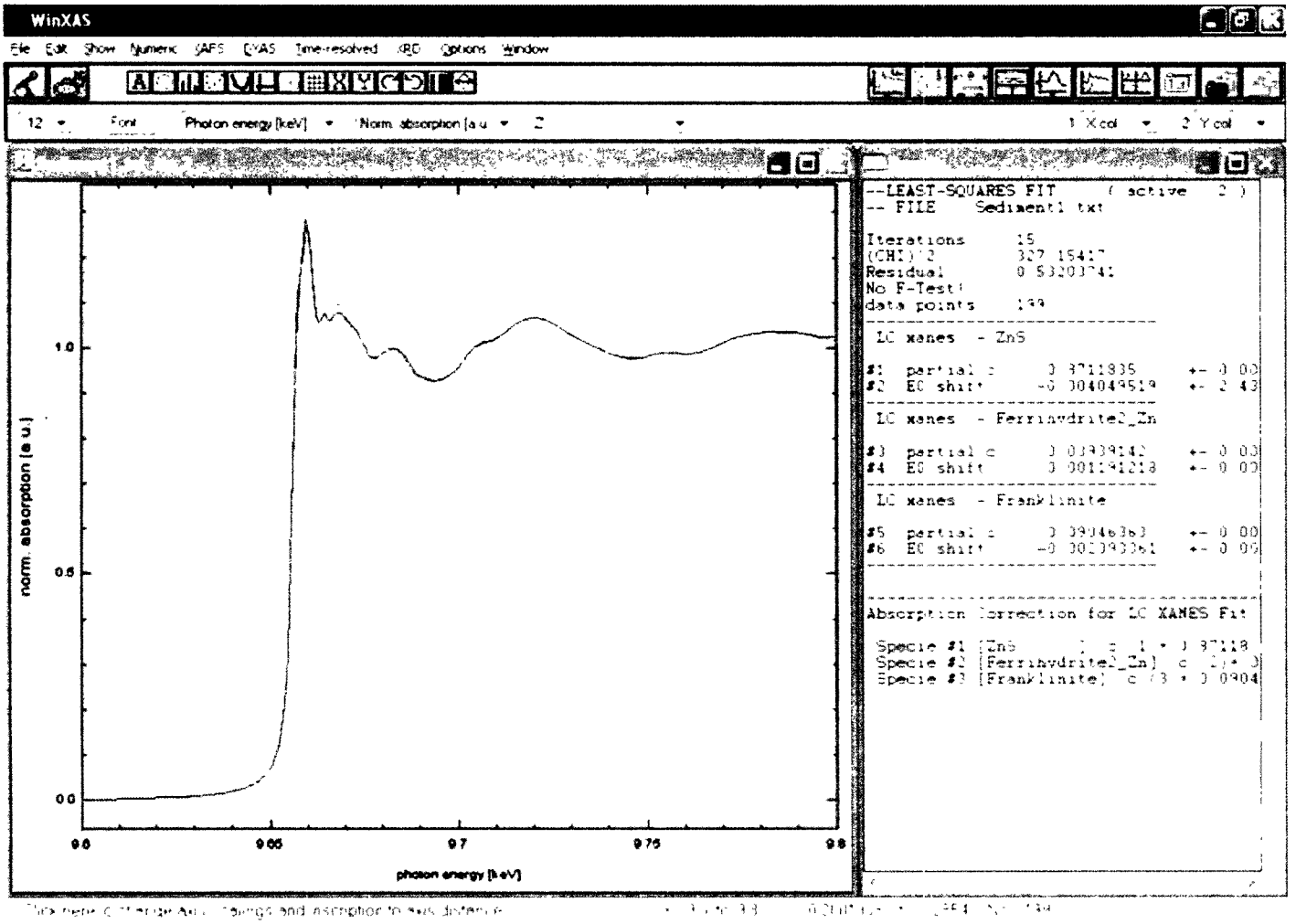


Figure C.20 *Linear combination fitting of X-ray absorption near edge spectroscopy data (LCF-XANES) for a sediment (Sediment1) sample with multiple Zn species. The red curve is the sample data, and the blue curve is the fitted result. The LCF-XANES results indicate Zn speciation as 87% ZnS, 4% Zn sorbed to ferrihydrite, and 9% $ZnFe_2O_4$ (franklinite).*